UNIVERSITA' DEGLI STUDI DELL'INSUBRIA

ISTITUTO SCIENTIFICO SAN RAFFAELE

PhD THESIS

Unravelling the physiopathological role of sacsin, the protein mutate□ in the autosomal recessive spastic ata□ia of Charlevoi□ Saguenay □ARSACS□

Fabiana Longo

Supervisor:

Dott.ssa Francesca Maltecca, Ospedale San Raffaele

Tutor:

Prof.ssa Daniela Parolaro, Università degli Studi dell'Insubria

DOTTORATO IN □EDICINA S□ERI□ENTALE E TRASLA□IONALE, □□□I ciclo, Curriculum □i Neuroscien□e

Francesca Maltecca's Laboratory:

Neurogenomics Unit

Division of Neuroscience

San Raffaele Scientific Institute,

Via Olgettina 60, 20132 Milan, Italy

Ph. +39 02 2643 9117

Academic Year 2018/2019

Ta□le of Contents

Results □□

Chapter □□□

□□Analy□ing the genotype□phenotype correlation of sacsin mutations in ARSACS □isease□□

Discussion

Conclusion

References

⬚u⬚lications

Summary

Sacsin is a large, multimodular protein encoded by the *SACS* gene and found only in vertebrates. It is expressed in the central nervous system, especially in Purkinje cells and corticospinal neurons. Bioinformatics' predictions suggest that sacsin plays a role in protein quality control. However, to date sacsin physiological functions and subcellular localization are still open questions.

Loss of function mutations in *SACS* gene cause Autosomal Recessive Spastic Ataxia of Charlevoix-Saguenay (ARSACS), an early-onset neurodegenerative disorder. Being sacsin function still unknown, the molecular pathogenesis leading to ARSACS has very poorly been investigated. My thesis is focused on exploring sacsin physiopathological role at the cellular level and on dissecting the pathogenesis of ARSACS.

First, we examined how sacsin mutations alter the residual amount of the protein in ARSACS patient cells, since until now it has never been evaluated, leaving a hole in the genotype-phenotype correlation in ARSACS.

At the same time, we investigated the effects of the lack of sacsin in different models depleted of its expression (ARSACS patient fibroblasts, *SACS* KO HeLa cells, *Sacs* KO mouse embryonic fibroblasts, and primary Purkinje neurons from the *Sacs* KO mouse model). We found alterations in mitochondrial dynamics, namely mitochondrial hyperfusion and, by dissecting the molecular mechanism, we demonstrated that the mitochondrial fission process was indeed impaired. In line with these results, we showed that mitochondrial hyperfusion has a strong impact on mitochondrial trafficking in primary Purkinje cells that lack sacsin expression. This highlights the importance of this phenotype in the pathogenesis of ARSACS, as Purkinje neurons are the first cells to be affected.

In sacsin-depleted cells, we detected a dramatic remodelling of the cytoskeletal network, particularly of intermediate filaments. Our data supports the hypothesis that sacsin may be involved in intermediate

filament remodelling in an indirect manner, such as by regulating their folding. This is also suggested by the predicted chaperone-like activities of certain sacsin domains. An intermediate filament reorganization and/or accumulation could sterically hinder both transport and distribution of mitochondria in Purkinje neurons of *Sacs* KO mouse. On the other hand, cytoskeletal derangement could be responsible for impairing DRP1 recruitment.

The cellular phenotypes that we have identified in the absence of sacsin are steps forward in understanding the pathogenetic cascade of ARSACS and shed light on potential sacsin functions.

Ac☐no☐le☐gements

I would like to thank people having supported me in these three years of my PhD journey. I want first to thank my supervisor Francesca Maltecca, for having accepted me to work in her laboratory. I will be forever grateful to her for the straightforward supervision and in deep tutoring activity on my entire PhD journey. Specially, I would thank her for the mentoring activity in regard to my educational and learning route but, above all, in regard to me as person and as rookie scientist.

My gratitude goes to my tutor of Università degli Studi dell'Insubria, professor Daniela Parolaro, for our enjoyable meetings, in which she followed the advances of my PhD project, and she gave me constructive scientific suggestions.

I would like also to thank my laboratory group, in particular my colleague Andrea Del Bondio for his practical help and scientific advices; the former member of the lab Susanna Tulli, for having introduced me in the lab and taught me a lot of experimental methods I still use.

My notable thanks also go to all the other group members, Daniele De Ritis, a recently graduated student working on a different part of the same project on which I work, for his brilliant help and our scientific discussions, particularly for driving all the bioinformatics analysis and the use of CRISPR-Cas9 technology for the generation of knockout and knockin models; the excellent recently graduated student Valentina Baderna for support and help, thank to her ability to face all with a smile; and the new skilful master's thesis student entry Davide Fraticelli.

I would certainly mention in my acknowledgements the former members of the lab of professor Giorgio Casari, with which I still have scientific contacts, as the senior postdoc Laura Cassina and the technician Maurizio De Fusco. I am grateful to professor Giorgio Casari, the scientific mentor of my supervisor Francesca (the former Head of Unit), who followed the advances of my work in the first year of my PhD. I would thank him for the impressive scientific discussions we had and the original points of view

that I perfectly still remember and whose I will jealously keep the memories.

I miei ringraziamenti di cuore vanno al mio fidanzato Ciro che ha sempre supportato e sostenuto me e il mio impegno nel mio lavoro, e alla mia famiglia che mi ha permesso di raggiungere tutti i miei traguardi, sin dall'inizio, e a cui devo semplicemente quello che sono.

My most sincere thanks,
Grazie di cuore,
Fabiana

A☐stract

Sacsin is a large, multimodular protein encoded by the *SACS* gene and found only in vertebrates. It is expressed in the central nervous system, especially in Purkinje cells and corticospinal neurons. Bioinformatics' predictions of sacsin protein structure have revealed the presence of domains sharing high similarity to known chaperone domains involved in proteostasis, as well as uncharacterized domains. This evidence suggests that sacsin plays a role in protein quality control. However, to date sacsin physiological functions and subcellular localization are still open questions, as its large size and complex architecture have so far hindered the progress of studies.

Loss of function mutations in *SACS* gene cause Autosomal Recessive Spastic Ataxia of Charlevoix-Saguenay (ARSACS) disease, a neurodegenerative disorder mainly characterized by early-onset cerebellar ataxia, lower limbs spasticity, and peripheral neuropathy. Being sacsin function still unknown, the molecular pathogenesis leading to ARSACS disease has very poorly been investigated. During my thesis project, I focused on exploring sacsin physiopathological role at the cellular level and dissecting the pathogenesis of ARSACS.

Until now we lack a clear genotype-phenotype correlation in ARSACS patients, as the residual amount of sacsin protein in patients has never been evaluated. Interestingly, we found that regardless of the nature of the mutations, sacsin is almost absent in a panel of different ARSACS patient fibroblasts. We ended up with the result that neither a faster post-translational degradation (e.g. by proteasome or autophagy) nor the formation of mutant sacsin aggregates proved to be the cause of the loss of mutant sacsin. Therefore, we hypothesized the existence of a co-translational quality control mechanism that prevented the complete translation of sacsin protein when it carries mutations in key structural residues. This is indeed possible for such a large multimodular protein as sacsin, whose translation may be preceded by single domains – sensed

as independent folding units by the translational machinery – resulting in a high energy-demand task for the cell.

At the same time, we investigated the effects of the lack of sacsin in different models depleted of its expression (ARSACS patient fibroblasts, *SACS* KO HeLa cells, *Sacs* KO mouse embryonic fibroblasts, and primary Purkinje neurons from the *Sacs* KO mouse model). We found alterations in mitochondrial dynamics, namely mitochondrial hyperfusion and, by dissecting the molecular mechanism, we demonstrated that the mitochondrial fission process was indeed impaired.

Dynamin-related protein 1 (DRP1) is the mediator of mitochondrial fission. It is recruited from the cytosol into the outer mitochondrial membrane, where it assembles into oligomers, hydrolyzes GTP, and constricts the membranes. Our studies showed compromised DRP1 recruitment and higher order oligomerization on the outer mitochondrial membrane of sacsin-depleted cells. In line with these results, we showed that mitochondrial hyperfusion has a strong impact on mitochondrial trafficking in primary Purkinje cells that lack sacsin expression. This highlights the importance of this phenotype in the pathogenesis of ARSACS, as Purkinje neurons are the first cells to be affected.

In sacsin-depleted cells, we detected a dramatic remodelling of the cytoskeletal network, particularly of intermediate filaments. Our data supports the hypothesis that sacsin may be involved in intermediate filament remodelling in an indirect manner, such as by regulating their folding. This is also suggested by the predicted chaperone-like activities of certain sacsin domains. An intermediate filament reorganization and/or accumulation could sterically hinder both transport and distribution of mitochondria in Purkinje neurons of *Sacs* KO mouse. On the other hand, cytoskeletal derangement could be responsible for impairing DRP1 recruitment. Further analyses are ongoing to understand how mitochondrial hyperfusion and intermediate filament rearrangement are linked.

The cellular phenotypes that we have identified in the absence of sacsin are steps forward in understanding the pathogenetic cascade of ARSACS and shed light on potential sacsin functions.

Introduction

⬚⬚ ⬚⬚⬚⬚ gene⬚genomic locali⬚ation an⬚ e⬚pression

1.1.1 – Characterization of SACS gene

SACS gene encodes for the protein sacsin and mutations in *SACS* lead to Autosomal Recessive Spastic Ataxia of Charlevoix-Saguenay (ARSACS). ARSACS is an early-onset neurodegenerative disease characterized by cerebellar ataxia, lower limbs spasticity and peripheral neuropathy (OMIM #270550). The ARSACS locus is localized on chromosome 13q12.12 and was cloned for the first time by Engert et al. in 2000 (Engert et al., 2000), who identified two mutations in the predicted coding sequence as leading to ARSACS. Initially, the gene was predicted to consist of a single giant exon, remarkably of 12800 bp, which contained an open reading frame (ORF) of 11500 bp. Then, other nine canonical exons were identified by retro-transcriptional PCR (RT-PCR) upstream the gigantic one, eight of which are coding, whereas one resides completely in the 5'UTR (Parfitt et al., 2009; Romano et al., 2013), for a total transcript of 15600 bp. The last gigantic exon is now known to be 12868 bp long, which is the longest exon ever identified in the vertebrate genome. The finally predicted ORF encodes for a protein of 4579 amino acids and has a molecular weight of 520 kDa. There are not paralogue genes to *SACS* in the human genome. However, sacsin is highly conserved in mammals. Mouse genome is predicted to express a homologue protein with length and weight identical to human sacsin.

1.1.2 – Expression of SACS gene in mammal tissues

Investigation of *SACS* expression and localization in mammalian tissues was initially carried out by Northern blot analysis, which revealed highest sacsin mRNA expression in human dermal fibroblasts and in different tissues, including: brain, heart, and skeletal muscles. A low expression was seen in pancreas and no expression was detected in lung, liver, and kidney (Engert et al., 2000). Further analysis of central nervous system

(CNS) tissues in human, rat, and monkeys by mRNA *in situ* hybridization confirmed general high expression in all the brain with the most intense areas being: the cerebral cortex, the hippocampus, and the granule cell layer of the cerebellum (Engert et al., 2000).

Parfitt et al. experimentally characterized sacsin protein for the first time (Parfitt et al., 2009). Analysis by Western blot (WB) on mouse and rat tissue extracts confirms that sacsin is specifically expressed in brain and particularly in cerebral cortex and cerebellum, whereas protein levels are low in heart and testis and absent in spinal cord, lung, liver, spleen and kidneys (Fig. Intro 1) (Parfitt et al., 2009).
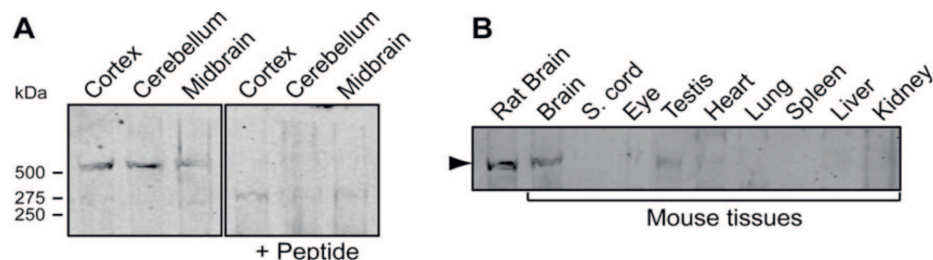
Fig. Intro 1. Sacsin expression in central nervous system by Western Blot (WB). WB analysis of different mouse and rat tissue extracts with polyclonal antiserum directed toward sacsin C-terminal region (residues 4489-4503). A band of 520 kDa is detected specifically in neuronal tissues (B), in particular in cerebellum and cerebral cortex (A). The band was not detected when the antiserum was pre-incubated with the immunizing peptide (Parfitt et al., 2009).

1.1.3 – Su☐cellular localization of sacsin protein

After 18 years since its discovery, sacsin subcellular localization is still unknown. Few works assessed experimentally sacsin localization (Parfitt et al., 2009; Girard et al., 2012) and results were irreproducible in our lab. Bioinformatics analysis reveals that sacsin does not possess any characterized protein sorting signal. Therefore, it is expected to stay in the cytosol. However, one exception regards nuclear localization signals (NLSs): WoLF PSORT – subcellular localization prediction software – identifies seven NLSs, which may suggest a cytosol-nucleus co-localization. The hypothesis of nuclear co-localization is fascinating since sacsin is homologous to Xeroderma Pigmentosum complementation group C (XPC) protein, related to the class of nuclear proteins Rad23, which are

involved in DNA binding and repair (Kamionka and Feigon, 2004). However, different algorithms and software tools do not consistently support such a prediction. Immunofluorescence (IF) analysis, using antibodies directed toward both N-terminal and C-terminal sacsin portion, gave the same staining pattern – a diffused cytosolic distribution, with some punctate spots in the nucleus (Fig. Intro 2, left) (Parfitt et al., 2009). Moreover, they reported partial co-localization to mitochondria by double labelling of sacsin and mitochondrial markers in different cell types (Fig. Intro 2, right) (Girard et al., 2012).
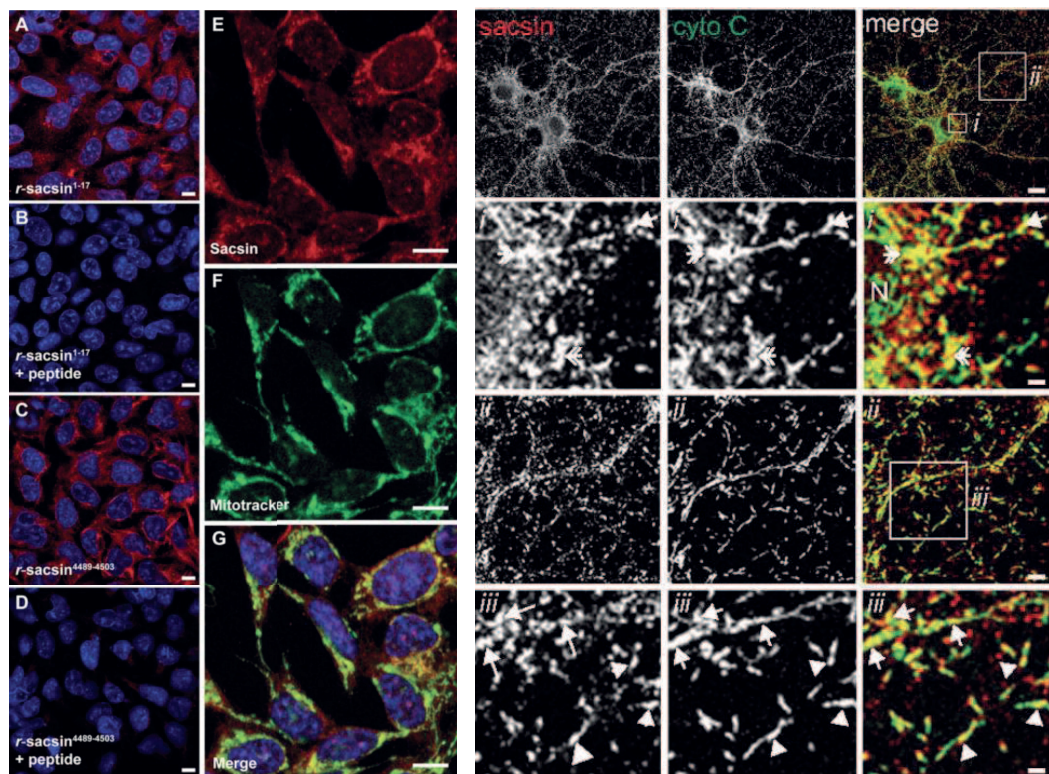
Fig. Intro 2. Sacsin subcellular localization in immunofluorescence (IF). Left: IF with antibodies directed toward N-terminal portion (a) and C-terminal portion (c) of sacsin protein in SHSY5Y cells. In red, the sacsin signal is shown. The signal was undetected when the antibodies were pre-incubated with the immunizing peptide (b, d). A merge (g) between sacsin signal in red (e) and Mitotracker signal in green (f) of a single field shows sacsin overlapping to mitochondria (Parfitt et al., 2009). Right: IF of COS-7 and HeLa cells marked with antibodies directed against sacsin (red) and cytochrome C (green). Merge shows partial overlapping of sacsin to mitochondria (Girard et al., 2012).

However, these results are not reproducible and so far, no sacsin antibodies have been reported consistently to use in IF. The hypothesis of

mitochondrial partial localization is interesting, since ARSACS pathogenesis is linked to impairment of mitochondrial dynamics, as will be demonstrated in Chapter 2. Moreover, due to sacsin's huge dimensions and lack of mitochondrial matrix targeting peptides in its sequence, it is highly unlikely that sacsin is translocated inside mitochondria. Also, sacsin's physical interaction with the mitochondria outer membrane (OMM) remains a controversial point. One key player in mitochondrial dynamics is Dynamin-related protein 1 (DRP1), a GTPase factor related to dynamins encoded by the DNM1L gene. DRP1 is diffused throughout the cytosol and upon stimuli it is recruited on the OMM, in foci that represent future points of fission (Girard et al., 2012; Tilokani et al., 2018). Interaction between endogenous DRP1 and an exogenous protein encoding a FLAG-tagged sacsin N-terminal fragment was reported by co-immunoprecipitation (Fig. Intro 3) (Girard et al., 2012). However, also this result was unconfirmed in our lab in endogenous conditions by co-immunoprecipating endogenous sacsin with available antibodies.
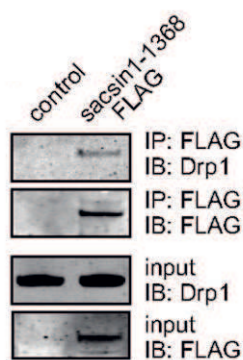
Fig. Intro 3. N-terminus of sacsin coimmunoprecipitates with DRP1. SHSY5Y were transfected with a construct encoding the FLAG-tagged N-terminal sacsin sequence (residues 1-1368). The figure shows the WB of anti-FLAG tag immunoprecipitation of N-terminus sacsin (IP: FLAG), and WB (anti-FLAG tag (IB: FLAG) or anti-DRP1 (IB: DRP1)). Input indicates the lysates that were not immunoprecipitated with anti-FLAG antibodies. IP: immunoprecipitation; IB: immunoblotting (Girard *et al.*, 2012).

Sacsin protein architecture and domains

1.2.1 – Sacsin architecture

Sacsin is a complex multimodular protein, with a total length of 4579 amino acids. Such huge dimension has hampered biochemical studies of the protein, due to the difficulty of cloning and expressing it in a heterologous system. The only available information on sacsin functions

have been obtained by bioinformatics analyses of the sequence and by the expression of small sub regions of the protein *in ⬚itro*.

Bioinformatics analysis reveals the presence, from the N-terminal to the C-terminal, of a Ubiquitin-Like domain (UbL) (Parfitt et al., 2009), three novel supra-domains defined as Sacsin Internal RePeaTs (SIRPT) 1, 2 and 3 (Anderson et al., 2010; Romano et al., 2013), each containing an H_ATPase_c domain homologous to Hsp90 chaperone family (Engert et al., 2000; Anderson et al., 2010), a Xeroderma Pigmentosum complementation group C (XPC) binding domain (XPCB) related to Rad23 (Kamionka and Feigon, 2004), a J domain, homologous to Hsp40 co-chaperone family (Engert et al., 2000; Parfitt et al., 2009) and a Higher Eukaryotes and Prokaryotes Nucleotide-binding domain (HEPN) (Grynberg et al., 2003). General view of sacsin architecture is displayed in Fig. Intro 4) (Parfitt et al., 2009).

Sacsin possesses different domains involved in proteostasis, which suggest it may have a role as a molecular chaperone or as a co-chaperone. The subsequent sections will elucidate in detail information available in literature in respect to each domain and the general picture will corroborate the idea of sacsin involvement in proteostasis. However, since many authors have focused more on specific domains and due to the presence of very uncommon modules, such as the HEPN, the XPCB and the SIRPTs; understanding how all the domain functions are integrated in the endogenous sacsin is still an open field of study.

1.2.2 – ⬚he ⬚terminal portion of sacsin contains a ⬚⬚⬚ ⬚omain

A putative UbL domain, detected by sequence similarity search, is present at the N-terminus of sacsin (Fig. Intro 5) (Parfitt et al., 2009). Ubiquitin-like proteins, such as NEDD8 and SUMO-1 are proteins evolutionarily related to ubiquitin. They are involved in post-translational modification of many protein substrates. Their covalent attachment mediates different functions and interactions. In particular, one that is especially understood is the targeting of many substrates to the proteasome for their degradation. Many multimodular eukaryotic proteins have also domains with sequence

and fold similar to ubiquitin. These domains may confer the same properties given by canonical ubiquitination, such as affinity to the proteasome. It has been shown that some proteins are able to bind the proteasome through their UbL domain (Hartmann-Petersen and Gordon, 2004). One case, especially characterized, is the UV excision repair protein Rad23. It is a protein shared by all eukaryotes and is involved in DNA repair after UV-damage. Rad23 is able to target misfolded chains to the proteasome through interaction between its N-terminal UbL domain and the proteasome (Schauber et al., 1998). Sacsin UbL domain has high significant homology with UbL domain of human homologue of Rad23, with an identity of 43☐ (Fig. Intro 6)) (Parfitt et al., 2009). Moreover, sacsin contains part of the consensus sequence identified to mediate proteasome interaction in Rad23 UbL domain (Parfitt et al., 2009). Interaction between 20S proteasome complex and an exogenous FLAG-tagged N-terminal sacsin fragment (residues 1-124), which contains the UbL domain, was reported by co-immunoprecipitation (Parfitt et al., 2009). Interestingly, the interaction was not detected if the N-terminal sacsin fragment contained changed residues in the conserved consensus binding site for the proteasome (Fig. Intro 5) (Parfitt et al., 2009).

```
Sacsin 22   TVAALASWTVRDVKERIFAETG---FPVSEQRLWRGGRELSDWIKIGDLTSKN---CHL
Rad23  19   KIRMEPDETVKVLKEKIEAEKGRDAFPVAGQKLIYAGKILSDDVPIRDYRIDEKNFVVV
Nedd8  14   EVDIEPTDKVERIKERVEEKEG---IPPQQQRLIYSGKQMNDEKTAADYKILGGSVLHL
Ubiqui 14   TLEVEPSDTIENVKAKIQDKEG---IPPDQQRLIFAGKQLEDGRTLSDYNIQKESTLHL
                                    **        *                        *
```

Fig. Intro 4. Ubiquitin-Like (UbL) of sacsin aligned with other ubiquitin related proteins. Multiple alignment between the putative UbL domain of sacsin and other ubiquitin related proteins and Rad23 UbL domain. Highly conserved residues are illustrated in bold. Residues that play a key role in proteasome binding are marked with a star (Parfitt et al., 2009).

	Input					IP-FLAG				
FLAG-HSJ1a	-	+	-	-	-	-	+	-	-	-
FLAG-sacsin[1-124]	-	-	+	-	-	-	-	+	-	-
L58A/D60A	-	-	-	+	-	-	-	-	+	-
R50A/L51A	-	-	-	-	+	-	-	-	-	+
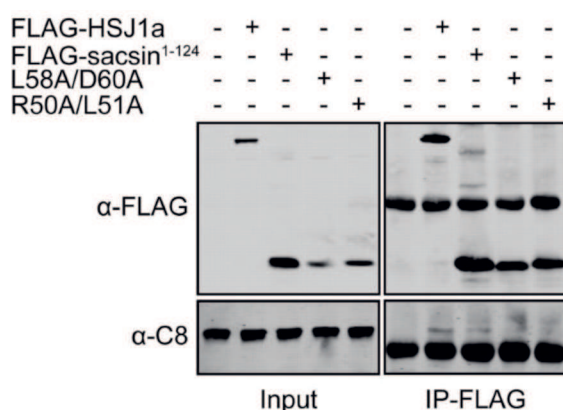
Fig. Intro 5. N-terminus of sacsin co-immunoprecipitates with C8 subunit of 20S proteasome. N-terminal sacsin fragment encoding the UbL domain (residues 1-124) with a FLAG-tag at its C-terminus, was over-expressed in CHO-1 cells. Cellular lysates were precipitated with an anti-FLAG antibody (IP-FLAG). WB were performed with antibodies directed against the C8 subunit of the 20S proteasome complex (☐-C8) and

17

against FLAG tag (￢-FLAG). Input indicates the lysates that were not immunoprecipitated with anti-FLAG antibodies. Interaction with C8 (black arrow) was not detected if the N-terminal sacsin fragment contained two changed residues in the conserved consensus binding site for the proteasome (L58A/D60A and R50A/L51A). FLAG-HSJ1a protein was used as positive control. Asterisk indicates immunoglobulin chains (Parfitt et al., 2009).

1.2.3 – ￢rom the ￢isco￢er￢ of S￢￢ 1￢2￢3 an￢ ￢￢C￢ ￢omain to the i￢entification of S￢￢￢ 1￢2￢3 ￢omains

Inside the sacsin sequence there is a novel supra-domain consisting of around 360 amino acids. Sacsin possesses three copies in tandem with this module that are called Sacsin Repeating Region (SRR) 1, 2 and 3. A supra-domain is defined as a combination of two or more adjacent domains that in turn behave as a functional unit in the evolution of new proteins. Often, a supra-domain displays a novel function beyond that of constituent domains. Constituent domains usually are found isolated or in different combinations in other proteins. The SRR supra-domain is special in regard to this since one of the two components is a novel recurrent sequence of around 200 amino acids that is always found linked downstream to a well-characterized ATPase domain homologous to that of Hsp90 chaperone family (H_ATPase_c domain).

Engert et al. already identified two regions of self-similarity inside sacsin (Engert et al., 2000). In these first studies, they also detected similarity between these repeated regions and Hsp90 family. Dot-plot analysis along the entire characterized sacsin protein sequence identifies three self-homologous regions, sharing 22￢ identity, of about 360 amino acids. These sequences are interspersed by less homologous traits (4￢ identity) of around 1000 amino acids (Fig. Intro 6) (Anderson et al., 2010).
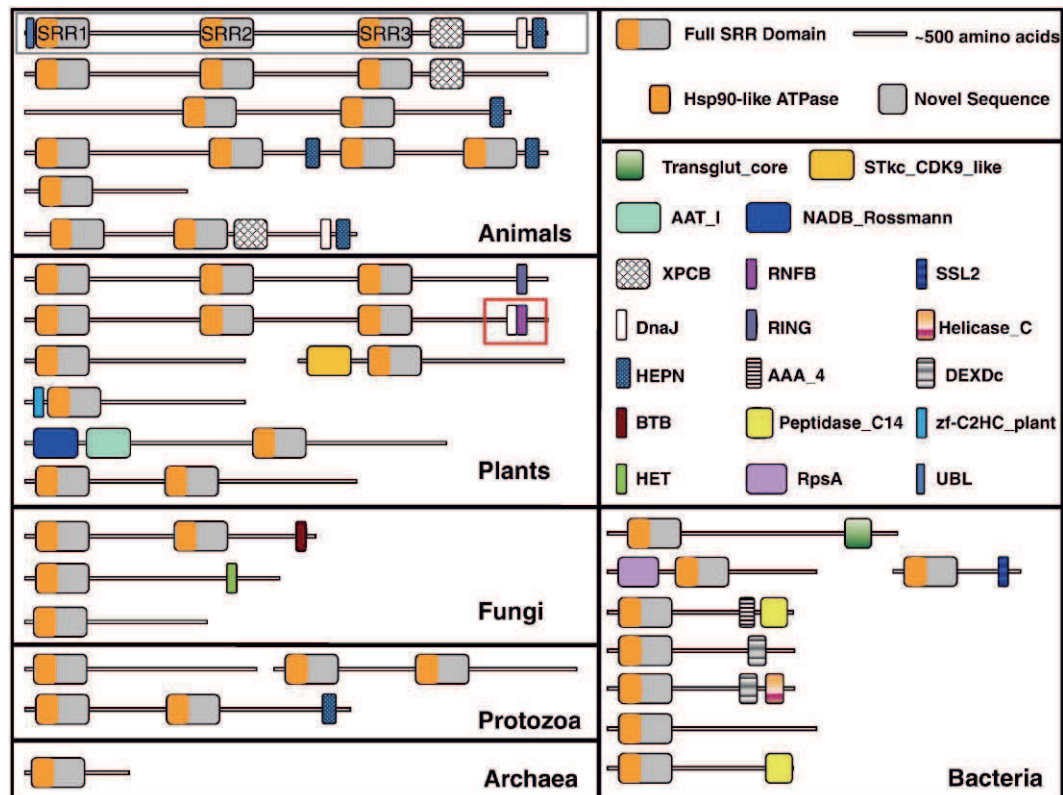
Fig. Intro 6. Scheme of sacsin repeating region (SRR) domain architecture and phylogenetic distribution based on Conserved Domain Database (CDD) (Anderson et al., 2010).

A pairwise alignment between each SRR and yeast Saccharomyces cerevisiae Hsp90 protein confirms that the N-terminal portion of each SRR shares high homology with the H_ATPase domain. PSI-BLAST analysis of the 200 residues in the C-terminal portion of SRRs reveals that this sequence is widely spread in all classes of living organisms (from Archaea to Eukarya) and it is always C-terminally linked to the H_ATPase domain homologous to Hsp90. This sequence never recurs isolated or in combination with other domains. Anderson et al. divided the proteins identified by this analysis into two classes: (1) the ꞏsacsin-like proteinsꞏ and (2) the ꞏSRR-containing proteinsꞏ

Sacsin homologues have been identified only in animals (Anderson et al., 2010; Romano et al., 2013). In particular, in all vertebrate genomes sequenced so far, a sacsin-like protein has always been identified. The percentage of amino acid identity ranges from 93-99ꞏ in mammals, to 83-84ꞏ in birds and reptiles and to 68-70ꞏ in fish (Fig. Intro 7) (Romano et

al., 2013). Moreover, all sacsin-like proteins share the very same architecture, namely three SRR, followed by an XPCB domain, a J domain and a HEPN domain. It is worth it to note that UbL domain is less conserved or not detected at all (Fig. Intro 7) outside mammals, suggesting that its inclusion may have represented a further complexification of sacsin function in the evolutionary tree.
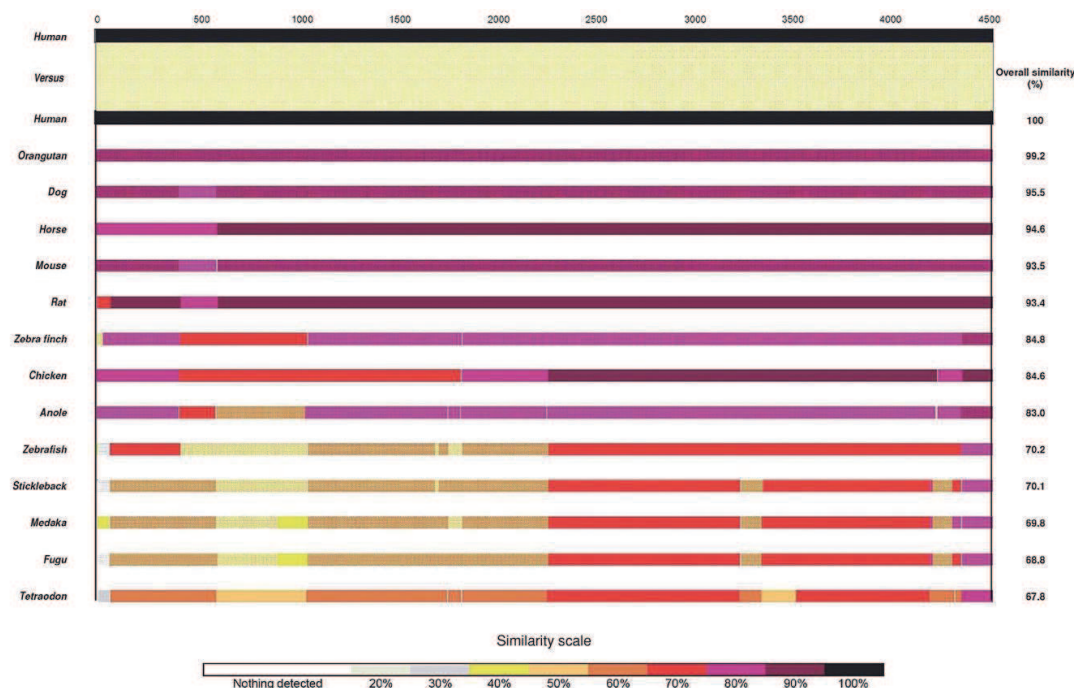
Fig. Intro 7. Analysis of sacsin sequence among different vertebrates. The similarity scale indicates to which homology degree corresponds each colour (Romano et al., 2013).

The SRR-containing proteins are proteins with at least one SRR, independently of the repeat number or the other domains with which they occur. It is the broadest class, with proteins spread in all kingdoms of living organisms (Archaea, Bacteria and Eukarya, included some animals, such as D. rerio) (Anderson et al., 2010). An important issue regards the number of SRR repetitions: as a trend, the number increases with the complexity of organisms, with prokaryotes having mostly single isolated SRR domains and eukaryotes having tandem repetitions of up to three SRRs (Fig. Intro 6) (Anderson et al., 2010). This may suggest not only a selective pressure in expressing adjacent SRR domains in the same

chain, but also an evolutionary convergence in taking together just three SRRs. In fact, the majority of complex SRR-containing proteins in non-animal Eukarya have three SRRs, like in animal's sacsin-homologous genes, and these proteins are not evolutionarily related. SRR domains contain a H_ATPase domain homologous to Hsp90 chaperone and this further suggests sacsin's role in protein quality control. In order to investigate if these Hsp90 domains are functional, Anderson et al. investigated the secondary structure of H_ATPase domain. The results showed a high structural resemblance with ATP binding domain of yeast Hsp90, with conservation in the same position of the majority of secondary structural elements (Anderson et al., 2010). The authors investigated also the ability of the SRR supra-domain to hydrolyze ATP. Interestingly, not only was the protein able to hydrolyze ATP, but also the catalysis kinetics (k_{cat}) was similar to that of yeast Hsp90 (Anderson et al., 2010). The k_{cat} of Hsp90 is known to be extremely low and this is functionally relevant to give time to misfolded or unfolded substrates to fold properly before being directed to degradation.

After the discovery of SRRs, in a more recent work Romano et al. identified further regions of self-homology, in human sacsin, embedded in the intervening regions of the three SRR sequences (Romano et al., 2013). Comprehensively, these analyses revealed that previously identified SRRs supra-domains form, with their adjacent C-terminal sequences, three large modules named Sacsin Internal RePeaTs 1, 2 and 3 (SIRPT 1, 2 and 3). Each module is long 1100 amino acids and share with each other around 18□ of homology; taken together the SIRPTs cover 84□ of all sacsin length (Romano et al., 2013). Each module has one copy of three sub-domains, sr1, sr2 and sr3, interspersed by more divergent sequences (Fig. Intro 8) (Romano et al., 2013). The previously identified SRR supra-domains consist of the N-terminal part of each SIRPT and are formed by the sr1 and sr2 sequences, with the H_ATPase domain embedded in the N-terminal half of sr1. A fourth sequence, srX, is present only in SIRPT 1 and 3. This compositional variability and low

homology between the overall SIRPTs may be functionally important. The three modules may not just be redundant, but may provide differential functions, such as different substrate specificity, in the hypothesis that the Hsp90 motif is functional as a chaperone.

Differently from SRRs, PSI-BLAST analysis of the newly discovered sr3 and srX sequences did not reveal homologous sequences in any database and SIRPT complex architecture is found in all vertebrates and only in this class (Romano et al., 2013). For this reason, sacsin may be involved in some new and complex process that appear with vertebrates. This may corroborate with sacsin high expression in central nervous system (see section 1.1.2).
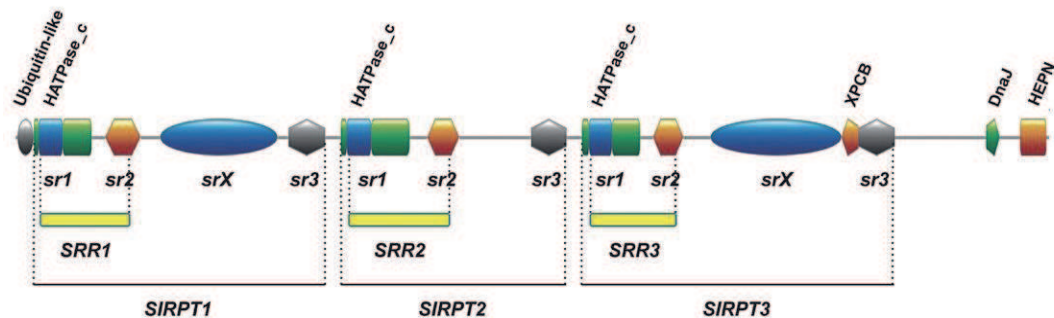
Fig. Intro 8. Scheme of sacsin architecture (Romano et al., 2013).

SIRPT 3 architecture is even more complex than the other SIRPT domains, as an XPCB domain is embedded in it, between the srX and sr3 motifs (Fig. Intro 8) (Romano et al., 2013). XPCB is an uncommon domain that is known to be present only in Rad23 proteins family. These proteins bind DNA and through XPCB domain they bind the XPC protein, which is involved in DNA repair pathway, known as nucleotide excision repair (NER) (Kamionka and Feigon, 2004). In the human genome, there are two Rad23 proteins: hHR23A and hHR23B (respectively homologous to yeast Rad23 protein A and B). Out of Rad23 family, XPCB has only been found in sacsin-like homologues (Kamionka and Feigon, 2004; Anderson et al., 2010) and very rarely in other SRR-containing proteins (Anderson et al., 2010). The Rad23 XPCB domain shares 35☐ identity with that of sacsin (Fig. Intro 9) (Kamionka and Feigon, 2004).

Fig. Intro 9. Multiple sequence alignment between human and mouse sacsin XPCB domain and Rad23 proteins from different species. Hydrophobic amino acids are shown in green (F, A, M, I, L, Y, V, W), negatively charged amino acids in red (D, E), positively charged amino acids in blue (H, K, R), polar amino acids in orange (N, □, S, T), and cysteine in yellow. Above: schematics of the five XPCB □-helices of hHR23A (□1-5) aligned with corresponding amino acid residues below (Kamionka and Feigon, 2004).

The XPCB domain of Rad23 has been shown to interact with the ubiquitin ligase Ube3A2. Ube3A2, encoded by UBE3A2 gene, is involved in Angelman syndrome (OMIM #105830), a neurodevelopmental disease. It has been speculated that sacsin may be a binding substrate of this enzyme through interactions with its XPCB domain (Greer et al., 2010).

1.2.□ – □he C□terminal portion of sacsin contains a □□omain

Similarity between sacsin sequence and J domain typical of Hsp40 co-chaperone family was previously detected (Engert et al., 2000). Hsp40 family encompasses a large set of proteins, expressed in all organisms that interact with the chaperone family of Hsp70 proteins. Sacsin putative J domain shares 60□ identity with different Hsp40 proteins, included DnaJ of E. coli (Fig. Intro 10) (Parfitt et al., 2009).

```
Sacsin  4295  -----KKLKVNSLPEILKEVTSVVEQAWKLPESERKKIIRRLYLKWHPDK
Hsj1    1     -------MAS--YYEILDVPR-------SASADDIKKAYRRKALQWHPDK
DnaJ    1     -------MAKQDYYEILGVSK-------TAEEREIRKAYKRLAMKYHPDR
HDJ1    1     --------MGKDYYQTLGLAR-------GASDEEIKRAYRRQALRYHPDK
TAg     1     MDRVLSRADKERLLELLKLPR-----QLWGDFGRMQQAYKQQSLLLHPDK
Hsc20   1     ----------MDYFTLFGLPA-----RYQLDTQALSLRFQDLQRQYHPDK
Con           -------------Y-ILG-----------AS--DIK-AYR-LA---HPD-

Sacsin  4309  NPEN----HDIANEVFKHLQHEINRL--EKQAFLDQNADRASRRTFSTSA
Hsj1    51    NPDN----KEFAEKKFKE-VAEAYEVLSDKHKREIY--DRYGREG
DnaJ    51    N----QGD-KEAEAKFKE-IKEAYEVLTDSQKRAAY--DQYGHAAFEQ
HDJ1    51    N----K-E-PGAEEKFKE-IAEAYDVLSDPRKREIF--DRYGEEGLKGSG
TAg     51    ---------GGSHALMQE-LNSLWGTFKTEVYNLRM--NLGGTGFQ
Hsc20   51    FASGSQAEQLAAVQQS-ATINQAWQTLRHPLMRAEY--LLSLHGFDLA
Con           ---------------F------A---L-D--KR--Y--D-----------
```

Fig. Intro 10. Multiple sequence alignment of sacsin J domain. Alignment with HSJ1 domain of human Hsp40, E. coli DnaJ, Homo sapiens HDJ1, antigen T of murine polyoma virus (Tag) and E. coli Hsc20. Highly conserved residues are indicated in the line below (Con☐consensus) (Parfitt et al., 2009).

Overexpression of sacsin J domain sub region has allowed to obtain its secondary structure and evaluate its functionality (Parfitt et al., 2009). Results showed that sacsin J domain has a secondary structure that resembles E. Coli DnaJ domain; organized in the same spatial orientation (Fig. Intro 11) (Parfitt et al., 2009).

Sacsin J domain functionality was evaluated in a bacterial complementation assay using an E. coli conditional-mutant strain defective for DnaJ gene that is unable to grow above 37☐C. Expression of an exogenous recombinant DnaJ protein, which possesses sacsin J domain, in this strain was able to rescue the phenotype, proving that the domain may be effectively functional (Fig. Intro 12) (Parfitt et al., 2009). On the contrary, expression in the same strain of the recombinant DnaJ protein, with sacsin J domain carrying a mutation in the crucial Histidine-Proline-Aspartate (HPD) motif, was unable to rescue the mutant phenotype, suggesting that sacsin J domain function depends on its ability to bind Hsp70 chaperone system (Fig. Intro 12) (Parfitt et al., 2009). However, it is important to note that this experiment is insufficient to state that sacsin J domain is functional in the context of mammalian cells.
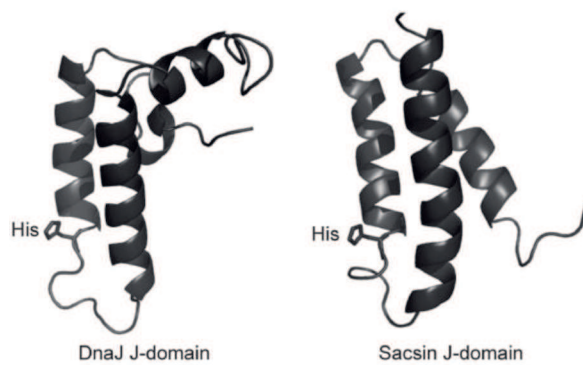
Fig. Intro 11. Sacsin J domain. Scheme of secondary structure of sacsin J domain compared to J domain of *E. coli* DnaJ, made with Pymol (Parfitt *et al.*, 2009).
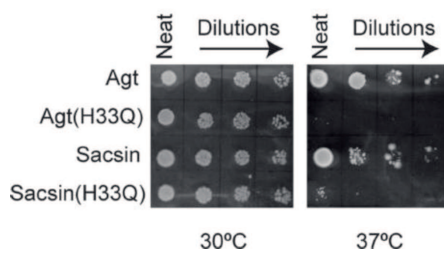
Fig. Intro 12. Bacterial complementation assay proves sacsin J domain is functional. Mutant *E. coli* strain OD259, defective for *dnaJ* and *CbpA* genes, is unable to grow above 37°C due to accumulation of misfolded and unfolded proteins. Expression in this strain of recombinant *Agrobacterium tumefaciens* (Agt) DnaJ protein with human sacsin J domain (Sacsin) can rescue the phenotype. Agt DnaJ with human sacsin J domain carrying a histidine to glutamine mutation in the HPD motif (Sacsin(H33Q)) is unable to rescue the mutant phenotype. Expression of wild type and H33Q Agt DnaJ protein was used as control (Parfitt *et al.*, 2009).

1.2.4 – The C terminal end of sacsin contains a HEPN domain

The last 110 amino acids of sacsin C-terminal portion were found to share homology with the HEPN domain by PSI-BLAST (Grynberg et al., 2003). HEPN is a quite uncommon and interesting protein domain, as it is found only in archaeal and bacterial proteins and in sacsin-like proteins. No HEPN domains have been found in the genome of lower eukaryotes with search similarity (Li et al., 2015b).

The crystal structure of human sacsin HEPN (corresponding to sacsin 4441-4579 residues) was reported by Kozlov et al. (Kozlov et al., 2011). In the crystal structure, four HEPN domains (here called protomers) assemble to form two dimers (Fig. Intro 13) (Kozlov et al., 2011). The propensity of HEPN domains to dimerize with each other was further evaluated measuring the molecular weight of HEPN protomers with molecular-exclusion chromatography that gave twice the predicted

molecular weight of the HEPN amino acid sequence ($\square$15 kDa) (Kozlov et al., 2011). Taken together, these results show that HEPN domain has the tendency to dimerize in solution and it is likely that sacsin protein dimerizes inside the cell through its HEPN domain. The HEPN domains of some bacterial proteins have been structurally characterized too, but their precise function remains unknown. In bacteria, HEPN domain is often associated with a nucleotidyltransferase (TD) domain, either encoded in the same polypeptide or in another subunit (Grynberg et al., 2003; Kozlov et al., 2011; Li et al., 2015b). The TD domain has been involved in resistance to antibiotics. Kanamycin-TD is an example of bacterial HEPN-containing enzyme, which is known to mediate aminoglycosides inactivation. The function of HEPN domain is to bind ATP necessary for the enzymatic reaction. It has been speculated if HEPN domain is able to bind ATP also in sacsin, a function that may facilitate the ATP hydrolysis or binding by the adjacent H-ATPase or J domains. This would be in accord with the hypothesis of sacsin being a chaperone. It was demonstrated through isothermal titration calorimetry and nuclear magnetic resonance that HEPN domain binds GTP with an affinity constant of 1.7 $\square$M (Fig. Intro 13) (Kozlov et al., 2011). It is likely that dimerization structure is necessary for HEPN domain to bind GTP or whatever substrate, and therefore dimerization is likely to be necessary for sacsin HEPN domain to function (Kozlov et al., 2011).
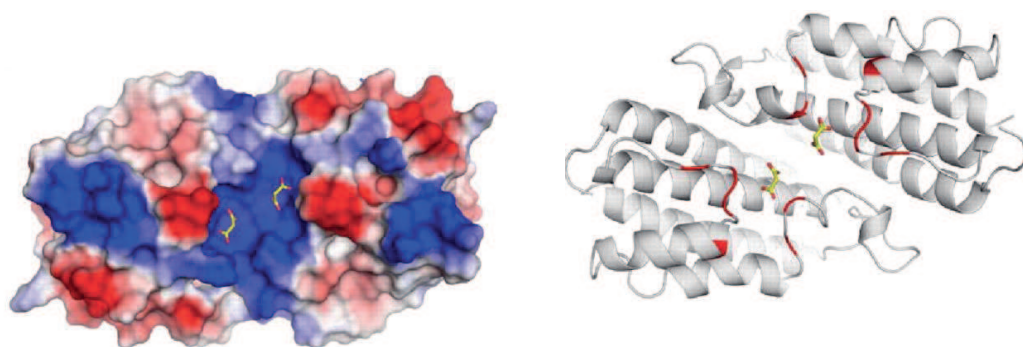
Fig. Intro 13. HEPN dimerization property. Left: electron potential at the surface of HEPN dimer crystal. The crystal structure revealed the binding of two malonate ions, present in buffer solution (in yellow), symmetrically positioned in a large pocket linked with positively charged amino acids, at the dimer interface. Since both protomers are involved in stabilization of each malonate ion through symmetrical residues, it is likely that

dimerization structure is necessary for HEPN domain to bind GTP. Positive charges are in blue, negative charges in red. Right: nuclear magnetic resonance reconstruction of HEPN dimer bound to GTP molecules (Kozlov et al., 2011).

In conclusion, sacsin is a multimodular protein of about 520 kDa, that contains:

-an UbL domain putatively able to bind the proteasome;

-an ATPase domain typical of Hsp90 able to hydrolyze ATP;

-an XPCB binding domain been speculated to bind the ubiquitin ligase Ube3A;

-a J domain with a conserved HPD motif typical of co-chaperone Hsp40 able to bind Hsp70;

-a HEPN domain able to bind GTP and analogues substrates.

These results highlight that sacsin may have a role in proteostasis. However, the validity of these results is limited due to the fact they were all obtained by generating and cloning a single domain of sacsin protein and therefore we do not know how the single domains work and integrate in the context of the entire protein. Moreover, data on UbL domain and J domain were obtained by overexpression conditions (even in non-mammalian cells in the case of J domain), which is far from a physiological state. Therefore, sacsin role inside the cell is still an open issue.

Autosomal Recessive Spastic Ataxia of Charlevoix Saguenay

1.3.1 – The Autosomal Recessive Spastic Ataxia of Charlevoix Saguenay is caused by mutations in SACS gene.

ARSACS (OMIM #270550) is a neurodegenerative disease characterized by early-onset cerebellar ataxia and caused by mutations in *SACS* gene, which encodes the protein sacsin. The disease name is given by the region of Charlevoix-Saguenay-Lac-Saint-Jean (CSLS), in Québec (Canada), where the frequency of healthy carriers is 1/22 (Engert et al., 2000; Bouhlal et al., 2011). The disease was first described in 1979 by Bouchard et al. (Bouchard et al., 1979) in the Québécois patients. In 2000, Engert et al. identified for the first time two mutations in the *SACS* gene in Québec ARSACS families. One mutation is a single base deletion

(g.8844delT) in homozygosis, which belongs to a major haplotype shared by 96☐ of ARSACS families by descending from an ancestral founder in the population that settled first in ☐u☐bec. The second mutation is a nonsense substitution (g.7504C☐ T), which belongs to a minor ARSACS haplotype and that was found in six families in heterozygosis with the major deletion. Both mutations occur in the last gigantic exon and should produce a truncated protein (Engert et al., 2000). Since these discoveries, ARSACS has been diagnosed worldwide, with the identification of more than 200 mutations in *SACS* gene. The disease is globally spread with no correlations (except the French-Canadian in ☐u☐bec) between specific ethnicities and specific allele or disease frequency. It is now considered the second most common recessive ataxia after Friedreich's ataxia (OMIM #229300). Most patients are compound heterozygotes for *SACS* mutations and any type of mutation has been reported; with missense substitutions and frameshift substitutions being the most represented, but also macrodeletions and nonsense mutations are seen (Romano et al., 2013; Synofzik et al., 2013). Table Intro 1 lists all the mutations known, until 2012 (Romano et al., 2013). Table Intro 2 reports all mutations updated to 2018 (The Human Gene Mutation Database (HMGD) software).

		Mutation		Amino-acid change		
Origin	Exon	Original nucleotide position reported[a] (see *Reference*, last column)	Newly assigned nucleotide position in CDS[b]	Original amino-acid position reported[c] (see *Reference*, last column)	Newly assigned amino-acid position in protein[d]	Reference
Synthetic construct	3	sdm	sdm	R50A	p.R50A	Parfitt et al., 2009
Synthetic construct	3	sdm	sdm	R51A	p.R51A	Parfitt et al., 2009
Synthetic construct	4	sdm	sdm	L58A	p.L58A	Parfitt et al., 2009
Synthetic construct	4	sdm	sdm	D60A	p.D60A	Parfitt et al., 2009
The Netherlands	7	c.502G>T	c.502G>T	p.D168Y	p.D168Y	Vermeer et al. (2008, 2009)
Synthetic construct		sdm	sdm	D168Y	p.D168Y	Anderson et al. (2010)
Belgium	7	c.602C>A	c.602C>A	p.T201K	p.T201K	Baets et al. (2010)
Italy	8	c.815G>A	c.815G>A	p.R272H	p.R272H	In house database
Maritime Canada (Acadian descent)	8	c.814C>T	c.814C>T	p.R272C	p.R272C	Guernsey et al. (2010)
Italy	8	c.826C>T	c.826C>T	p.R276C	p.R276C	Prodi et al. (2012)
Aragona-Spain/Croatia	8	c.832C>T	c.832C>T	p.Q278X	p.Q278X	Gazulla et al. (2012)
Japan	8	922C>T	c.922C>T	L308F	p.L308F	Takado et al. (2007)
The Netherlands	8	c.961C>T	c.961C>T	p.R321X	p.R321X	Vermeer et al. (2008, 2009)
Italy	8	c.1373C>T	c.1373C>T	p.T458I	p.T458I	In house database
Italy	8	c.1420C>T	c.1420C>T	p.R474C	p.R474C	In house database
The Netherlands	8	c.1475G>A	c.1475G>A	p.W492X	p.W492X	Vermeer et al. (2008, 2009)
France	8	c.1607C>T	c.1607C>T	p.P536L	p.P536L	Anheim et al. (2008)
Morocco	8	c.1667T>C	c.1667T>C	p.L556P	p.L556P[c]	Baets et al. (2010)
Aragona-Spain	8	c.1894C>T	c.1894C>T	p.R632W	p.R632W	Gazulla et al. (2012)
The Netherlands	9	c.2182C>T	c.2182C>T	p.R728X	p.R728X	Vermeer et al. (2008, 2009)
UK	10	c.2224C>T	c.2224C>T	p.R742X	p.R742X	Terracciano et al. (2010)
Japan	10	g.2405T>C	c.2405T>C	L802P	p.L802P	Kamada et al. (2008)
Belgium	10	c.2971T>C	c.2971T>C	p.C991R	p.C991R	Baets et al. (2010)
Japan	10	987T>C	c.3161T>C	F304S	p.F1054S	Shimazaki et al. (2005)
Aragona-Spain	10	c.3198T>A	c.3198T>A	p.C1066X	p.C1066X	Gazulla et al. (2012)
Belgium	10	c.3491T>A	c.3932T>A	p.M1164K	p.M1311K	Ouyang et al. (2008)
Japan	10	3774C>T	c.4033C>T	Q1198X	p.Q1345X	Okawa et al. (2006)
Italy	10	1858C>T	c.4108C>T	Q620X	p.Q1370X	Grieco et al. (2004)
Turkey	10	g.2018T>C	c.4182T>C	C648R	p.C1398R	Richter et al. (2004)
Italy	10	c.4198T>A	c.4198T>A	p.Y1400N	p.Y1400N	In house database
Italy	10	c.4567T>C	c.4567T>C	p.W1523R	p.W1523R	In house database
Serbia	10	c.4724G>C	c.4724G>C	p.R1575P	p.R1575P	Baets et al. (2010)
Spain	10	c.4748C>G	c.4748C>G	p.P1583R	p.P1583R	In house database
Belgium	10	c.4760A>G	c.4760A>G	p.H1587R	p.H1587R	Baets et al. (2010)
Algeria	10	c.4934G>A	c.4934G>A	p.R1645Q	p.R1645Q	In house database
The Netherlands (Turkish descent)	10	c.4957G>T	c.4957G>T	p.E1653X	p.E1653X	Vermeer et al. (2008, 2009)
The Netherlands	10	c.5125C>T	c.5125C>T	p.Q1709X	p.Q1709X	Vermeer et al. (2008, 2009)
The Netherlands	10	c.5143A>T	c.5143A>T	p.K1715X	p.K1715X	Vermeer et al. (2008, 2009)
Italy	10	c.5629C>T	c.5629C>T	p.R1877X	p.R1877X	Anesi et al. (2011)
Italy	10	c.5639C>T	c.5639C>T	p.T1880I	p.T1880I	In house database
Algeria	10	c.5719C>T	c.5719C>T	p.R1907X	p.R1907X	Prodi et al. (2012)
Tunisia	10	3662T>C	c.5836T>C	W1196R	p.W1946R	El Euch-Fayache et al. (2003)
Japan	10	6355C>T	c.6355C>T	R2119X	p.R2119X	Hara et al. (2007)
Algeria	10	c.6409C>T	c.6409C>T	p.Q2137X	p.Q2137X	H'mida-Ben Brahim et al. (2011)
Italy	10	c.6680T>C	c.7121T>C	p.L2374S	p.L2374S	Terracciano et al. (2009)
Belgium	10	c.7276C>T	c.7276C>T	p.R2426X	p.R2426X	Baets et al. (2010)
Quebec	10	g.5254C>T	c.7504C>T	R1752X	p.R2502X	Engert et al. (2000)
France	10	c.7673C>T	c.7673C>T	p.A2558V	p.A2558V	Anheim et al. (2008)
Spain	10	7848C>T	c.8107C>T	R2556C	p.R2703C	Criscuolo et al. (2005)
France	10	c.8289_8291delTTC	c.8289_8291delTTC	p.Y2763X	p.Y2763X	In house database
Morocco	10	c.8393C>A	c.8393C>A	p.P2798Q	p.P2798Q[f]	Baets et al. (2010)
Aragona-Spain/Italy	10	c.8677A>T	c.8677A>T	p.R2893X	p.R2893X	In house database
Aragona-Spain	10	c.9670C>T	c.9670C>T	p.R3224X	p.R3224X	Gazulla et al. (2012)
Japan	10	7492T>C	c.9742T>C	W2498R	p.W3248R	Ogawa et al. (2004)
Tunisia	10	c.10290C>G	c.10290C>G	p.Y3430X	p.Y3430X	H'mida-Ben Brahim et al. (2011)
The Netherlands (English descent)	10	c.10442T>C	c.10442T>C	p.L3481P	p.L3481P	Vermeer et al. (2008, 2009)
The Netherlands	10	c.10906C>T	c.10906C>T	p.R3636X	p.R3636X	Vermeer et al. (2008, 2009)
Belgium	10	c.10907G>A	c.10907G>A	p.R3636Q	p.R3636Q[f]	Baets et al. (2010)
Belgium	10	c.10934T>C	c.10934T>C	p.L3645P	p.L3645P	Baets et al. (2010)
Belgium	10	c.10954C>A	c.10954C>A	p.P3652T	p.P3652T[f]	Baets et al. (2010)
Belgium	10	c.10517T>C	c.10958T>C	p.F3506S	p.F3653S	Breckpot et al. (2008)
Italy	10	c.10743C>T	c.11185C>T	p.Q3582X	p.Q3729X	Kamionka and Feigon (2004), Masciullo et al. (2008)
Tunisia	10	c.11374C>T	c.11374C>T	p.R3792X	p.R3792X	Bouhlal et al. (2008)
Maritime Canada (Acadian descent)	10	c.11707C>T	c.11707C>T	p.R3903X	p.R3903X	Guernsey et al. (2010)
The Netherlands	10	c.12160C>T	c.12160C>T	p.Q4054X	p.Q4054X	Vermeer et al. (2008, 2009)
Tunisia	10	c.10046G>C	c.12220G>C	p.A3324P	p.A4074P	El Euch-Fayache et al. (2003), H'mida-Ben Brahim et al. (2011)
Italy	10	c.12428_12429insA	c.12428_12429insA	p.Y4143X	p.Y4143X	Prodi et al. (2012)
Japan	10	10723C>T	c.12973C>T	R3575X	p.R4325X	Takiyama (2006), Yamamoto et al. (2006)
The Netherlands	10	c.12992G>A	c.12992G>A	p.R4331Q	p.R4331Q	Vermeer et al. (2008, 2009)
Synthetic construct		sdm	sdm	R4331Q	p.R4331Q	Parfitt et al., 2009
Italy		c.12991C>T	c.12991C>T	p.R4331W	p.R4331W	Prodi et al. (2012)
Synthetic construct		sdm	sdm	H4337Q	p.H4337Q	Parfitt et al., 2009
Belgium	10	c.13027G>A	c.13027G>A	p.E4343K	p.E4343K	Baets et al. (2010)
Italy	10	c.13132C>T	c.13132C>T	p.R4378X	p.R4378X	Anesi et al. (2011)
UK	10	c.13237C>T	c.13237C>T	p.Q4413X	p.Q4413X	Terracciano et al. (2010)
Aragona-Spain	10	c.13405G>C	c.13405G>C	p.A4469P	p.A4469P	Gazulla et al. (2012)
Belgium	10	c.13523A>C	c.13523A>C	p.K4508T	p.K4508T	Baets et al. (2010)
Turkey	10	g.11471A>G	c.13645A>G	N3799D	p.N4549D	Richter et al. (2004)
Synthetic construct		sdm	sdm	N4549D	p.N4549D	Kozlov et al. (2011)

Table Intro 1. Pathogenic mutations identified in *SACS* gene of ARSACS patients, updated to January 2012. The list includes 41 missense, 28 nonsense substitutions, and 2 frameshift mutations. The table contains also 8 artificial site-directed mutations generated by different authors in order to study sacsin function: 4 in the UbL domain, 1 in H_ATPase domain, 2 in J domain, 1 in HEPN domain (Romano et al., 2013).

Gene Symbol	Chromosomal location	Gene name	cDNA sequence
SACS (Aliases: available to subscribers)	13q12	Spastic ataxia of Charlevoix-Saguenay (sacsin) (Aliases: available to subscribers)	

Mutation type	Number of mutations
Missense/nonsense	98
Splicing	1
Regulatory	0
Small deletions	43
Small insertions	16
Small indels	1
Gross deletions	9
Gross insertions/duplications	1
Complex rearrangements	0
Repeat variations	0
Public total (HGMD Professional 2018.3 total)	**169** (262)

Disease/phenotype	Number of mutations
Spastic ataxia, Charlevoix-Saguenay	150
Ataxia	5
Spastic ataxia	4
Cerebellar ataxia	3
Neuropathy, prominent sensorimotor	2
ARSACS without leg spasticity	1
Ataxia, early-onset	1
Sacsin-related ataxia	1
Spastic ataxia, Charlevoix-Saguenay ?	1
Spastic paraplegia, non-ataxic, and peripheral neuropathy	1

Table Intro 2. The Human Gene Mutation Database (HMGD) pathogenic mutations identified in *SACS* gene of ARSACS patients, updated to December 2018.

The recessive pattern of clinical phenotype, and the fact that many of the mutations should lead to the production of a truncated protein, suggests that the molecular pathology mechanism is associated with loss of function of sacsin protein (Baets et al., 2010; Bouhlal et al., 2011; Romano et al., 2013; Synofzik et al., 2013). However, any characterization of the outcomes of sacsin mutations at the protein level has never been performed.

1.3.2 – A□SACS clinical manifestations

ARSACS is a neurodegenerative disease characterized by cerebellar ataxia, spasticity, and peripheral neuropathy. Progressive degeneration of

the cerebellar vermis has been documented in patients who underwent magnetic resonance imaging (MRI) and post-mortem analysis (Bouchard et al., 1979; Bouhlal et al., 2011; Synofzik et al., 2013).   Other typical signs include: distal amyotrophy (likely as consequence of neuropathy), dysarthria, limb weakness, sensory loss, pyramidal signs, and cerebellar eye manifestations (e.g. nistagmus). The clinical picture in French-Canadian patients of which the majority harbour the same mutation in homozygosis (g.8844delT), is rather homogeneous as described by Bouchard et al: signs of spasticity first appear between 12-24 months in the lower limbs and unsteady gait is noticed when the patients begin walking. Patients become wheelchair bound by the mean age of 41, with a reduced life expectancy (50 years) (Bouchard et al., 1979; Bouhlal et al., 2011). The discovery of many clinical cases throughout the world has expanded the clinical spectrum, showing much more phenotype variability, especially regarding age of onset and presence of spasticity. In some patients, the disease starts later in childhood, but rarely after 12 years of life. Moreover, there are case reports of patients who do not develop spasticity in their lower limbs. On the other hand, dysarthria has been described as a common feature and it is likely a consequence of ataxia. The speech is slurred in childhood and becomes incomprehensible by adulthood (Bouchard et al., 1979).

Post-mortem brain analysis from ARSACS patients and MRI studies revealed a remarkable atrophy of anterior vermis of cerebellum, associated with loss of Purkinje cells, starting very early in the disease course. Instead, the cerebellar hemispheres are less affected. Bilateral demyelination of both the corticospinal tract (that can account for spasticity and pyramidal signs common in ARSACS patients) and of the dorsal spinocerebellar tract were also observed. Of course, the high specific expression of sacsin in central nervous system and in particular in cerebellum and cerebral cortex (see section 1.1.2), is in accordance with the primary relevance of these tissues and cell types to the development of the disease.

ARSACS diagnosis includes MRI, neurological evaluation and sensory and nerve conduction studies. However, since ARSACS patients present high clinical variability and many symptoms are shared by other recessive spinocerebellar ataxia, the ultimate diagnosis is made by genetic testing in order to identify mutations in *SACS* gene. The process is time consuming and expensive, as the entire gene, which is very large, must be sequenced. Moreover, in many cases with uncertain variants it is still necessary to sequence other sets of ataxia-related genes in order to exclude alternative diagnosis (Silvestri et al., 2012). As of today, there are no curative therapies available for ARSACS patients, and the treatments on the market only alleviate the symptoms of the disease.

1.3.3 – Genotype phenotype correlation in ARSACS

All ARSACS patients from different ethnicities show a similar clinical phenotype with ataxia, neuropathy, and a similar disease progression. Greater variability regards specific symptoms, such as retinal hypermyelination, mental retardation, and age of disease onset. Moreover, spasticity was not observed in some patients (Bouhlal et al., 2011). These variations do not correlate with specific mutations. Variability has been observed even in the presence of the same mutation. For example, one mutation was found to segregate in two ARSACS Tunisian families. In one family, the disease appeared at 3 years of age and was associated to skeletal abnormalities, whereas in the other family the onset was after the age of 10, and patients did not show skeletal problems. On the contrary, a study conducted with over 23 German patients from 16 different families that had 16 different mutations showed a very similar clinical phenotype (Bouhlal et al., 2011).
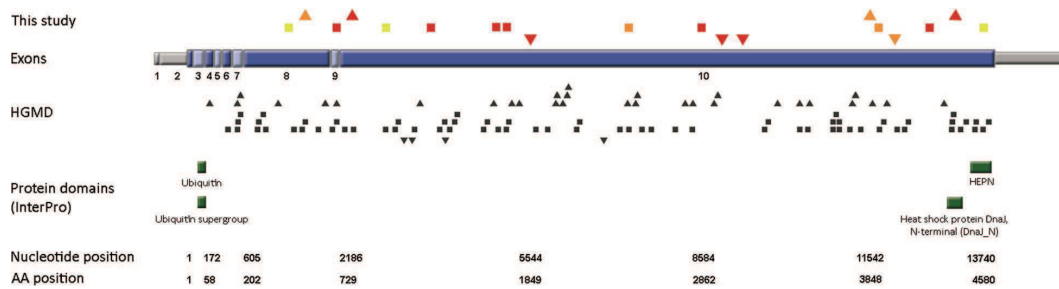
Fig. Intro 14. Representation of SACS sequence variants. Variants have been summarized from ARSACS patients (Synofzik et al., 2013) and HMGD, aligned to sacsin domains (green rectangles). Squares ☐ missense mutations; triangles with downward orientation ☐ indels; triangles with upward orientation ☐ deletions. Red ☐ pathogenic variant, orange ☐likely pathogenic, yellow ☐uncertain (Synofzik et al., 2013).

Besides the individual clinical variability, there is not a clear genotype-phenotype correlation considering the nature, the localization of the mutations and the disease severity, as the first missing point is a correlation with the residual amount of sacsin in different ARSACS-causing mutations. Indeed, any type of analysis on mutant sacsin protein has not been performed, so there is no information about the retention or the lack of sacsin functional domains. Moreover, mutations spread randomly all over the gene. Patients with macrodeletions that lead to loss of more than 3000 amino acids have similar phenotype to those that harbour single base insertion/deletions (indels) in the C-terminal end of the protein or that have missense substitutions (Fig. Intro 14) (Synofzik et al., 2013). However, in a comprehensive work, Romano et al. discovered that missense mutations in heterozygosis with truncating mutations (nonsense substitutions or indels) in charge of the DnaJ domain are associated with patients with more severe spastic ataxia (SPAX) scores. Interestingly, the SPAX scores of these patients are similar to those of patients carrying truncating mutations on both alleles, which are expected to be more deleterious (Fig. Intro 15) (Bouhlal et al., 2011). These results may suggest a critical function of DnaJ domain.
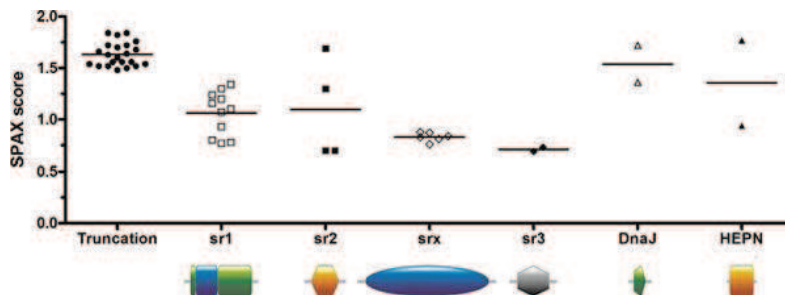
Fig. Intro 15. SPAX score of ARSACS patients. The score evaluates the spastic and ataxia severity of patients; it is reported for patients carrying a missense mutation, in charge of different sacsin domains, in heterozygosis with a truncating mutation (which is expected to lead to protein absence); SPAX scores for patients carrying truncating mutations in both alleles are reported for comparison. Horizontal lines indicate mean values (Romano et al., 2013).

1.3. – *Phenotype of cellular models of sacsin absence*

The study of sacsin domains, recapitulated in section 1.2, allows us to suppose that this protein is involved in protein quality control. The presence of UbL domain and J motif suggests that sacsin may interact with the proteasome or the Hsp70 chaperone family or both. Hsp70 protein family is involved in the response induced by cellular stress due to the presence of misfolded or unfolded protein aggregates. Such aggregates are extremely toxic for the cell and have been widely associated to neurodegeneration pathologies. Ataxin-1 (encoded by the ATXN1 gene) is a chromatin-binding factor that belongs to the well-known class of polyQ containing proteins. Mutations leading to expansion of polyQ tract have been demonstrated to lead to toxic aggregations of the protein that cause Spinocerebellar Ataxia 1 (SCA1) (OMIM #164400). Hsp70 is found to be actively recruited to these aggregates. In one experiment, SHSY5Y human cells were transfected with wild type ataxin-1 linked to GFP (GFP-ataxin-1) or with one of two mutated GFP-ataxin-1 forms with expanded polyQ tract (GFP-ataxin-1 30Q and GFP-ataxin-1 82Q, respectively with 30 and 82 glutamine residues). Labelling endogenous sacsin has revealed that the protein co-localizes to foci of large GFP-ataxin-1 82Q aggregates in the nucleus of the cells (Fig. Intro 16) (Parfitt et al., 2009).
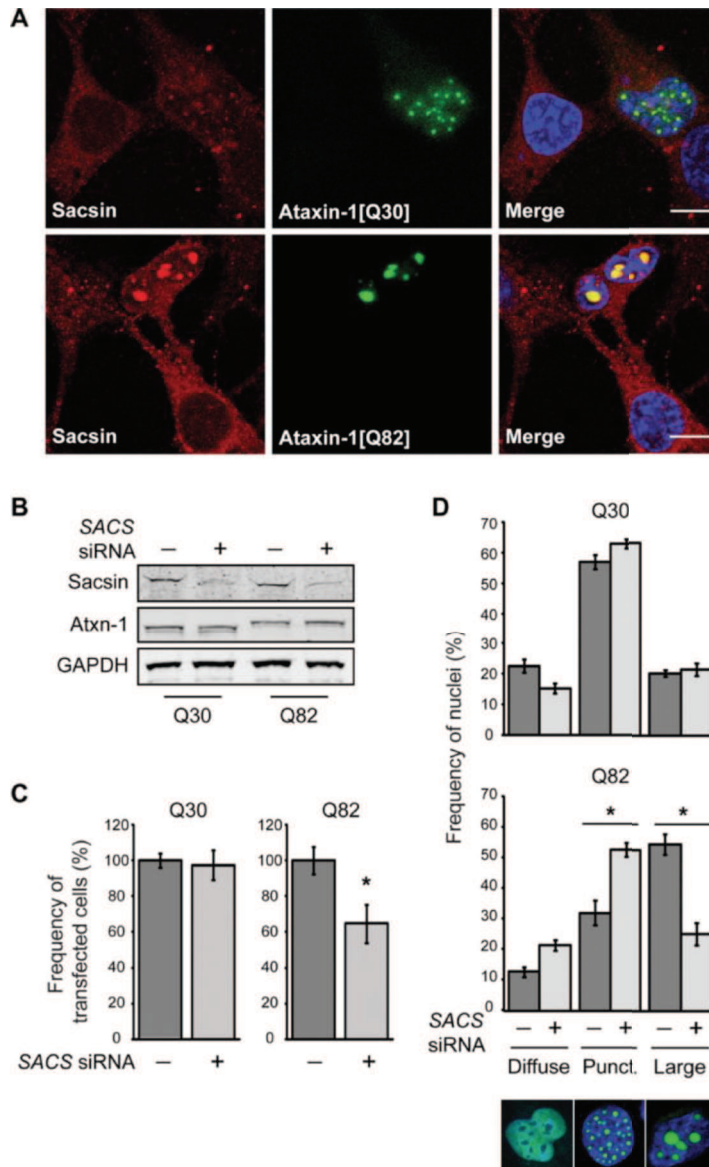
Fig. Intro 16. Sacsin is recruited to ataxin-1 aggregates that accumulate in the nucleus, in particular to larger inclusions consisting of GFP-ataxin-1 82 . (A) IF of SHSY5Y cells transfected with GFP-ataxin-1 82 or GFP-ataxin-1 30 and sacsin. (B) Evaluation of sacsin knockdown and ataxin expression. (C) Comparison of total number of cells that express mutated GFP-ataxin-1 in cells transfected with *SACS* siRNAs relative to cells transfected with scrambled siRNAs. Sacsin reduction causes a reduction in the number of cells expressing GFP-ataxin-1 82 , but not of cells expressing GFP-ataxin-1 30 (D) Quantification of mutated ataxin-1 distribution in the nucleus in cells co-transfected with GFP- ataxin-1 82 or GFP-ataxin-1 30 and *SACS* siRNAs. Ataxin-1 is found inside the nucleus in a diffused manner (Diffuse), in smaller foci (Punct.) or in large inclusions (Large). Reduction of sacsin causes a reduction in the number of cells with large inclusions that express GFP- ataxin-1 82 due to death of these cells (Parfitt et al., 2009).

As a further proof, siRNAs-mediated *SACS* knockdown SHSY5Y cells

transfected with GFP-ataxin-1 82 showed an increased toxicity of the

mutated ataxin-1 form, with an increased number of cells with ataxin-1 aggregates in the nucleus and an increased cell mortality correlated with the reduction of cells with very large inclusions of ataxin-1 in the nucleus (Fig. Intro 16) (Parfitt et al., 2009). These results may confirm a role of sacsin in proteostasis, particularly in protecting neurons from stress induced by protein aggregation. This would thus explain neuron degeneration in the absence of the protein. However, these studies are limited due to overexpression of an exogenous aggregating protein and we do not have data on sacsin's role with endogenous protein aggregates. Moreover, direct interaction between ataxin-1 aggregates and sacsin is based on IF of endogenous sacsin, but all available sacsin antibodies tested in our lab are unable to work in IF.

Other interesting lines of research in cellular models of sacsin absence are connected with the hypothesis of sacsin involvement in basic processes of mitochondrial biology, such as mitochondrial dynamics, functionality, and transport in neurons.
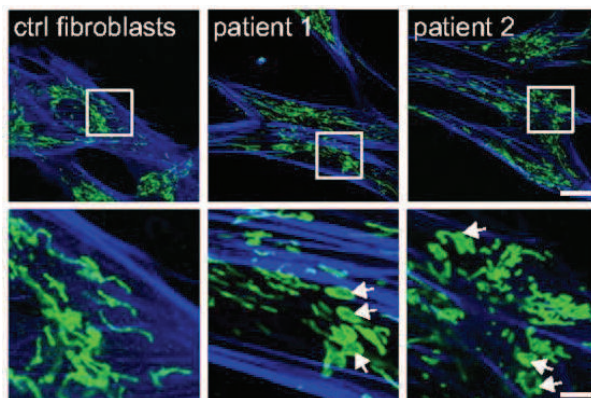
Fig. Intro 17. Mitochondrial bulbed structures in ARSACS patient fibroblasts. IF using antibody against TOM20 (green), a mitochondrial marker and against phalloidin (blue), which marks actin filaments. Arrows indicate bulbed-like mitochondria, which are mitochondria extremely fused (Girard et al., 2012).

Sacsin involvement in mitochondrial dynamics has been firmly established by investigating mitochondrial morphology both in siRNA-mediated *SACS* knockdown in SHSY5Y cells and in patient fibroblasts cells. In these models, the mitochondrial network appears more fused than in the wild

type (WT) conditions. In patient fibroblasts, in particular, bulbed mitochondria are present, which are a typical sign of extreme mitochondrial hyperfusion (Fig. Intro 17) (Girard et al., 2012).

Mitochondrial morphology and shape is a consequence of fusion and fission rate (mitochondrial dynamics) of this extremely dynamic organelle (Chen and Chan, 2009; Wai et al., 2016). As discussed in section 1.1.3, DRP1 is a key player in mitochondrial dynamics, as it mediates mitochondria division by oligomerizing on OMM in foci that represent future points of fission (Kraus and Ryan, 2017). Deregulation of DRP1 in the absence of sacsin was investigated in literature as previously shown in Fig. Intro 3. Girard et al. identified, through immunoprecipitation, an interaction between the N-terminal 1368 amino acids of sacsin (encompassing the UbL domain and first SRR) and DRP1 (Girard et al., 2012). Bradshaw et. al investigated the recruitment of DRP1 to OMM in different cellular models in absence of sacsin. The number of DRP1 foci on OMM is both lower in patient and in siRNA-mediated *SACS* knockdown fibroblasts. Additionally, those foci have smaller diameter and reduced signal intensity relative to controls (Bradshaw et al., 2015). In contrast, the size of cytosolic DRP1 foci was equivalent.

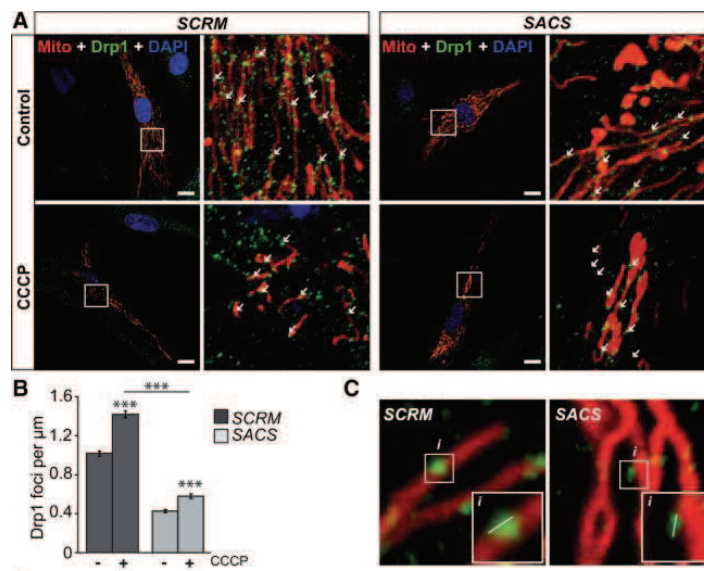Fig. Intro 18. *SACS* siRNA fibroblasts show reduced mitochondrial fragmentation compared to scrambled. (A) IF on human primary fibroblasts (*SACS* siRNA or scramble siRNA) after 48 hours of treatment with CCCP. In green labelled DRP1 and in blue nuclei

with DAPI. Arrows indicate DRP1 foci associated with mitochondria. (B) Quantification of DRP1 foci per mitochondrial length in *SACS* siRNA or scramble siRNA fibroblasts. (C) Enlargement of DRP1 punctae along mitochondria length in *SACS* siRNA or scramble siRNA fibroblasts (Bradshaw et al., 2015).

Moreover, after carbonyl cyanide m-chlorophenyl hydrazone (CCCP) treatment (an uncoupling agent that dissipates mitochondrial potential and leads to DRP1-driven mitochondrial fragmentation) the degree of fragmentation (calculated as the ratio of fragmented mitochondria between CCCP-treated and vehicle-treated controls) was lower in *SACS* knockdown cells relative to scrambled-siRNA-transfected controls and the increase of DRP1 foci on OMM was significantly less (Fig. Intro 18) (Bradshaw et al., 2015). These data were confirmed also in patient fibroblasts. This indicates an impairment of DRP1 recruitment to OMM in absence of sacsin, causing therefore the hyperfused morphology seen in ARSACS patient cells. However, in recent literature, in contrast with the commonly accepted pathway where cytosolic DRP1 is directly recruited to a constriction site through its membrane-anchored adaptors, a 'targeted equilibrium' has been proposed. In this model, dimeric and oligomeric forms of DRP1 are in constant balance between the cytosol and mitochondria. Mitochondria-bound DRP1 puncta can merge into a mature-sized DRP1 complex capable of moving laterally along the mitochondrial tubule, inducing constriction and eventually fission (Tilokani et al., 2018). In this new view, IF methods of DRP1 do not reveal the active DRP1 oligomers, as they do not distinguish between inactive oligomers and active high order DRP1 complexes. Moreover, levels of total DRP1 were not reduced in WB analysis, corroborating that decrease of OMM foci is not due to a general reduction of DRP1, but a problem in DRP1 mobilization and recruitment.

Mitochondrial fission is a crucial process to isolate those parts of the mitochondrial network that are damaged, in order to target unhealthy mitochondria to mitophagic pathway, a highly selective form of autophagy specialized in degrading mitochondria (Chen and Chan, 2009; Youle and Narendra, 2011). This is crucial for mitochondrial quality control, as it

maintains functional mitochondria with intact membrane potential. Indeed, impairment of mitochondria bioenergetics, measured as membrane potential integrity, has been assessed in models of sacsin absence. A defect in Tetramethylrhodamine methyl ester (TMRM) loading in mitochondria, measuring membrane potential integrity, has been found in models of sacsin absence. TMRM is a red-orange fluorescent dye, which enters functional mitochondria driven by membrane potential. Its signal accumulation is therefore an indicator of membrane potential integrity. At steady state, both siRNA-mediated *SACS* knockdown in SHSY5Y cells and ARSACS patient fibroblasts have reduced membrane potential, seen as lower TMRM intensity signal, indicating a general altered functionality of mitochondria (Girard et al., 2012). Moreover, SHSY5Y cells stained with the red fluorescent dye Mitotracker, which marks specifically mitochondria, were treated with the uncoupling agent CCCP. Since Mitotracker accumulation in mitochondria is sensitive to alterations in membrane potential, treatment with CCCP, that dissipates the potential, cancels the Mitotracker fluorescent signal, whereas CCCP washout is expected to recover fluorescent signal. In SHSY5Y knockdown cells the recovery of signal is much slower than in the control condition (Girard et al., 2012). Bradshaw et al. further demonstrated impairment of mitochondrial bioenergetics in ARSACS patient fibroblasts and SHSY5Y knockdown cells. In both models, they found by microarray analysis, a reduction of expression of genes encoding the oxidative phosphorylation (OXPHOS) complexes and an increase in the expression of genes related to oxidative stress, suggesting an accumulation of oxidative damage in absence of sacsin, a clear consequence of mitochondrial impairment (Bradshaw et al., 2015). Moreover, in ARSACS patient cells and SHSY5Y *SACS* knockdown cells, oxygen consumption rate was reduced, compared to control, both in basal conditions and upon inhibition of complex IV with oligomycin, upon the uncoupling agent FCCP and inhibition of complex I and III with rotenone and antimycin A (Fig. Intro 19) (Bradshaw et al., 2015).
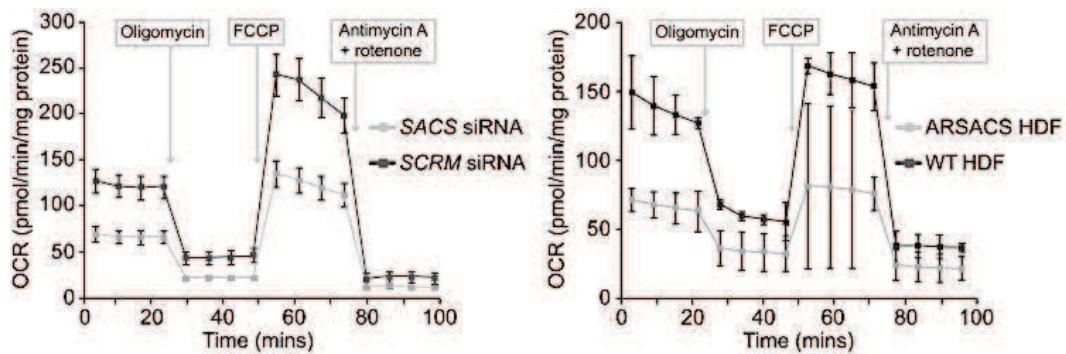
Fig. Intro 19. Reduced Oxygen Consumption Rate (OCR) of *SACS* siRNA and ARSACS cells. OCR in cells transfected with *SACS* siRNA relative to control transfected with scrambled siRNA (left) and ARSACS fibroblasts relative to controls (right) (Bradshaw et al., 2015).

Finally, Girard et al. characterized for the first time the mitochondrial functionality of cultured cells derived from *Sacs* knockout (KO) mouse model (*Sacs* KO). This mouse was obtained by gene targeting in embryonic stem cells (ESCs), replacing the last *Sacs* exon with the IRES-☐Gal cassette (see section 1.3.5). Purkinje cells, the primary cell type involved in ARSACS disease course, derived from *Sacs* KO mice were stained with the mitochondrial affine cationic JC-1 fluorescent dye and compared to Purkinje cells from WT mice. JC-1 dye is a probe sensitive to membrane potential. It accumulates inside mitochondria and emits a green band when the potential is weakly polarized, whereas red band is emitted when the polarization is stronger. Purkinje cells from KO mouse showed decreased mitochondrial potential, detected as a lower red to green ratio JC-1 signal (Girard et al., 2012).

Another aspect of mitochondrial biology affected in absence of sacsin is mitochondrial transport and localization within neurons. siRNA-mediated *Sacs* knockdown in cultured murine hippocampal neurons showed indeed a reduced number of mitochondria localized to distal dendrites and an abnormal accumulation, as well as aggregation of mitochondria in the soma and proximal regions of dendrites (Fig. Intro 20) (Girard et al., 2012). In these neurons, dendrite morphology was altered (observing a reduction in number and thinner diameter) with respect to controls (Fig. Intro 20).

Although hippocampal neurons seem not to be involved in ARSACS, hence not being the best model to study mitochondrial dynamics, a suggestion is that mitochondrial defective transport may be likely a consequence of deregulated fusion-fission balance (Chen and Chan, 2009).
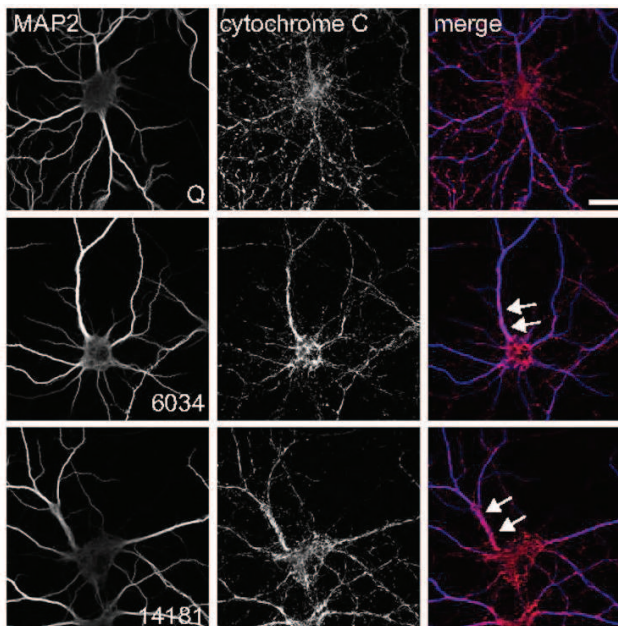
Fig. Intro 20. Improper distribution of mitochondria in *Sacs* siRNA hippocampal neurons. Cultured hippocampal neurons transfected with *Sacs* siRNAs (6034 and 14181) and scrambled siRNA (□). IF with antibodies directed against Cytocrome C (in red). Arrows indicate accumulated mitochondria in proximal dendrites (Girard *et al.*, 2012).

1.3.□ – Sacs □noc□out murine mo□el

Mitochondria are essential to sustain local biology of dendrites far away from the cellular soma and therefore altered mitochondrial distribution may contribute to neuronal cell degeneration, as well as the accumulation of damaged mitochondria within the cells (Chen and Chan, 2009).

Both bioinformatics and *in □itro* approaches illustrated so far have intrinsic limitations as they cannot assess or predict the function of a protein in the context of a complex living organism. Moreover, cellular models used *in □itro* were often more or less far away from the primary cell types involved in ARSACS. To study sacsin function in a physiological context, *Sacs* KO mice have been generated by gene targeting in ESCs cells and their characterization was assessed in two different works (Girard et al., 2012;

Larivière et al., 2015). Because they recapitulate main ARSACS symptoms, these murine lines were evaluated as good models of ARSACS. *Sacs* KO mice start to show gait disorder and tremors after seven months of age, and these signs progressively get worse. Tests conducted to investigate balancing, motor coordination and muscular strength revealed significant differences relative to WT. *Sacs* KO mice show early-onset and progressive deficit in balance, a feature in line with possible cerebellar involvement. Moreover, mice develop associated muscular wasting, which is also in line with ARSACS patients (Larivière et al., 2015). Purkinje cell loss in *Sacs* KO begins by day 90 of animal life, in the anterior medial cerebellum, similar to ARSACS (Fig. Intro 21) (Larivière et al., 2015). However, unlike patients, Purkinje cell loss in KO mice is not limited to vermis, but spreads to cerebellar hemispheres. Moreover, Purkinje cell axons show progressive swelling starting from day 30 of life, suggesting that there is an axonal degeneration that precedes the loss of the cell body (Fig. Intro 21). Although silver staining of corticospinal tract shows signs of neurodegeneration, histological examination does not reveal, differently from ARSACS patients, morphological alteration or reduction of axon number in mice up to 2 years of age. On the contrary, peripheral neuropathy is observed in *Sacs* KO mice as reduction (of about 25 in respect to control) of spinal motor neurons total number at 2 years of age and reduction of myelinated axons of diameter larger than 7-10 m with concomitant increase of number of myelinated axons of smaller dimension (3-4 m). Consequently, muscle wasting in lower limbs is also observed.

In conclusion *Sacs* KO mouse model recapitulates well the main signs of ARSACS, showing ataxia due to cerebellar degeneration, with loss of Purkinje cells, neuropathy and consequent muscle wasting, although spasticity seems to be less severe than in patients (Larivière et al., 2015). For this reason, it provides a suitable tool to further investigate ARSACS cytopathology and therapeutic treatments.
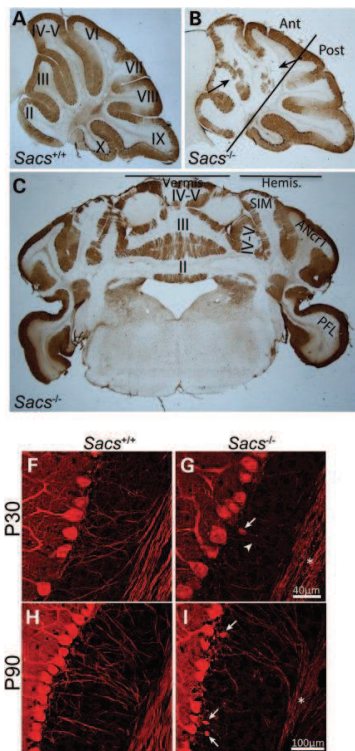
Fig. Intro 21. Progressive Purkinje cell loss and axonal swellings in *Sacs* KO mouse. (A–C) Anti-calbindin immunohistochemistry on mid-sagittal brain sections from 365-day-old *Sacs* WT (A) and *Sacs* KO (B) mice revealed Purkinje cell loss in the cerebellar anterior lobules. (F–I) Anti-calbindin labeling of cerebellar parasagittal brain sections of 30-day-old (P30) *Sacs* KO mice revealing dystrophic axons (asterisk and arrowhead in G) and occasional torpedo swellings in the proximal axonal segment (arrow in G) compared with *Sacs* WT mice (F). (I) Numerous axonal swellings (arrows) and beaded axons (asterisk) were present in *Sacs* KO samples at 90 days of age (P90) compared with age-matched controls (H) (Larivière *et al.*, 2015).

Neurofilaments (NF) are intermediate filaments expressed by neurons; they consist of three subunits that undergo cytoskeletal phosphorylation and dephosphorylation cycles: one heavy chain (NFH), one light chain (NFL) and one medium chain (NFM) (Lowery et al., 2015). Immunohistochemical examination of 14 day-*Sacs* KO mice compared to WT controls has revealed that they show accumulation of NFH, marked with pan-NFH antibody (that is against both phosphorylated and non-phosphorylated NFH subunit), in proximal dendrites in many areas of central nervous system, especially in thalamus, Purkinje cells in cerebellum, deep cerebellar nuclei, and superior olivary nucleus (Fig. intro 22) (Larivière et al., 2015). The deregulation in NF distribution has been found to be the first sign of cytopathological alteration, both in *Sacs* KO mice and in ARSACS patient neurons (Larivière et al., 2015). A similar accumulation of NFH in proximal dendrites has been observed in corticospinal neurons of layer 5 and in Purkinje cells from an ARSACS

patient (Fig. Intro 22, e-j). These cell types are the first seen to degenerate (see section 1.3.2) and have the highest expression of sacsin (see section 1.1.2). IF of Purkinje cell layer in tissue section derived from *Sacs* KO mice with antibodies specific for non-phosphorylated NFH (npNFH) (abbreviated SMI32) showed increased signal in soma and dendrites in respect to WT mice, whereas staining with antibodies specific for phosphorylated forms (pNFH) (abbreviated SMI31) failed to show significant differences (Fig. intro 23) (Larivi□re et al., 2015). Similar results, increased npNFH to total NFH ratio in *Sacs* KO mice relative to controls and unchanged levels of pNFH, have been confirmed also by WB, on cerebellar extracts, with pan-NFH, SMI31 and SMI32 (Larivi□re et al., 2015). In conclusion, sacsin loss leads to abnormal npNFH accumulation in dendrites in large areas of the brain. An open issue regards how sacsin is involved in NF cytoskeleton regulation.
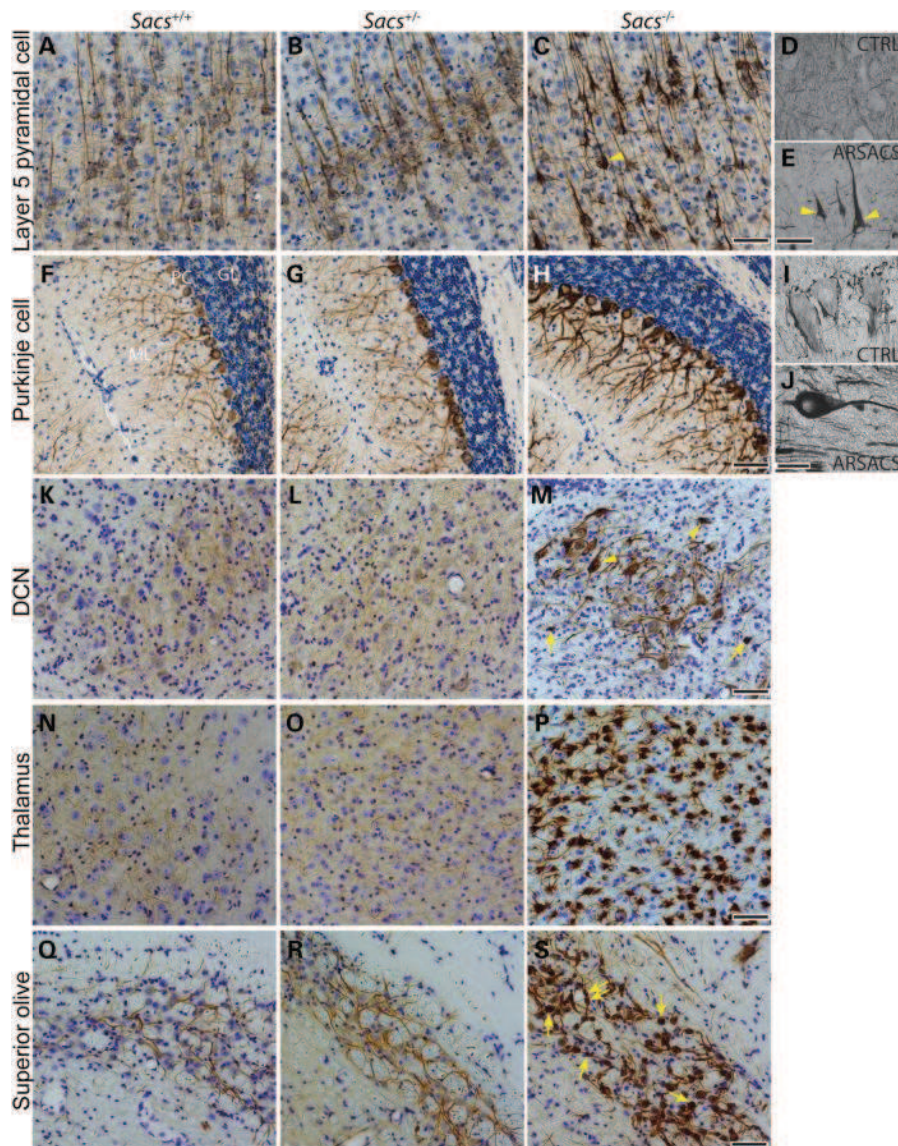
Fig. Intro 22. Accumulation of neurofilament heavy subunit (NFH) in immunohistochemistry on *Sacs* KO mouse and ARSACS brain. Immunohistochemistry of sagittal sections of brain from 180 days *Sacs* KO mice control (A, B, C, F, G, H, K, L, M, N, O, P, □, R, S) and from autopsy of ARSACS patient brain (E and J) and autopsy from controls (D and I), stained with panNFH. Accumulation of NFH is different in many neuronal population both in KO mice and patients relative to control (Larivi□re et al., 2015).
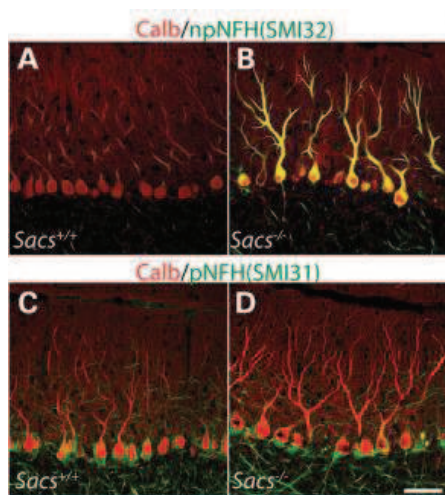
Fig. Intro 23. npNFH accumulation in Purkinje cell layer in *Sacs* KO mice. IF of Purkinje cells from *Sacs* KO mice and WT controls with antibodies directed against calbindin (in red) and against npNFH (in green) (calb/npNFH in A and B) and with antibodies against calbindin and pNFH (calb/pNFH in C and D). Intense npNFH staining is visible in B relative to the control in A, whereas no differences are seen with pNFH signal (Larivière *et al.*, 2015).

Aim of the project

Mutations in the *SACS* gene are causative of ARSACS, a complex neurodegenerative disorder characterized by early-onset cerebellar ataxia, pyramidal tract signs and peripheral neuropathy. Sacsin protein represents one of the biggest proteins of human genome with a size of 520 kDa. Due to its enormous dimension, functional studies on sacsin protein have been limited over time. In the end, the difficulties in managing such a large protein have hindered studies trying to examine the role of sacsin both at physiological and at pathological level. Therefore, ARSACS molecular pathogenetic cascade remains unclarified.

Most of the available information derives from sacsin single domain sub cloning experiments and bioinformatics prediction studies. These approaches have left huge knowledge holes; mainly on sacsin subcellular localization and on sacsin molecular function.

My PhD thesis work is focused on trying to address the gaps on sacsin knowledge: first, we sought to uncover the genotype-phenotype correlation in ARSACS, by investigating how different kinds of *SACS* mutations impact on sacsin levels, a topic that has never been taken into consideration. In this part of the work, we studied mutant sacsin protein stability, proposing a molecular hypothesis of the cause of sacsin absence in ARSACS. Second, we have aimed to examine the still undiscovered subcellular localization of sacsin. Third, we focused on unraveling the functional consequences of sacsin's absence in different sacsin-depleted cells/models we generated in our lab.

In the first chapter (Chapter 1) of my thesis we went in depth in the analysis of the reasons why sacsin mutations lead to ARSACS. As it emerges from literature, ARSACS causing-mutations are missense, nonsense, frameshift, small or gross deletions, found in both homozygous or compound heterozygous state and all of them lead to the loss of function of sacsin protein. However, a clear genotype-phenotype correlation does not exist in ARSACS because sacsin levels have not yet

been measured in association to different mutations. Moreover, ARSACS clinical severity seems to be not associated with the nature/position of the mutations on *SACS* gene (Baets et al., 2010; Synofzik et al., 2013). It is reasonable that in an autosomal recessive disorder caused by the loss of function of the protein of interest, such as ARSACS, the abolishment of sacsin could derive from either transcriptional degradation of mutant *SACS* mRNA or faster post-translational degradation of the mutant protein. Curiously, this is not the case for sacsin protein. Thus, a crucial element missing in the ARSACS genotype-phenotype correlation is the molecular cause of sacsin absence.

In the second part of my work (Chapter 2 and Chapter 3), we studied the functional consequences of sacsin's absence at cellular level. As we previously asserted, sacsin's function inside the cell remains unknown. What has been reported in literature mainly concerns studies observing the presence of mitochondrial hyperfusion in ARSACS fibroblasts and of cytoskeletal components accumulation in *Sacs* KO mouse.

To gain insight into the molecular mechanisms involved in ARSACS, we utilized ARSACS patient fibroblasts, CRISPR/Cas9 *SACS* KO HeLa cells, mouse embryonic fibroblasts (MEFs) and neuronal models from *Sacs* KO mouse. In particular:

- in Chapter 2 we explore the outcomes of sacsin absence at the mitochondrial level and the underlying molecular mechanisms;

- in Chapter 3 we unravel the relationship of sacsin with cytoskeletal components and organization, analyzing the consequences of sacsin absence at the level of cytoskeleton remodelling.

In the first part of the Chapter 2 we also describe the strategy and the generation of a new tool containing HA tagged endogenous sacsin (by CRISPR/Cas9 knockin (KI) technology in HeLa cells). We set up this technology to uncover the still mysterious sacsin subcellular localization. Our strategy assumes a certain relevance in the sacsin knowledge field since all antibodies generated until now do not work in IF. The purpose of this model is to provide a novel tool to study sacsin subcellular localization

at the ultrastructural level. We can employ Halo-tag or GFP-tag instead of HA and then apply Correlative and Light Microscopy (CLEM) approaches, thus combining and linking ultrastructural to functional information and also overcoming overexpression artefacts. The HA tag would also be suitable to perform and improve immunoprecipitation experiments in order to isolate sacsin interactors, shedding light on sacsin physiological function.

Materials and methods

Cell culture

Human primary skin fibroblasts and mouse derived embryonic fibroblasts (MEFs) were cultured in D-MEM medium supplemented with 20% FBS, 1 mM sodium pyruvate, 2 mM L-glutamine and 100 U/mL penicillin-streptomycin (GIBCO). HeLa cells were cultured in D-MEM medium supplemented with 5% FBS, 1 mM sodium pyruvate, 2 mM L-glutamine and 100 U/mL penicillin-streptomycin (GIBCO).

Cell lysis, SDS and Native PAGE and Western Blot analyses

Cells were lysed in 100 mM Tris-HCl pH 7.4, 150 mM NaCl, 1 mM EDTA pH 8 + protease inhibitor cocktail (SIGMA) and centrifuged at 8000g x 10 minutes. Supernatants were collected and quantified by Bradford procedure. Samples were boiled in sodium dodecyl sulfate (SDS) Sample buffer: 5,8 mM TrisHCl pH 6.8, 5% glycerol, 1,6% SDS, 0,1 M dithiothreitol (DTT), 0,002% bromophenol blue, and loaded in SDS-PAGE or Native-PAGE (standard polyacrylamide gel without SDS detergent and samples resuspension in non-reducing non-denaturing sample buffer). Standard Western Blot (WB) procedure was followed. Secondary antibodies used are conjugated with HRP and detected by Chemiluminescence HRP Substrate Reagent (Immobilion Western, Millipore). WB bands were analyzed by ImageJ software.

RNA extraction and Real Time PCR

Total mRNA from primary fibroblasts patients was extracted with Trizol Reagent as followed:

-cells were lysed in 1 mL Trizol for 10 cm2 of dish area;

-0.2 mL of chloroform were added per 1 mL of TRIZOL Reagent;

-cells were centrifuged at 12000g 15 minutes at 4°C;

-sovranatant was recovered (aqueous phase) and 0.5 mL of isopropyl alcohol was added (for 1 mL of Trizol Reagent);

-aqueous phases were incubated for 10 minutes;

-centrifuged at 12000g 10 minutes at 4□C;

-sovranatant was removed (the pellet was RNA);

-pellet was washed in 1 mL of 75□ ethanol;

-centrifuged at 7500g 5 minutes at 4□C;

-the dried pellet was resuspended in water.

RNA was retrotranscribed in cDNA using SuperScript III Reverse Transcriptase (ThermoFisher Scientific) with random hexamers. After setting up a standard curve for determining the optimal concentration of cDNA to use and the specificity of the primers, Real Time-PCR (qRT-PCR) was performed based on SYBR Green chemistry (Light Cycler 480, SYBR Green I master, Roche). qRT-PCR amplified a region of the *SACS* cDNA downstream all the ARSACS mutations of PN_1 and PN_2. This determined the *SACS* mRNA levels in patients and controls. To normalize *SACS* mRNA levels, we used TATA Binding Protein (□□□) mRNA levels.

SACS primers: left primer: 5' TTTTCAGTTGCGAGGGGTTG 3'; right primer: 5' TCCTGGCTTGGGAGGTAAAG 3'

TBP primers: left primer: 5' ACGCCGAATATAATCCCAAG 3'; right primer: 5' GCACACCATTTTCCCAGAAC 3'

Cell culture treatments

Primary fibroblasts were plated in 6 multiwell plates and after 24 hours treated with different compounds: 1 □M MG132 24 hours (SIGMA), 20 □M Chloroquine (C□) 24 hours (SIGMA) or together (0,25 □M MG132 + 10 □M C□, 18 hours); protease inhibitors (0,1 mM AEBSF, 50 □M Leupeptin, 0,1 mM Orto-phenantroline, 5 □M E64, 10 □M Bestatin, 5 □M Pepstatin, 48 hours (SIGMA)). After the mentioned hours of treatments, cells were harvested and lysed for biochemical assays.

Aggregate detection methods

1) Soluble and insoluble fractions

Cells were lysed by using Dounce homogenizer in 100 mM Tris-HCl pH 7.4, 150 mM NaCl, 1 mM EDTA pH 8 + protease inhibitor cocktail (SIGMA), centrifugated 1000g x 10 minutes. Post-nuclear supernatant (PNS) was collected, and pellets were resuspended in 500 µL lysis buffer and sonicated (20 seconds pulse-10 seconds stop; repeated twice). PNS and pellet were quantified and equal amount were loaded on SDS-PAGE.

2) Total homogenates in agarose-acrylamide gel

Whole cellular pellets were lysed in SDS Sample Buffer 2X and sonicated to break the DNA as described in 1).

Stacking gel was prepared at 2% acrylamide concentration. Resolving gel at 2,7%. To the standard ingredients of an acrylamide gel was added a 0,5% agarose solution both in the resolving and in the stacking gel.

Radioactive pulse of newly synthesized sacsin protein

We radioactively pulse-labelled human primary fibroblasts for two time points (4 and 8 hours), by culturing them in 35S-L-methionine, 35S-L-cysteine medium (EasyTag™ EXPRESS35S Protein Labeling Mix, [35S], PerkinElmer). We harvested and lysed cells in RIPA buffer (150 mM sodium chloride, 1.0% NP-40, 0.5% sodium deoxycholate, 0.1% SDS, 50 mM TrisHCl pH 8.0) for 30 minutes on ice, centrifuged at 13000g x 10 minutes and collected supernatants.

We immunoprecipitated sacsin by incubating cell lysates 18 hours with anti-sacsin antibody conjugated-magnetic Dynabeads (#10002D Dynabeads Protein A, ThermoFisher Scientific) (as described for sacsin immunoprecipitation in mouse cerebellum) and eluted the immunoprecipitated fraction in SDS Sample Buffer to then perform SDS-PAGE electrophoresis. Gel was transferred onto a 3 MM filter paper and dried by vacuum (Gel Dryer). Then the gel was exposed to a GE storage phosphor screen (GE Healthcare). Signals were acquired on Typhoon FLA-9000 with a phosphorimaging filter.

Su☐cellular fractionation

We followed the abcam protocol for subcellular fractionation: https://www.abcam.com/protocols/subcellular-fractionation-protocol.

In brief:

1.Cells were transferred from 10 cm2 plates into 500 ☐L fractionation buffer (20 mM Hepes pH 7.4; 10 mM KCl; 2 mM MgCl2, 1 mM EDTA, 1 mM EGTA), by scraping and incubated 15 minutes on ice.

2.Using 1 mL syringe cells were passed through a 27 gauge needle 10 times.

3.Lysed cells were incubated on ice for 20 minutes. Then, centrifuged at 720g x 5 minutes.

5.The pellet is containing nuclei and the supernatant is containing cytoplasm, membrane and mitochondria. Supernatant was transferred into a fresh tube and kept on ice. This was dealt with in Steps 8–11.

6.Nuclear pellet from Step 4 was washed with 500 ☐L fractionation buffer and dispersed with a pipette. Then it was passed through a 25 gauge needle 10 times. After centrifugation at 720g 10 minutes, supernatant was discarded, keeping the pellet that contained nuclei.

7.Pellet was resuspended from Step 6 in TBS with 0.1☐ SDS and sonicated to shear genomic DNA and homogenize the lysate.

8.The supernatant recovered in Step 5 was centrifuged 10000g 5 minute and then collected: this was the cytoplasm and the membrane fraction.

9.The mitochondrial pellet from Step 8 was processed as described for the nuclear pellet in Step 7, to obtain mitochondrial lysate in TBS/0.1☐ SDS.

10.For the membrane fraction, supernatant from Step 8 was centrifuged in ultracentrifuge at 100000g 1 hour. Pellet was washed by adding 400 ☐L of fractionation buffer and resuspended by pipetting and pass through a 25 gauge needle. Then it was re-centrifuged 45 minutes. The membrane pellet was resuspended in the same buffer as used for the nuclei.

Mitochondrial fractionation

1. Differential centrifugation method

Mitochondria were isolated by differential centrifugation from fibroblasts (Robinson, 1996). In brief, tissues were homogenized in an appropriate isotonic buffer (0.25 M sucrose, 20 mM 3-(N-morpholino) propanesulfonic acid (MOPS), pH 7.2, 1 mM EDTA, 0.1% Bovine Serum Albumin (BSA) fatty acid free) using a glass-glass homogenizer. Cell debris and nuclei were pelleted by centrifugation at 2500g x 5 minutes at 4°C. Supernatants were centrifuged at 12000g x 25 minutes at 4°C, and the mitochondrial pellet was resuspended in an isotonic buffer (0.5 M sucrose, 20 mM MOPS, pH 7.2, 1 mM EDTA).

2. Mitochondrial purification with anti-TOM22 magnetic beads

Mitochondria Isolation Kit, human was used (#130-094-532, MACS Miltenyi Biotec) following instructions. Briefly, after cell lysis, mitochondria were magnetically labelled with Anti-TOM22 MicroBeads, which bind to the translocase of the outer mitochondrial membrane 22 protein (TOM22). The sample was loaded onto an LS Column placed in a magnetic (QuadroMACS) separator. After washing, only magnetically labelled mitochondria were retained on the column. The column was removed from the separator and functional human mitochondria were eluted from the column in appropriate buffer (Franko et al., 2013).

Generation of SACS knockin HeLa cells by CRISPR/Cas9 mediated genome editing

Plasmid for expression of *SACS* sgRNA and Cas9 was provided by Sigma Aldrich (SIGMA CRISPR Plasmid, target gene *SACS*, lot number 11211602MN). *SACS* sgRNA sequence 5' GAGGTTGCTATGAGGGTGA 3' was designed by Sigma Aldrich and cloned under U6 promoter; spCas9-RFP proteins are under CMV promoter control and are separated by a T2A peptide so that they are translated as different proteins. Primers for molecular screening were also designed and provided by Sigma. *SACS*_FW primer sequence was 5' CCAACTGCACTTGCTCAG 3';

*SACS*_REV primer sequence was 5' CGTTGGTATTCATGTTCATAAC 3'. The predicted cutting site of *SACS* sgRNA is 59bp upstream the insertion site, i.e. the *SACS* natural STOP codon.

For homology directed repair (HDR) template, we designed single-stranded oligodeoxynucleotides (ssODNs) with 40bp homology arms identical to *SACS* sequence upstream the Cas9 cutting site and downstream *SACS* natural STOP codon. Since there is a distance of 59 bp between the Cas9 cutting site and the natural STOP codon, the endogenous *SACS* region of 59bp was inserted between the homology arms followed by the sequence encoding the Linker-HA-PsiI-STOP construct. The endogenous *SACS* region of 59 bp in HDR template was recoded to avoid HDR in this region (Paquet et al., 2016). A mutation proximal to 42 spCas9 PAM in HDR template was also included in order to avoid cutting by the Cas9 itself. The amino acidic linker sequence was GSGGG and was designed by studying literature (Chen et al., 2013; Klein et al., 2014). PsiI restriction site was inserted together with HA tag to perform restriction fragment length polymorphisms (RFLP) assay, after having checked this restriction site was not present in the WT in the region between *SACS*_FW and *SACS*_REV primers (referred to genome reference hg38).

The ssODNs were ordered as synthetic DNA oligo from Metabion international AG. FW_HA oligo sequence was:
5'G☐C☐T☐TCCCTTTCCTCAGATCCCAAATGACAGGTTCACTTCTGAGGT TGCTATGAGGGTAATGGAGTGCACCGCTTGCATTATTATTAAGCTCG AGAACCTCATGCAGCAGAAGGTAGGATCCGGCGGAGGATACCCATA CGATGTTCCAGATTACGCTTTATAAAGATATTTAACGAAAAAAAAGGT AG ATCTTGAATGTG☐T☐T☐G 3'

REV_HA oligo sequence was:
5'C☐A☐A☐CACATTCAAGATCTACCTTTTTTTTCGTTAAATATCTTTATAA AGCGTAATCTGGAACATCGTATGGGTATCCTCCGCCGGATCCTACCT TCTGCTGCATGAGGTTCTCGAGCTTAATAATAATGCAAGCGGTGCAC TCCATTACCCTCATAGCAACCTCAGAAGTGAACCTGTCATTTGGGATC

TGAGGAAAGGGA□A□G□C 3'. Asterisks indicate phosphorothioate internucleotide linkages which were included to provide higher stability of HDR template in order to increase HDR efficiency (Renaud et al., 2016). Oligos were inserted in cells both as ssODNs and as annealed dsDNA molecules. Annealing was performed as described above.

HeLa cells were nucleofected with CRISPR plasmid and FW or REV or annealed HA-oligo. Cells nucleofected with CRISPR plasmid only were used for CEL-I endonuclease assay. Transfections were performed with 4D-Nucleofector system (Lonza), following manufacturer's instructions for HeLa cells. Final concentration of oligo was 10 □M; CRISPR plasmid amount was 2 □g. After being nucleofected, cells were recovered for 24 hour incubation and then harvested and resuspended in their medium at a concentration of □20□106 cells/mL.

RFP positive cells were sorted through FACS at San Raffaele Institute Flow cytometry facility. Sorting was performed with BD FACS Aria Fusion instrument and BD FACS DivaTM 8.0 software. For each nucleofected sample, cells with RFP signal 102 times higher than in negative control were collected and recovered for 24 hours. Then cells were trypsinized and monoclonal cell lines were derived for each nucleofection condition, by serial dilutions as described above. Genomic DNA was also extracted from nucleofected cell populations to perform molecular analyses.

CE□□assa□

PCR using *SACS*_FW and *SACS*_REV primers was made from genomic DNA extracted from cells nucleofected only with SIGMA CRISPR plasmid and from untreated cells. CEL-I assay was then made to detect the level of mutagenesis induced by Cas9 at genomic target locus. CEL-I was from IDT- Integrated DNA Technologies (Surveyor□ mutation detection kit), and protocol was carried on according to manufacturer. Briefly, PCR products from nucleofected and untreated samples were mixed at 1:1 ratio and hybridized by a temperature gradient; then 1 □L of Surveyor nuclease S was added and the mix was incubated at 42□C for 1 hour. Finally, 2 □L were loaded on high sensitivity D1000 ScreenTape electrophoresis

system (Agilent); quantification was made with TapeStation software. Expected CEL-I cleavages bands were 221bp and 175bp; WT expected band was 396bp.

PsiI assay

Genomic DNA from cells co-nucleofected with the CRISPR plasmid and HA oligo and from untreated cells was PCR amplified with *SACS*_FW and *SACS*_REV primers. PCR products were purified with PCR purification kit (QIAGEN), diluted in CutSmart 10X buffer (New England Biolabs inc.) and digested with 0,05 U/μL of PsiI enzyme (New England Biolabs inc.). Digestion was carried out for 5 hours at 37°C and then inactivated at 65°C for 5 minutes. Finally, 2 μL of each sample were loaded on high sensitivity D1000 ScreenTape electrophoresis system (Agilent); quantification was made with TapeStation software. Expected PsiI cleavages bands were 279bp and 162bp; WT expected band was 396bp.

Intracellular staining and flow cytometry for detection of HA integration in HeLa cells

HeLa cells were harvested by trypsin and washed two times in PBS by centrifuging 10 minutes at 800g. Intracellular staining was then performed in V bottom 96 multiwell plates. Cells were resuspended and fixed with 2% paraformaldehyde for 30 minutes on ice and washed three times in cold PBS. Then cells were blocked and permeabilized by incubation with PBS, 5% BSA, 0,1% Triton-X100 for 30 minutes at room temperature in agitation. After washing with PBS, 1% BSA cells were incubated with anti-HA Alexa-fluor 488 antibody buffered in PBS, 1% BSA, 0,05% Triton-X100 for 2 hours at room temperature in agitation. Finally, cells were washed in cold PBS, 1% BSA and resuspended in cold PBS. Cells were then analyzed with CytoFLEX S cytometer (Beckman Coulter) and Cytexpert software. Monoclonal cell lines that showed an increase in fluorescence signal relative to WT were then screened by WB. Analyses of fluorescence were made with FCS Express software.

Analysis of mitochondrial morphology

20000 human primary skin fibroblasts were plated on a bottom-glass culture dish (Matteck) and 24 hours later infected with lentivirus expressing mito-DsRed2 (1:200 from 4,67☐108 U/ml). After 48 hours, cells were splitted and 24 hours later (72 hours after the infection) mitochondrial network morphology was evaluated in live imaging with using an Axio Observer.☐1 inverted microscope (☐eiss). At least 100 cells per each cell line on average were evaluated in a single experiment. Three categories (fused/intermediate/fragmented) were created based on the mitochondrial length to describe the network morphology between the genotypes.

Immunofluorescence analysis

Human primary fibroblasts or MEFs were plated at a density of 20000 cells/13mm glass slide area (while HeLa cells 35000/13mm) and after 24 hours were washed in PBS. In experiments with Mitotracker staining, cells were incubated with MitoTracker☐ Red CM-H2XRos M7513 (ThermoFisher Scientific), which is a mitochondrial membrane potential sensitive dye that labels living mitochondria, for 10 minutes in cell incubator and then washed with PBS. Cells were fixed with 4☐ paraformaldehyde/PBS, then permeabilized and blocked in 10☐ normal goat serum (NGS), 0.5☐ Triton X-100 in PBS for 1 hour and incubated overnight at 4☐C with primary antibodies in 5☐ NGS, 0.1☐ Triton X-100 in PBS. Cells were incubated with species specific Alexa Fluor Secondary Antibodies (ThermoFisher Scientific) in the dark for 1 hour; rewashed and stained with DAPI for nuclei, lastly mounted with FluorSave Reagent (Calbiochem International) on microscope slides for immunofluorescence acquisition. At least 100 cells per line on average were evaluated in a single experiment.

Immunoprecipitation in endogenous condition

1‐Sacsin immunoprecipitation in hela cells

Cells were collected and freshly lysed in detergent-free soluble protein lysis buffer (5 mM EDTA pH 8.0 in PBS + fresh PIC) with a Dounce homogenizer. Total homogenate was centrifuged 8000g for 20 minutes at 4℃ to discard cell debris and supernatant was collected. 1mg of total protein of lysate was incubated overnight at 4℃ with 4 µg of immunoprecipitating antibody (Ab1). After the immunoprecipitation of the antigen (Ag) in the lysate, this was incubated with protein G-Sepharose beads (ThermoFisher Scientific) at 4℃ under rotary agitation for 4 hours to bind the Ab-Ag complex and after 4 washes in lysis buffer, the Ag-Ab complex was eluted from the beads boiling sample SDS Sample Buffer for 5 minutes and loaded on a SDS-PAGE for WB analysis.

2‐Sacsin immunoprecipitation in mouse cerebellum

The first steps of the immunoprecipitation procedure were the same as for Hela cells. 1 mg of total protein of lysate was incubated 2 hours with magnetic Dynabeads Protein A (ThermoFisher Scientific) to depauperate the lysate for the aspecific interactions/Ags with the beads; new Dynabeads Protein A were linked to the same Ab for 30 minutes at room temperature and then Dynabeads-Ab complex was incubated with the precleared lysate over night at 4℃ on a wheel. After 4 washes in lysis buffer, Ag was eluted from the Dynabeads-Ab in 0.2 M glycine pH 2.6 on rotation for 3 minutes and the pH adjusted adding 20µ 1 M Tris HCl pH 7.4. Immunoprecipitating eluates were sent to Mass Spectrometry facility for LC-MS/MS and loaded in SDS Sample Buffer on SDS-PAGE for WB analysis.

Proteasomal activity assay

20S chymotrypsin-like proteasome activity was measured using 20S Proteasome Activity Assay Kit (# APT280, Chemicon International) according to the manufacturer recommendations. Freshly collected mouse cortex and cerebellum were homogenized by Dounce homogenizer in ice-

cold buffer (25 mM HEPES, pH 7.5, 0.5 mM EDTA, 0.05□ NP-40 and 0.01□ SDS). Homogenates were centrifuged at 13000g x 10 minutes at 4□C, supernatants were collected, and protein concentration was determined with Bradford. Assays were conducted using equal amounts of proteins from tissue lysates (80 □g). Levels of 7-amino-4- methylcoumarin (AMC) after cleavage from succinyl-LLVY- AMC were determined by the measurement of fluorescence intensity using a microplate reader (Victor3 Plate Reader, PerkinElmer). The resulting fluorescence, reflecting activity of 20S proteasome activity, was presented as relative fluorescence units (RFU). Tissues from three different mice for each genotype was evaluated, each in technical triplicate.

Aggresome □etection metho□

20000 fibroblasts were plated in 24 multiwell plates on slides and after 24 hours treated with 1 □M MG132 for 18 hours (positive control) or vehicle (DMSO). Then, cells were processed by using ProteoStat□ Aggresome Detection Kit, following manufacturer recommendations (#EN□-51035-K100, EN□O Life Science). 63X objective was used to acquire images. At least 100 cells per line were evaluated in a single experiment.

Electron microscopy analysis

These experiments were done in collaboration with the unit of Neuropathology of San Raffaele Institute. Human primary fibroblasts were harvested by trypsin, washed with PBS and centrifuged at 1000g x 10 minutes 3 times and then put in glutaraldehyde fixative to perform standard electron microscopy (EM) experiments. At least 30 cells per line were evaluated in a single experiment.

□icroscope ac□uisition an□ live imaging analysis

We used Microscope Axio Imager A2 □eiss (Upright Fluorescence Microscope) and Confocal PerkinElmer UltraVIEW ERS to acquire immunofluorescence images. Images were taken with 40X dry or 63X oil

immersion lens using Upright Fluorescence Microscope, or with 63X oil immersion lens using Confocal PerkinElmer UltraVIEW ERS. For live imaging experiments, we used the Axio Observer.□1 inverted microscope (□eiss). For EM experiments, TEM Vision- Leo912ab was used.

Statistical analyses

For statistical evaluation of *SACS* mRNA levels in patients and controls we performed unpaired t-test, 2 tails. For mitochondrial morphology evaluation □-square analysis, 2 degrees of freedom was performed. For statistical evaluation of vimentin cage-presenting cells; sacsin - npNFH - LC3II - WB band intensities and volume of dendritic mitochondria in primary Purkinje cells, t-test 2 type and 2 tails was performed.

□rimary anti□o□ies use□

Antibody target	WB dilution	IF dilution	Brand
Anti-sacsin Ab1 ab181190	1:2500	-	Abcam
Anti-sacsin Ab2 sc-515118 F-1	1:250	-	Santa Cruz
Anti-sacsin Ab2 sc-515118 G-3	1:250	-	Santa Cruz
Anti-spectrin MAB1622	1:20 000	-	Chemicon/Millipore
Anti-p53	1:3000	-	Santa Cruz
Anti-ubiquitin ab134953	1:2500	-	Abcam
Anti-p62/S□STM1 P0067	1:1000	-	SIGMA
Anti-HA Alexa-fluor 488 #901509	FACS 1:10000	-	Biolegend

Anti-calnexin C4731	1:20000	-	SIGMA
Anti-lamin B sc-6216	1:1000	-	Santa Cruz
Anti-GAPDH sc-32233	1:20000	-	Santa Cruz
Anti-TIM44 ab194829	1:4000	-	Abcam
Anti-Na/K ATPase 05-369	1:10000	-	Millipore
Anti-p70 S6 Kinase	1:1000	-	Cell signaling
Anti-AFG3L2	1:6000	-	Home-made
Anti-conjugated actin	1:2000000	-	Developmental Studies Hybridoma Bank (DSHB)
Anti-HA 16812	1:500	-	Covance
Anti-MFN1 ab57602	1:4000	-	Abcam
Anti-MFN2 ab56889	1:4000	-	Abcam
Anti-Hsp60 ADI-SPA-806	1:7000	-	EN☐O Life Science
Anti-OPA1 612607	1:2500	-	BD Bioscience
Anti-DRP1 Clone-8	1:4000	-	BD Bioscience
Anti-DRP1 ab184247	1:1000	-	Abcam
Anti-☐ tubulin	1:4000	-	Home-made

Anti-calbindin CB38	-	1:250	Swant
Anti-COXIV 459600	-	1:200	ThermoFisher Scientific
DAPI D1306	-	1:20 000 (1:7000 on Purkinje cells)	ThermoFisher Scientific
Anti-vimentin ab92547	1:10000	1:1000	Abcam
Anti-npNFH NE1023	1:1000	-	Calbiochem
Anti-NFL sc-20012	1:1000	-	Santa Cruz
Anti-LC3 A/B ab58610	1:3000	-	Abcam

Results

Chapter □

□□Analy□ing the genotype□phenotype correlation of sacsin mutations in ARSACS □isease□

□□□ARSACS patient fi□ro□lasts sho□ a □ramatic re□uction of sacsin levels□

The identified ARSACS causing mutations are missense, nonsense, frameshift, small or gross deletions found in either homozygous or compound heterozygous state (http://www.hgmd.cf.ac.uk/). Until now, a clear genotype-phenotype correlation does not exist in ARSACS, as patient disease severity does not seem to be associated with the nature/position of the mutation on *SACS* gene (Baets et al., 2010; Synofzik et al., 2013). Additionally, there is insufficient information regarding the consequences of the various mutations at the protein level.

In order to address this issue, we used primary skin fibroblasts from two compound heterozygous ARSACS patients (patient 1-PN_1, patient 2-PN_2) to study the residual amount of sacsin protein. PN_1 and PN_2 present a very severe phenotype (PN_26.1 and PN_53.1 described by Baets et al. (Baets et al., 2010)). They carry the following mutations: both have two identical missenses on one allele (p.R3636□; p.P3652T) and a different frameshift mutation on the other allele (PN_1: p.L3745fs; PN_2: p.C72fs) (Fig. Results 1 A-B). For sacsin detection in WB, we set up two different commercially available antibodies (Ab1-Ab2), which detect different portions of sacsin protein. Independently from the nature of the sacsin mutation, we found that the amount of sacsin protein is dramatically reduced in ARSACS patients using both Ab1 and Ab2 (Fig. Results 1 C). In collaboration with other groups, we obtained data from a panel of ARSACS patient fibroblasts carrying different mutations. In agreement, other ARSACS cells (Fig. Results 1 D) showed drastic reduction or totally absence of sacsin protein (Fig. Results 1 E and Duncan EJ et al. 2017 (see Publications)).

Interestingly, these results suggest a loss of function mechanism for ARSACS, as sacsin protein is almost absent in patients.
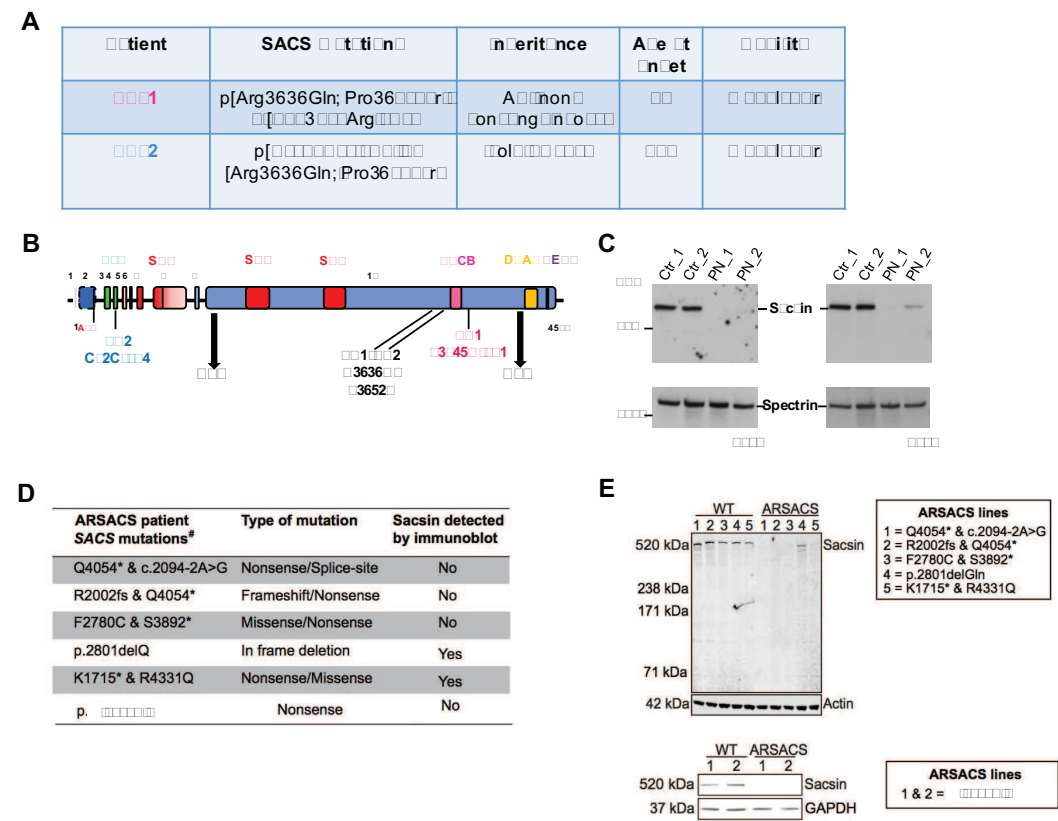
A

□□tient	SACS □□t□ti□n□	in□erit□nce	A□e □t □n□et	□□□i□it□
□□□1	p[Arg3636Gln; Pro36□□□□r□ □[□□□3□□□Arg□□□□	A□□non□ □on□□ng□n□o□□□	□□□□	□ □□□□□□□□n
□□□2	p[□□□□□□□□□□□□□□□ [Arg3636Gln;□Pro36□□□□r□	□ol□□□□ □□□□	□□□	□ □□□□□□□□n

B

C

D

ARSACS patient SACS mutations#	Type of mutation	Sacsin detected by immunoblot
Q4054* & c.2094-2A>G	Nonsense/Splice-site	No
R2002fs & Q4054*	Frameshift/Nonsense	No
F2780C & S3892*	Missense/Nonsense	No
p.2801delQ	In frame deletion	Yes
K1715* & R4331Q	Nonsense/Missense	Yes
p. □□□□□□	Nonsense	No

E

ARSACS lines
1 = Q4054* & c.2094-2A>G
2 = R2002fs & Q4054*
3 = F2780C & S3892*
4 = p.2801delGln
5 = K1715* & R4331Q

ARSACS lines
1 & 2 = □□□□□□

Fig. Results 1. ARSACS PN_1 and PN_2 used in this work present drastic reduced sacsin levels, as confirmed in different ARSACS patient mutations. (A) ARSACS patient mutations and some clinical features. (B) Mutation-localization on *SACS* gene and epitopes recognized by the two antibodies we used. (C) WB analyses showing sacsin levels in patients and controls, normalized on spectrin, with Ab1 (left) and Ab2 (right). (D) Panel of other ARSACS mutations and (E) sacsin protein levels by WB. (C-D-E) Figures published in Duncan et al., 2017.

□□ □utant sacsin mRNA is sta□le an□ the protein is not rescue□ □y inhi□iting □egra□ative systems□

Due to the nature of ARSACS patient mutations we analyzed (Fig. Results 1 A), we did not expect such a strong reduction of sacsin levels. Indeed, we had presumed missense mutations led to a full-length (even if mutant) sacsin protein, while frameshift mutations should encode for a truncating protein. Therefore, at least for the missense mutations on one *SACS*

allele, we expected half of the amount of sacsin protein in both PN_1 and PN_2 compared to the wild type (WT). Being this expectation in contrast with our results showing high sacsin reduction in patient cells (Fig. Results 1 A), we evaluated a possible transcriptional instability and degradation of the mutant mRNA. Said degradation may be a consequence of the frameshift mutations as expected from nonsense-mediated mRNA decay (NMD) (Nasif et al., 2017). However, after performing a qRT-PCR in ARSACS patient fibroblasts using a couple of primers annealing downstream *SACS* PN_1 and PN_2 mutations, we found no difference in the amount of *SACS* mRNA in patients and controls, excluding NMD of the mutant mRNA (Fig. Results 2 A). We then decided to explore a second alternative hypothesis, i.e. if mutant sacsin could be post-translationally unstable and have a faster turnover compared to the WT.

Indeed, unfolded or aberrant proteins are usually targeted by proteolytic systems, such as ubiquitin proteasome system and autophagy, the main molecular pathways involved in cellular protein quality control. Efficient proteasomal or autophagic degradation oversee cellular proteostasis (Morimoto and Cuervo, 2014). Therefore, we blocked cellular degradative systems to rescue mutant sacsin levels in ARSACS fibroblasts in order to understand which is the degradative mechanism activated. The inhibition of ubiquitin-proteasome system by MG132 (1 uM, 24 hours) was unable to recover sacsin amount in patients (Fig. Results 2 B-C). Surprisingly, by blocking the proteasomal pathway, a reduction of WT sacsin levels was seen in controls (Fig. Results 2 C). This data suggests that autophagy could be boosted in response to proteasomal inhibition. Prolonging the time of MG132 treatment in control cells, we found a further reduction in the amount of sacsin protein (Fig. Results 2 D). To strengthen this result, we evaluated if sacsin was ubiquitinated. We immunoprecipitated endogenous sacsin in HeLa cells and performed immunodecoration with anti-ubiquitin antibody, which revealed that sacsin does not undergo ubiquitination (Fig. Results 2 E). Additionally, an autophagy block by using C☐ (20 uM, 24 hours, an autophagosome-lysosome fusion blocker) does

not rescue sacsin levels (Fig. Results 2 F-G). Prolonged time treatment with C☐ demonstrated sacsin is almost stable (Fig. Results 2 H). Combined treatment (autophagy plus proteasome block – 0,25 ☐M MG132 +10 ☐M C☐, 18 hours –) (Fig. Results 3 A) does not neither rescue sacsin levels in patients nor increase the protein in controls.

At this point we analyzed if sacsin could be degraded by specific proteases and we tested this hypothesis by inhibiting all proteases one by one. We used AEBSF for serine proteases, bestatin for amino peptidases, E64 for cysteine proteases, leupeptin for serine and cysteine proteases, orto-phenantroline for metallopeptidases, pepstatin for aspartyl proteases. Yet, even after blocking individual proteases, the amount of mutant sacsin remained low (Fig. Results 3 B). These results indicate that the drastic reduction of mutant sacsin in ARSACS patients is not caused by a faster post-translational degradation of the protein.

☐☐ ☐utant sacsin ☐oes not aggregate in ARSACS patient fi☐ro☐lasts☐
We took in consideration that mutant sacsin could be completely translated, but undetectable by standard WB procedures due to its misfolding and/or aggregation. To address this hypothesis, we performed different experiments to solve aggregates in biochemical assays. First, we checked for the putative mutant sacsin aggregates by loading in SDS-PAGE both the soluble and the insoluble fractions of control and patient fibroblasts (PN_1, PN_2) trying to detect mutant sacsin in the insoluble fraction (Fig. Results 4 A). We were unable to detect sacsin aggregates in patients. To avoid a lack of material during the fractionation procedure, we checked also total homogenates directly from patients (PN_1, PN_2) and controls. We loaded total homogenates in 2.7☐ acrylamide-agarose mixed-gels, which have much larger pores than pure acrylamide gels, allowing the passage and an acceptable resolution of large complexes (Weiss et al., 2008) (Fig. Results 4 B). Again, we did not rescue any mutant sacsin level in this experiment.
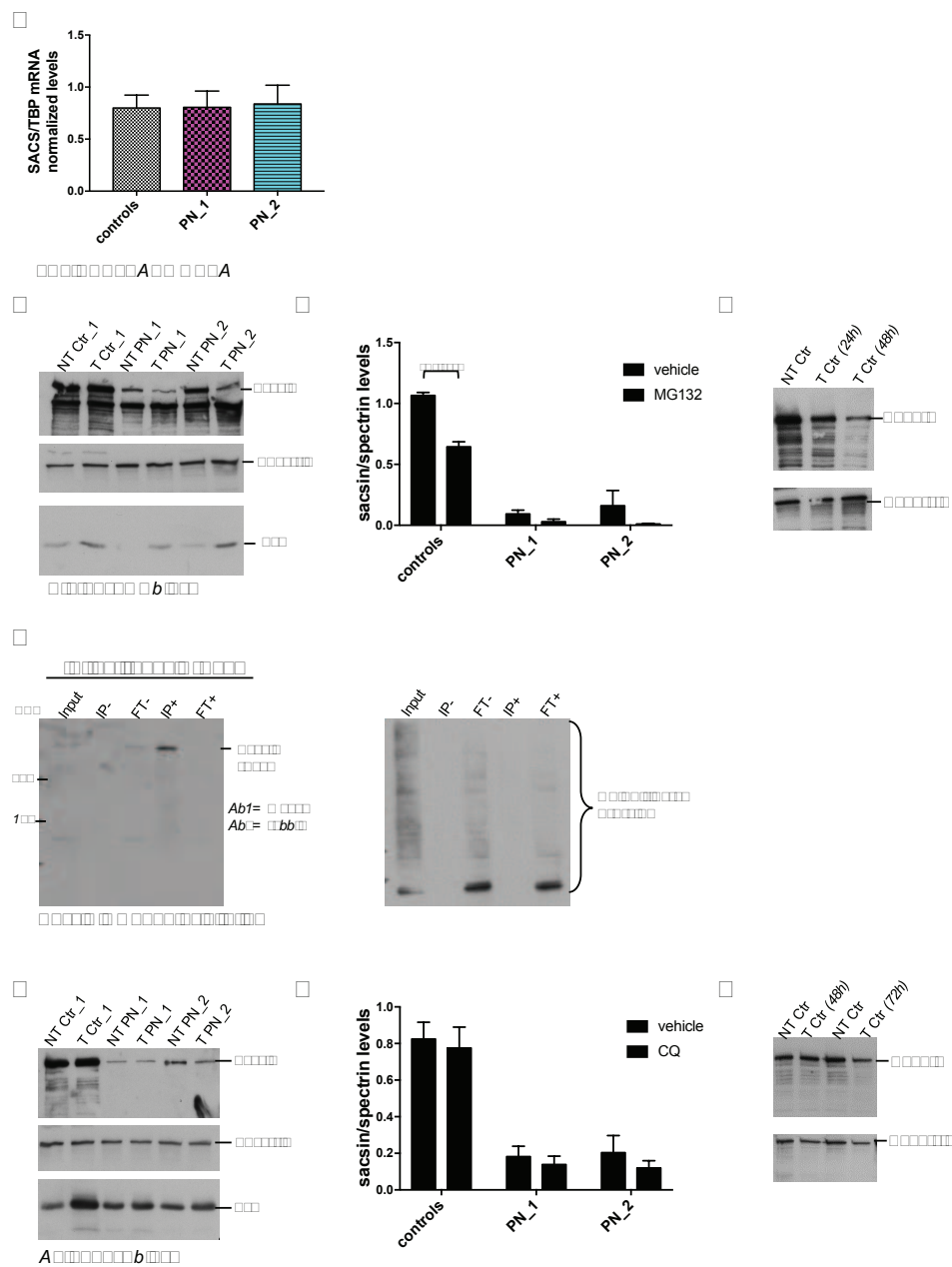
Fig. Results 2. *SACS* mRNA is stable and sacsin protein is not degraded by proteasome or autophagy. (A) qRT-PCR performed on ARSACS patient fibroblasts and controls (n☐3). (B) Representative WB of proteasome block experiments, by using MG132, and (C) quantification, showing no rescue of sacsin levels in patients and a reduction in controls (n☐5, mean☐SEM). (D) WB of longer time points of MG132 treatment on control cells. (E) Immunoprecipitation of endogenous sacsin in HeLa cells confirming that sacsin is not ubiquitinated as the proteasomal substrates. (F) Representative WB of autophagy block experiments, by using C☐, and (G) quantification, showing no rescue of sacsin levels in patients and controls (n☐5, mean☐SEM). (H) WB of longer time points of C☐ treatment on control cells.

68

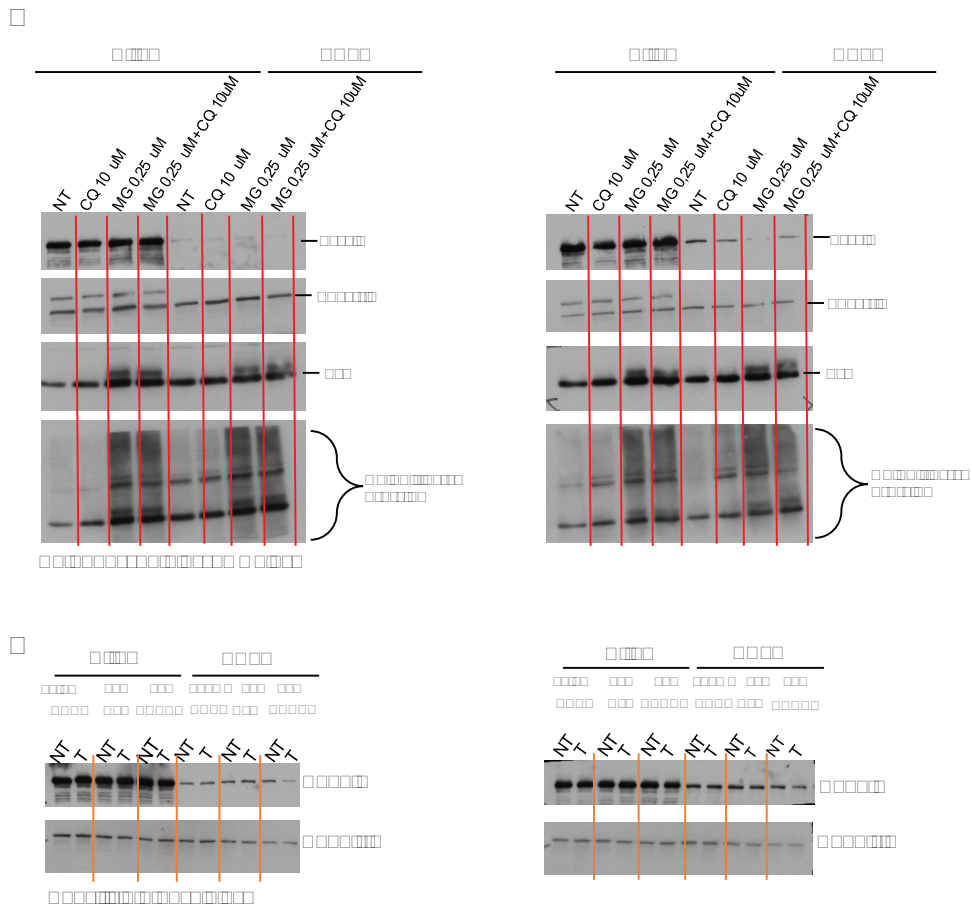Fig Results 3. Mutant sacsin protein is not rescued upon combined proteasome and autophagy block or upon single protease inhibition. (A) Representative WB of combined inhibition of proteasome plus autophagy. (B) Representative WB experiments of inhibition of some proteases on patients and controls.
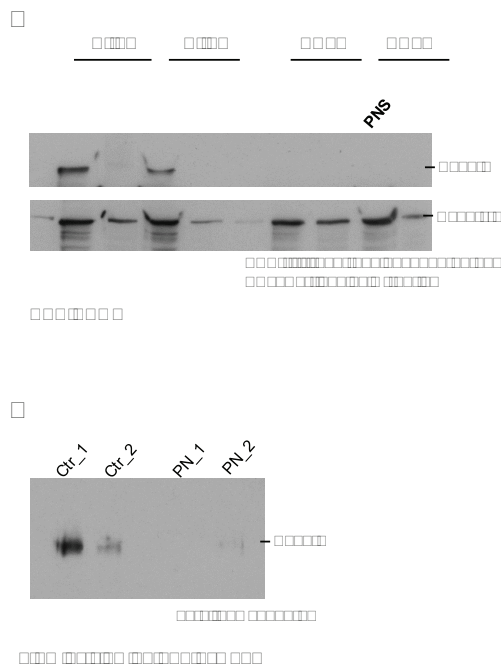
Fig. Results 4. Mutant sacsin protein does not form aggregates. (A) SDS-PAGE, followed by WB of sacsin, of patients and controls soluble and insoluble fractions.
(B) Acrylamide-agarose gel, followed by WB of sacsin, of patient and control total homogenates.

Ongoing work investigating the hypothesis of a co-translational quality control of mutant sacsin

Altogether, our results excluded any mechanism acting on transcriptional control of mutant *SACS* mRNA (mRNA degradation) or on post-translational control of mutant sacsin protein (faster degradation of unstable protein). Our current working hypothesis concerns a quality control at the co-translational level of sacsin protein.

There is emerging evidence that, in addition to the canonical post-translational protein quality control (QC) pathways (e.g. proteasomal degradation and autophagy), cells have evolved a co-translational QC pathway to degrade aberrant proteins. Nascent chains are tagged for destruction before they leave the ribosome, thus avoiding translation and folding of aberrant protein products (Pechmann *et al.*, 2013; Lykke-Andersen and Bennett, 2014). This mechanism is plausible in case of

mutation of big and multi-domain proteins (Pechmann et al., 2013), whose translation and folding is extremely time and energy consuming for the cell. Therefore, it is plausible for sacsin. Mechanistically, co-translational □C senses the folding or maturation state of nascent chains while they are being translated. One part of co-translational □C mechanism has been deeply characterized, being coupled to the mRNA degradation mechanism. Nascent polypeptides encoded by aberrant mRNAs undergo co-translational ubiquitination operated by a specific E3 ubiquitin ligase (Listerin). They are then extracted by the valosin-containing protein (VCP) complex and targeted by the proteasome for rapid degradation (Lykke-Andersen and Bennett, 2014). The specificity of Listerin for nascent chains is guaranteed by nuclear export mediator factor (NEMF), which binds Listerin and stabilizes its association to ribosomes (Pechmann et al., 2013; Inada, 2017) (Fig. Results 5 A). A different co-translational □C mechanism has also been described, especially occurring during active translation of mRNAs that do not undergo degradation. However, the molecular players have not been clearly identified (Wang et al., 2015) (Fig. Results 5 A, in red square) and we are now involved in evaluating this hypothesis.

To test our hypothesis, we collected other ARSACS patient fibroblasts, carrying a panel of different mutations compared to PN_1, PN_2 we already studied, in particular: PN_3- p.E723fs; p.F3209fs; PN_4- p.L2374S; deleted_allele [(Terracciano et al., 2009)]; PN_5- p.G188E + p.S2465L ; p.L3916W) (Fig. Results 5 B). We analyzed sacsin levels by WB in these patient fibroblasts. We found a total absence of full-length sacsin protein in PN_3 as expected by sacsin truncating mutations. In PN_4 we expected to find half the amount of sacsin protein. However, the results from WB indicated a total absence of sacsin. In PN_5 we expected to see the whole amount of sacsin, but we detected a very faint residual level of the protein. (Fig. Results 5 C). In line, experiments of qRT-PCR on *SACS* mRNA showed halved amounts of *SACS* mRNA in PN_3 (probably due to NMD of one of the two frameshift mutations). Yet, there are unchanged levels of *SACS* mRNA in PN_4 and increased levels in PN_5 (Fig. Results 5 D),

probably indicating a 'flooding' of ribosomes in the attempt to translate the mutant protein. The end result is the accumulation of *SACS* mRNA.

Now, our goal is to try to evaluate putative co-translational □C of sacsin at this purpose. We are generating a new N-terminal sacsin antibody to recognize putative N-terminal sacsin arrest products upon blocking proteasomal degradation. Additionally, we are trying to understand which are the players involved in this co-translational machinery. Therefore, we want to silence the known ones (Listerin/NEMF) to study the effect on the mutant sacsin amount. We are aware that the feasibility of our strategy depends on whether the rate of sacsin synthesis is compatible with the proposed experimental setup (proteasomal block/silencing). Half-life of WT sacsin has never been investigated, but since sacsin is a big protein it is expected to have a very long turnover. We assayed the rate of sacsin synthesis experimentally by radioactively pulse-labelling human fibroblasts followed by sacsin immunoprecipitation, SDS-PAGE and autoradiography. Our results demonstrated that sacsin is efficiently □e *no*□o synthesized already in 4 hours (Fig. Results 5 E).

□□□□□□□□	□□□□□□ □□□□□□□□
P□□□□	p□□□2□f□□□5 □p□□□20□f□□□□
P□□□□	p□□2□□□□□ □de□eted□a□e□e □□erra□□iano□200□□
P□□□5	p□□□□□□□ □p□□□2□□□5□ □p□□□□□□□□□

Western Blot, anti-actin

| | Sol□□□e □□action□ | □□ea□ in□o□□□□e □□action□ |

SACS/TBP mRNA normalized levels

□□□□□□□□□, □□□□□□ m□□□□

controls   PN_3   PN_4   PN_5

2.0
1.5
0.5
0.0

Inp: input
IP: immunopre□ipitated fra□tion
□□: f□o□ t□rou□□

□□ead□
□a□□in□

250 —
□50 —
□00 —

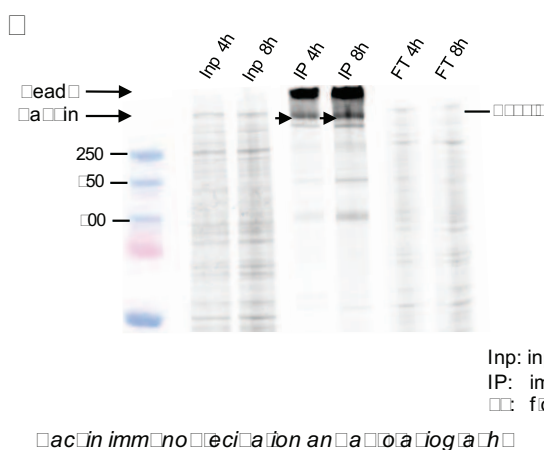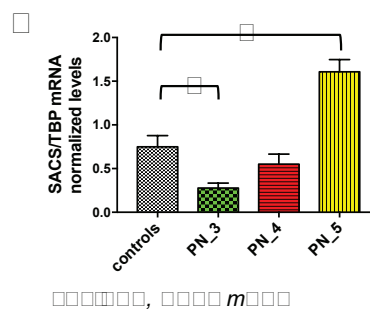□□ac□in immu□no□□eci□□a□ion an□□a□□o□a□iog□a□h□
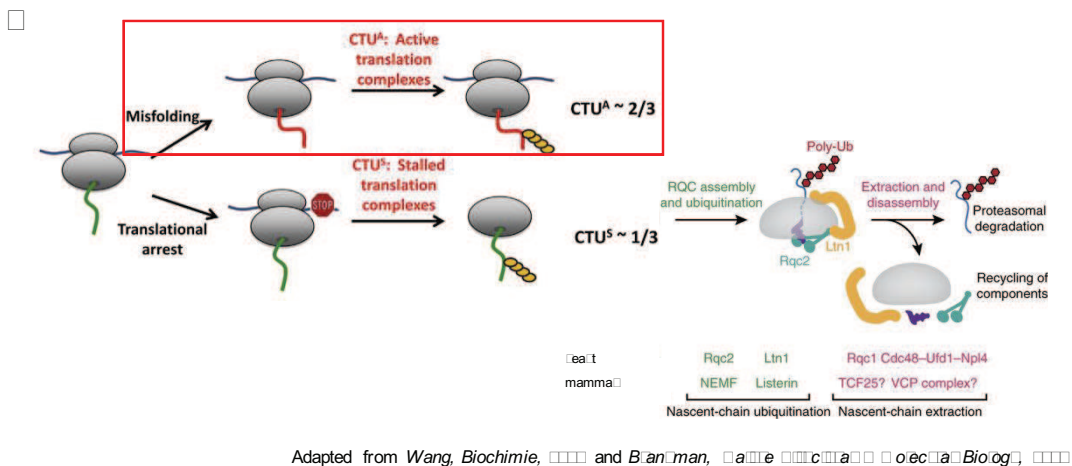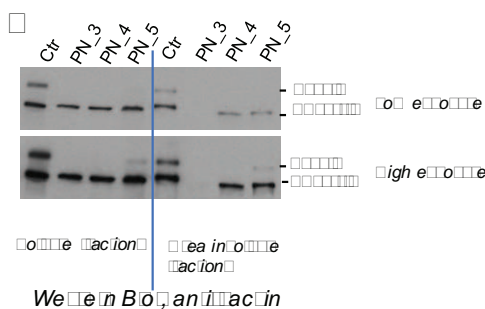
Fig. Results 5. Co-translational quality control (□C) hypothesis for sacsin. (A) Cartoon showing co-translational □C pathways, in particular the two possible co-translational ubiquitination (CTU) situations: CTU^A has been proposed to target misfolded nascent chains that are being actively translated, whereas CTU^S is proposed to ubiquitinate

nascent chains arising from irreversibly stalled translation complexes (Wang et al., 2015). In this second pathway, the main players involved in recognition, ubiquitination, and targeting of aberrant polypeptidic nascent chains to the proteasome are shown (Brandman and Hegde, 2016). The red square indicates our more plausible working hypothesis, being mutant *SACS* mRNA present. (B) Table showing ARSACS patient mutations newly enrolled in our study. (C) Sacsin protein levels by WB in control fibroblasts versus PN_3, PN_4, PN_5, normalized on spectrin, loaded as soluble fractions on the left, and urea insoluble fractions on the right. (D) qRT-PCR on controls and ARSACS patients PN_3, PN_4 and PN_5 (n□3, mean□SEM, □p□0,05). (E) Autoradiography of sacsin immunoprecipitation after 4 and 8 hours of radioactive pulse-labelling.

Chapter □

□□ Investigating the outcomes of sacsin a□sence i□□ mitochon□rial net□or□ hyperfusion□

□□□ Sacsin is □ioinformatically pre□icte□ to □e cytosolic an□ nuclear□

Sacsin subcellular localization is still a big unknown topic. Actually, there are no available antibodies working properly in IF able to detect endogenous sacsin. We therefore started investigating sacsin (referred to RefSeq NP_055178.3) subcellular localization with a bioinformatic approach. Analysis by WoLF PSORT (https://www.genscript.com/wolf-psort.html), a state-of-the-art tool in the field of subcellular localization prediction (Horton et al., 2007), reported the protein to be cytosolic. Sacsin is predicted to be cytosolic with a score of 11.5 out of 32, against a score of 10.5 out of 32 for nuclear localization. Beside these results, the score for cytosol-nuclear co-localization is 11.5 (Results Table 1). These results suggest that sacsin is cytosolic, but it may also shuttle between the nucleus and the cytosol, due to a nuclear score parameter of 3.06, based on the presence of seven Nuclear Localization Signals (NLS) and DNA binding site motifs identified by WoLF PSORT in sacsin sequence (Results Table 2).

Such hypothesis of nuclear co-localization is interesting given the fact that sacsin has high homology with the Rad23a protein family, with which it shares both the UbL and the XPCB domain. Rad23a localizes in the nucleus and both the UbL and XPCB domains have been involved in DNA repair pathways. It was speculated that the same domains may be involved in protein quality control in the nucleus (Kamionka and Feigon, 2004). Using various softwares, such as NucPred (https://nucpred.bioinfo.se/nucpred/) only one NLS, located at position 2776, was consistently predicted with a probability of 0.83. To investigate the cytosol-nucleus shuttling hypothesis, we analyzed Nuclear Export Signals (NES) with different available online softwares, without revealing the presence of NES sequences in sacsin. The search was limited to canonical Crm1-exportin binding site consensus sequence. Analysis of the

mouse sacsin orthologue by WoLF PSORT showed the same results, with prediction of seven NLSs with conserved amino acid residues and at conserved positions relative to human sacsin (Results Table 3). ⬚uerying other state-of-the-art software, confirmed sacsin to be cytosolic, thus in accordance with general prediction of WoLF PSORT. Finally, neither WoLF PSORT nor any other software did predict sacsin to have characterized protein sorting signal, included both endoplasmic reticulum (ER) and mitochondrial targeting peptides, apart from the above discussed NLSs.

153431625032623 WoLFPSORT prediction cyto: 11.5, cyto_nucl: 11.5, nucl: 10.5, pero: 3, cysk: 3

PSORT features and traditional PSORTII prediction

id	site	distance	identity	comments
				32 Nearest Neighbors
NOP5_HUMAN	nucl	62.5317	4.73903%	[Uniprot] SWISS-PROT45:Nuclear; nucleolar. GO:0005730; C:nucleolus; Evidence:TAS.
NOP5_RAT	nucl	62.6736	4.80454%	[Uniprot] SWISS-PROT45:Nuclear; nucleolar. GO:0005730; C:nucleolus; Evidence:ISS.
KU86_MOUSE	nucl	63.7937	6.48613%	[Uniprot] SWISS-PROT45:Nuclear. GO:0005634; C:nucleus; Evidence:IDA.
BAL_HUMAN	nucl	65.4066	6.92291%	[Uniprot] SWISS-PROT45:Nuclear.
ADAS_CAVPO	pero	66.3274	5.37235%	[Uniprot] SWISS-PROT45:Peroxisomal.
CYG3_BOVIN	cyto	70.3882	5.85281%	[Uniprot] SWISS-PROT45:Cytoplasmic.
CHKA_HUMAN	cyto	73.6872	4.58615%	[Uniprot] SWISS-PROT45:Cytoplasmic.
CTNA_DROME	cysk	76.246	7.46888%	[Uniprot] SWISS-PROT45:Found only at cell-cell boundaries. GO:0005915; C:zonula adherens; Evidence:NAS.
XDH_CALVI	pero	76.463	9.41254%	[Uniprot] SWISS-PROT45:Peroxisomal.
CHKA_RAT	cyto	78.2415	4.30225%	[Uniprot] SWISS-PROT45:Cytoplasmic.
CACH_RAT	cyto	78.6851	4.91374%	[Uniprot] SWISS-PROT45:Cytoplasmic.
SEN6_HUMAN	cyto	80.4752	8.23324%	[Uniprot] SWISS-PROT45:Cytoplasmic.
NO56_HUMAN	nucl	81.5753	5.39419%	[Uniprot] SWISS-PROT45:Nuclear; nucleolar. GO:0005730; C:nucleolus; Evidence:TAS.
CPSB_XENLA	cyto	81.591	6.77004%	[Uniprot] SWISS-PROT45:Cytoplasmic.
CLUS_PIG	extr	82.5479	4.21489%	[Uniprot] SWISS-PROT45:Secreted.
SPO1_XENLA	extr	83.3652	6.70452%	[Uniprot] SWISS-PROT45:Secreted. Extracellular matrix (By similarity).
CHKA_MOUSE	cyto	84.2667	4.47696%	[Uniprot] SWISS-PROT45:Cytoplasmic.
AOFA_HUMAN	mito	84.44	4.80454%	[Uniprot] SWISS-PROT45:Mitochondrial outer membrane.
CC45_XENLA	nucl	84.7404	5.43787%	[Uniprot] SWISS-PROT45:Nuclear.
CIC2_MOUSE	plas	85.151	8.14588%	[Uniprot] SWISS-PROT45:Integral membrane protein.
E2F1_CHICK	nucl	85.6906	4.12754%	[Uniprot] SWISS-PROT45:Nuclear.
TUI4_MOUSE	cyto	87.2994	9.93667%	[Uniprot] SWISS-PROT45:Cytoplasmic.
TUI4_HUMAN	cyto	89.0136	10.3298%	[Uniprot] SWISS-PROT45:Cytoplasmic.
AL6B_HUMAN	nucl	89.3566	4.06202%	[Uniprot] SWISS-PROT45:Nuclear. GO:0005634; C:nucleus; Evidence:IDA.
CTN1_MOUSE	cysk	89.6841	7.16314%	[Uniprot] SWISS-PROT45:Found at cell-cell boundaries and probably at cell-matrix boundaries. GO:0005915; C:zonula adherens;
CC45_MOUSE	nucl	89.7695	5.37235%	[Uniprot] SWISS-PROT45:Nuclear.
REP2_HUMAN	cyto	90.1329	6.09303%	[Uniprot] SWISS-PROT45:Cytoplasmic.
CTN1_HUMAN	cysk	90.2348	7.1413%	[Uniprot] SWISS-PROT45:Found at cell-cell boundaries and probably at cell-matrix boundaries.
EF1A_CAEEL	cyto	90.8888	4.45512%	[Uniprot] SWISS-PROT45:Cytoplasmic.
XDH_CHICK	pero	90.9221	9.74012%	[Uniprot] SWISS-PROT45:Peroxisomal.
PIA4_MOUSE	nucl	90.9498	4.60799%	[Uniprot] SWISS-PROT45:Nuclear. GO:0016363; C:nuclear matrix; Evidence:IDA.
CC45_HUMAN	cyto_nucl	91.055	5.15396%	[Uniprot] SWISS-PROT45:Cytoplasmic and nuclear. GO:0005634; C:nucleus; Evidence:TAS.

Results Table 1. Output of sacsin sequence analysis by WoLF PSORT software. The figure displays the 32 proteins most similar to sacsin in WoLF PSORT dataset. For each protein, id (gene name and species), site (subcellular localization site), distance (measure of the similarity between WoLF PSORT parameters values calculated for sacsin sequence and proteins in the dataset), amino acid identity and GO terms are given. It can

be noticed that majority of neighbour proteins localize in the nucleus or in the cytosol. Sacsin sequence is referred to NP_055178.3.

Sequence	Position	Type
RKFLASLTDTSEKEKRI	906	Bipartite
RRIISEGIWSLIREKRQ	2427	Bipartite
PKRHKAL	2502	Pat 7
KRKQFHASVIDSVTKKR	2778	Bipartite
KRPK	3171	Pat 4
PRKLKVN	4298	Pat 7
PESERKK	4324	Pat 7

Results Table 2. Human sacsin NLS analysis according to WoLF PSORT. Seven NLSs are identified by WoLF PSORT software. For each site is given the sequence, the amino acid start position and the type of NLS. Pat 4: 4 residue pattern, composed of 4 basic amino acids (K or R), or composed of three basic amino acids (K or R) and either H or P; pat7: 7 residue pattern, composed of P followed within 3 residues by a basic segment containing 3 K/R residues out of 4; bipartite: composed of 2 basic residues, 10 residue spacers, and another basic region consisting of at least 3 basic residues out of 5 residues.

Sequence	Position	Type
RKFLASLTDSSEKEKRI	904	Bipartite
RRIISEGIWSLIREKKQ	2425	Bipartite
PKRHKAL	2500	Pat 7
KRKQFHASVIDSVTKKR	2776	Bipartite
KRPK	3169	Pat 4
PKKLKVN	4295	Pat 7
PESERKK	4321	Pat 7

Results Table 3. Mouse sacsin orthologue NLS analysis by WoLF PSORT software. For each site is given the sequence, the amino acid start position and the type of NLS (refer to Results Table 1 for the meaning of each NLS type). Interestingly, the same number of NLSs as in human sacsin is predicted, with conserved residues at conserved amino acid positions. Also in this case, only NLS at 2778 is consistently reported by other online software, included NucPred with a probability of 0,83.

Subcellular fractionation experiments demonstrate that sacsin is cytosolic with a partial mitochondrial localization.

Since we have commercial antibodies perfectly working in WB, to address sacsin subcellular localization issue, we performed fibroblast subcellular fractionation. We confirmed that sacsin is predominantly cytosolic and totally absent from nuclei. This is in contrast with bioinformatic predictions. Interestingly, we detected sacsin in mitochondrial and membrane fractions (Fig. Results 6 A).

Previous reports showed impaired mitochondrial transport in sacsin knockdown hippocampal neurons and hyperfused mitochondria in ARSACS fibroblasts (Girard et al., 2012), suggesting a role of sacsin at the mitochondrial level. To perform an in-depth study about this role, we first strengthened sacsin presence in mitochondrial fraction by performing two different experiments: a standard mitochondrial-cytosolic subcellular fractionation, using differential centrifugation to enrich mitochondria (Fig. Results 6 B) and a new method of mitochondrial purification that uses TOM22-conjugated magnetic beads to highly purify mitochondria (method (Franko et al., 2013), Fig. Results 6 C). As previously described in Fig. Results 6 A, sacsin is mostly cytosolic, but it also shows mitochondrial localization, as demonstrated by sacsin in the M (mitochondrial) fractions, immunoblotted also for mitochondrial and cytosolic markers (Fig. Results 6 B-C)
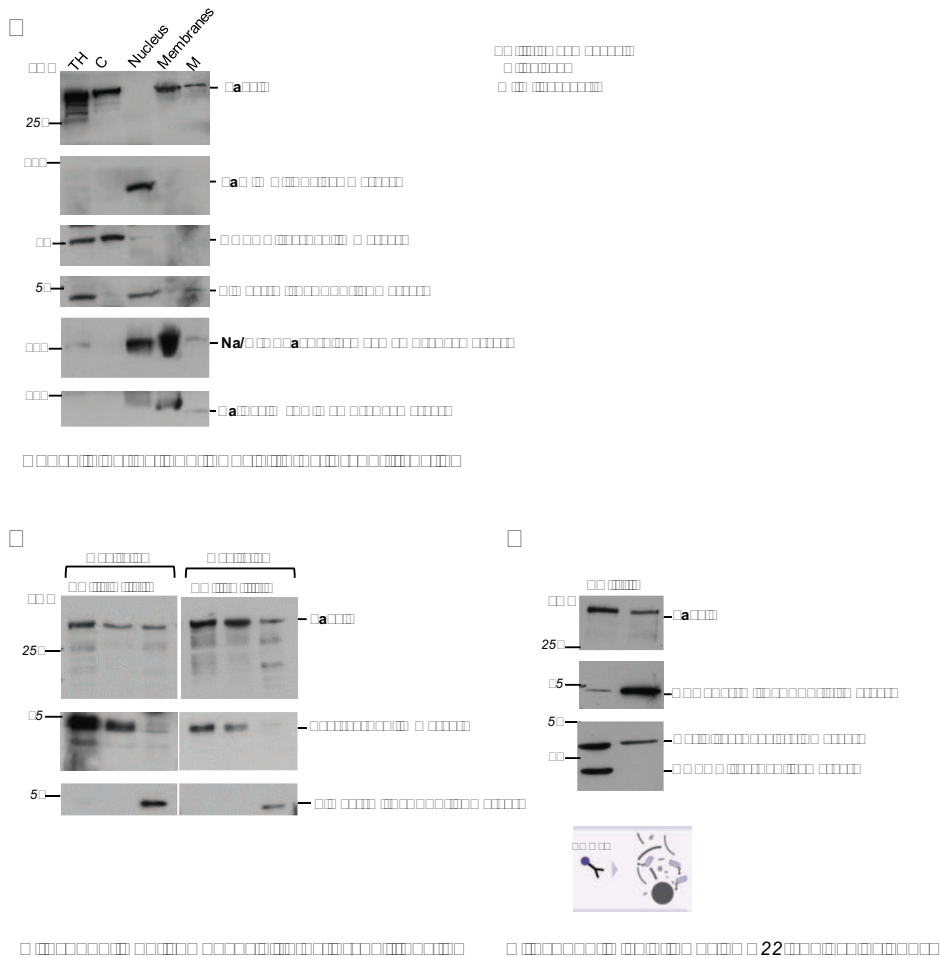
Fig. Results 6. Sacsin is localized in cytosol and partially on mitochondria in subcellular fractionations. (A) WB showing different fractions from subcellular fractionation. Each compartment is labelled with a specific antibody. (B) WB of mitochondrial enrichment by differential centrifugation. (C) WB of mitochondrial purification using specific isolation protocol based on anti-TOM22 immunoprecipitation of mitochondria, obtaining pure mitochondrial fraction, avoid of cytosolic contamination.

□□ □□□□□□A □noc□in □ela cells generation □y CRIS□R□Cas□□ me□iate□ genome e□iting to clarify sacsin su□cellular locali□ation□

To unravel sacsin subcellular localization, we designed a CRISPR/Cas9-knockin (KI) system to fuse a protein-tag sequence to the C-terminal region of sacsin endogenous coding sequence. Briefly, in CRISPR/Cas9-KO strategy, Cas9 mutagenic activity gives origin to insertion/deletions

(indels) mutations at the double strand break (DSB) sites, inducing the error-prone non-homologous end joining (NHEJ) pathway of DNA repair and finally inactivating the coding sequence of a locus of interest. On the other hand, in CRISPR/Cas9-KI strategy, homology directed repair (HDR) of DSBs is exploited to insert or replace a sequence inside the targeting region. CRISPR/Cas9-KI allows the insertion of a sequence at a precise genomic locus by CRISPR/Cas9-mediated genome editing. In particular, it requires that Cas9-induced DSB at that locus is repaired by HDR and therefore an exogenous DNA molecule acting as donor for repair (HDR template) must be delivered into the cells. HDR template includes the DNA sequence to insert, flanked by homologous sequences (homology arms) that mediate HDR with the endogenous locus.

HDR is a very rare and inefficient event in mammalian cells in respect to NHEJ repair pathway of DSBs (Mao et al., 2008; Komor et al., 2017). Until now endogenous gene tagging by CRISPR/Cas9-based HDR in human cells has been carried out in few studies and for few loci, mainly to insert fluorescent tags or reporters, which allow selection of edited cells by FACS (Ratz et al., 2015; Roberts et al., 2017).

Moreover, to the best of our knowledge, endogenous gene tagging by CRISPR/Cas9-mediated HDR has never been reported for a giant and complex protein like sacsin. Due to these challenges, the project was carried out in collaboration with a genome editing expert research group inside our Institute community. In order to prove our novel CRISPR-KI strategy works, we first attempted to insert a HA-epitope protein tag sequence fused to sacsin coding sequence in HeLa cells. We opted for HA tag since it is a small tag and allows for shorter HDR template.

2.3.1 C□S□□□□□strateg□ an□ □esign

We designed a CRISPR-KI strategy to fuse HA protein tag sequence C-terminally to *SACS* open reading frame in HeLa cells (Fig. Results 7). We designed the insertion of HA epitope along with a short flexible linker (GSGGG) between the tag and the endogenous sacsin protein. Since we

know that our collaborators failed to clone sacsin if the tag sequence was placed at the N-terminus, we decided to tag sacsin protein at the C-terminus. The linker sequence was designed by studying literature (Chen et al., 2013; Klein et al., 2014). In general, poly-GS and poly-G are flexible linkers, commonly used in combination for expression of recombinant proteins, which are able to keep separated different protein segments and therefore to expose the epitope to the solvent (Chen et al., 2013). The length of the linker was limited to 5 residues to avoid folding of the linker on itself, which can mask the epitope. Together with the linker-HA sequence, the system was designed to introduce also a new restriction site (RS) for PsiI restriction enzyme, which is not present in the surrounding genome sequence (referred to hg38). This new RS allows us to detect the integration of the tagged sequence at genomic level by restriction fragment length polymorphism (RFLP) assay.

We used a plasmid-based strategy for the delivery of Cas9:sgRNA complexes. In this approach, an all-in-one episomal plasmid encodes both the Cas9 and the sgRNA specific for the locus of interest. An advantage of this approach is that it sustains for longer Cas9 expression in the cell, which increases its cleavage activity. For HDR template, we decided to use single-stranded oligodeoxynucleotides (ssODNs), which have been already efficiently employed for genome editing in different systems, including human cell lines (Paquet et al., 2016; Komor et al., 2017; Li and Wang, 2017; Xu et al., 2018).

Sigma Aldrich designed the best sgRNA targeting region (Fig. Results 7) in the 3' terminal part of *SACS* coding sequence in exon 10 (referred to RefSeq NM_014363.5). The plasmid encodes also RFP fluorescent protein to select positively transfected cells by FACS. *SACS* sgRNA predicted cutting site is positioned 59 bp upstream the insertion site for tag sequence, which corresponds to the natural STOP codon of *SACS* open reading frame. This represented the main problem of our CRISPR-KI design, as the increasing distance between the insertion site and the DSB greatly reduces the efficiency of homologous recombination (Elliott et al.,

1998). For this reason, we designed the sequence of HDR template, including the 59 terminal coding bases of sacsin sequence, followed by the linker-HA-PsiI-STOP sequence. This sequence was flanked by 40 bp homology arms identical to sacsin coding region upstream the Cas9 cutting site and to 3'UTR region downstream sacsin natural STOP codon (Fig. Results 7).
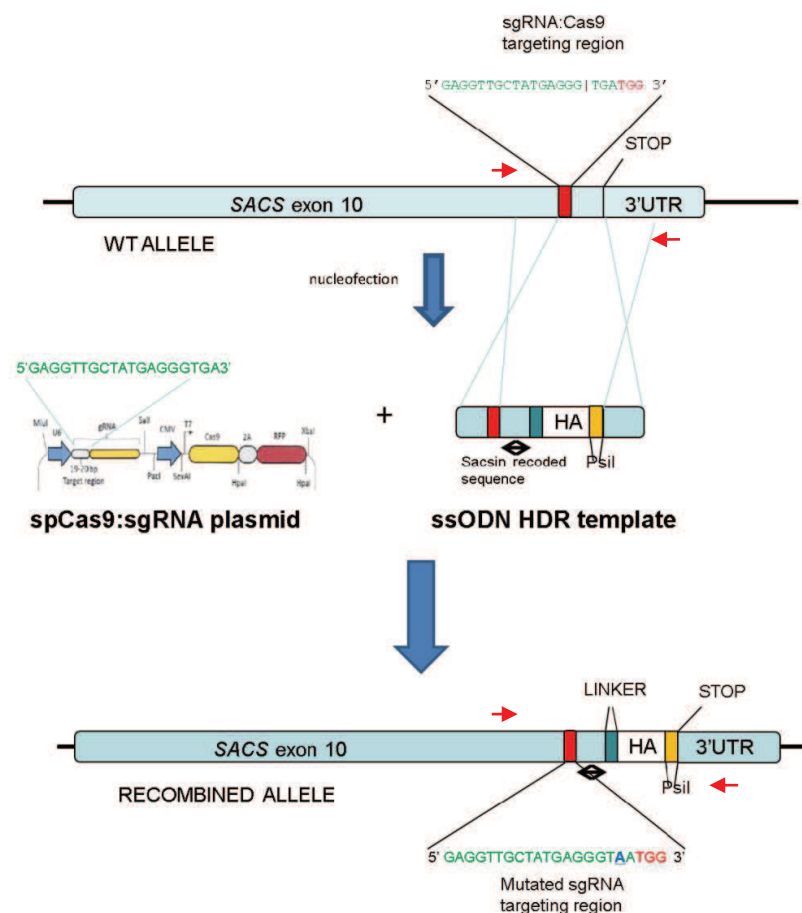

Fig. Results 7. Strategy for HeLa *SACS*-HA generation by CRISPR/Cas9 technology. Cells are nucleofected both with a plasmid encoding Cas9-RFP protein plus the sgRNA and with homologous donor template in the form of single-stranded oligodeoxynucleotide (ssODN). Green: sgRNA targeting region; red: PAM; black line: predicted Cas9 cut site; blue lines: regions of homology; red arrows: primers used for PCR amplification. Note that in the homology donor template the region between the homology arms (included one base upstream the PAM) has been recoded, in order to reinsert the 3' terminal region of sacsin coding sequence and to avoid homologous recombination in the intervening region between Cas9 cutting site and the wanted insertion site.

2.3.2 *Molecular analysis of HeLa cells nucleofected with Cas9:sgRNA and HDR template*

WT HeLa cells were co-nucleofected with the Cas9:sgRNA all-in-one plasmid together with HA donor ssODN in one of three different forms: the ssODN encoding the forward filament of HDR template (named FW HA-oligo), the ssODN encoding the reverse filament of HDR template (named REV HA-oligo), and the two FW and REV HA-oligo annealed to form a double-stranded HDR template (named annealed HA-oligo). RFP positive cells were sorted by FACS, to enrich the population with gene edited cells. We then performed molecular analysis and subsequently we generated clonal cell lines from this population.

An important validation step of our CRISPR-KI strategy included first the evaluation of the on-target cleavage activity of our designed Cas9:sgRNA novel system. To assess this question, we performed a CEL-I-endonuclease mismatch assay to detect the degree of indel mutations induced by Cas9 at the target genomic locus of HeLa cells nucleofected only with the all-in-one plasmid. Genomic target locus was PCR-amplified from this cell population and then digested with CEL-I endonuclease. Data showed that the Cas9 had an efficient cutting activity at the expected target site with 25% of genomic DNA population being digested by CEL-I endonuclease (Fig. Results 8 A). This result is particularly important, since high efficiency cutting increases HDR frequency by creating more DSBs that can be available for HDR machinery. Usually, a frequency of at least 25% is required to have efficient HDR at the target site.

To investigate if this cleavage activity is sufficient to induce recombination with the HDR template, we then performed RFLP assay on cells co-nucleofected both with the plasmid encoding the Cas9:sgRNA and one of three different constructs encoding the HDR template. Genomic target locus was PCR-amplified and then digested with PsiI enzyme. The results were positive for all three HDR template delivery systems (FW HA-oligo, REV HA-oligo and annealed HA-oligo), showing integration of PsiI site in at most 5% of genomic DNA population in the cells nucleofected with FW

HA-oligo and 3□ in cells nucleofected with annealed HA-oligo (Fig. Results 8 B). On the contrary, integration efficiency with REV HA-oligo was lower. These results were particularly encouraging since homologous recombination frequency in mammalian cells is reported to be less than 5□ (1□ on average) (Mao et al., 2008; Komor et al., 2017). We expected different efficiency using one strand filament rather than other, since it is known that HDR machinery binds with different efficiency the negative or positive strand of HDR template, depending on many variables, including the reciprocal position of DSB and insertion site and which genomic strand is released first by Cas9 after cleavage (Renaud et al., 2016; Richardson et al., 2016; Song and Stieger, 2017).

Taken together, these results show that the designed system is able to cleave and induce homologous recombination, with insertion of the HA-tag, at relatively high efficiency in HeLa cells.
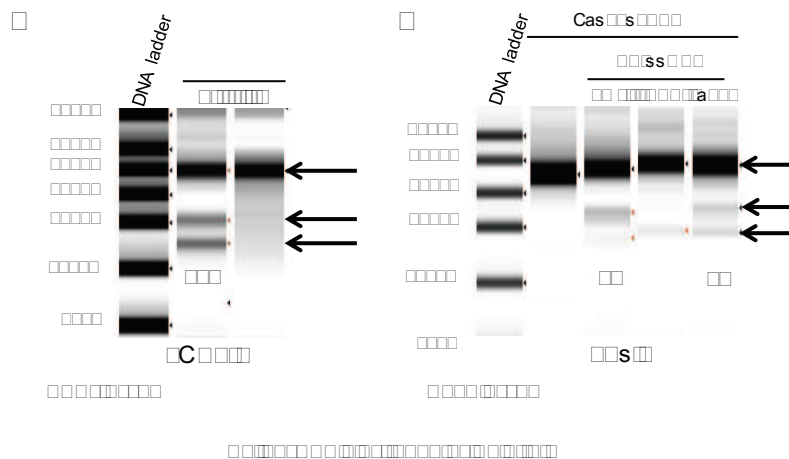

Fig. Results 8. Molecular analysis of HeLa nucleofected with Cas9:sgRNA and homology directed repair (HDR) template validates our CRISPR-KI strategy. (A) Results for CEL-I endonuclease assay on genomic DNA extracted from RFP positive cells nucleofected with the plasmid encoding Cas9-RFP and the sgRNA, relative to WT cells. Detection of NHEJ DNA repair, using the CEL-I enzyme, which cuts at mutated DNA sites. Arrows indicate heights of expected digestion bands. The two cleavage products bands are detected only in nucleofected sample, with an efficiency calculated to be 25□. (B) Results of RFLP assay on genomic DNA extracted from RFP positive cells nucleofected with the plasmid encoding Cas9-RFP and the sgRNA and the donor template. Detection of recombination and HA integration by using PsiI restriction enzyme. Arrows indicate heights of expected digestion bands. PsiI cleavage products appear only in cell populations nucleofected both with the Cas9:sgRNA and the HDR template, whereas no bands appear after digestion of DNA from untreated cells. Efficiency of PsiI integration was quantified to be 5□ in cells nucleofected with FW HA-oligo and 3□ in annealed HA-

oligo. Samples were loaded on high sensitivity screenTape (Agilent) electrophoresis platform. ann.: annealed.

2.3.3 Anal☐sis of the clones ☐eri☐e☐ from cells nucleofecte☐ ☐ith Cas☐sg☐☐A an☐☐☐☐ template

We generated monoclonal cell lines from the population of RFP positive cells nucleofected with the all-in-one plasmid and the FW HA-oligo, as this condition gave the maximum HDR efficiency (Fig. Results 8 B).
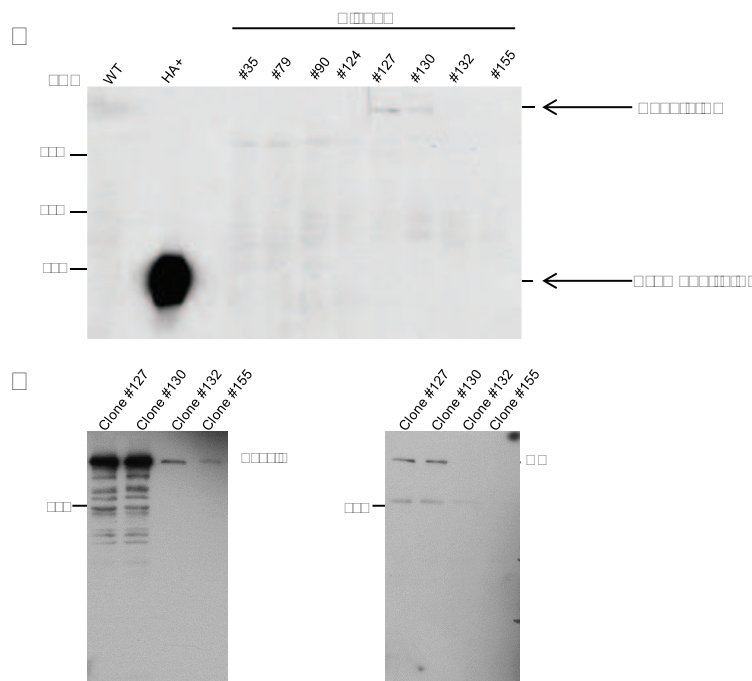

Fig. Results 9. WB analysis of HeLa monoclonal cell lines derived from population of RFP positive cells nucleofected with the all-in-one plasmid and the FW HA-oligo. (A) Two clones positive for HA integration detected by WB with antibodies against HA tag, as a specific band appeared at sacsin height (black arrow, sacsin-HA). Cells transfected with uromodulin-HA were used as positive control. (B) WB with HA antibodies (at higher concentration than in (A) and sacsin antibodies shows that HA integrated in clones 127 and 130 since a specific band is present at the same molecular weight of sacsin (black arrow). Antibody against HA was from mouse, antibody against sacsin was from rabbit.

Extensive screening of clones is necessary since there is no way to select edited cells, as it would be possible using a fluorescent tag that allows to select edited cell by FACS. A total of 174 clones were pre-screened by intracellular staining with an anti-HA antibody conjugated with a fluorophore followed by flow cytometry analysis. Those clones that

showed increased fluorescence signal were re-screened via WB and we found two clones in which HA peptide integrated at sacsin molecular weight (Fig. Results 9). Due to HA and sacsin relative signal intensity, it is likely that the integration occurred in heterozygosis, as it is expected due to extremely low efficiency of homology recombination in mammalian cells. Full molecular characterization of these two clones is now ongoing.

▢▢ ▢itochon▢rial net▢or▢ in ARSACS patient fi▢ro▢lasts is more fuse▢ than controls▢

The partial co-fractionation of sacsin with mitochondria prompted us to investigate the functional sacsin role at the mitochondrial level. To study the consequence of sacsin absence on mitochondrial morphology, we analyzed mitochondrial network morphology by infecting primary fibroblasts with mito-DsRed2 and performing live imaging microscopy. We found a significant increased number of patient cells presenting a fused mitochondrial network compared to control cells showing intermediate and fragmented network (Fig. Results 10 A-B). This finding was also confirmed in IF experiments with Mitotracker Red, where we better appreciated mitochondrial morphological structures strongly suggestive of hyperfusion, indicated by the presence of balloon-like or bulbed mitochondria (Fig. Results 10 C). To confirm that this phenotype was due to sacsin absence, we analyzed mitochondria network also in mouse embryonic derived-fibroblasts (MEFs) from *Sacs* KO mouse and CRISPR/Cas9 *SACS* KO HeLa cells we generated in our lab. Accordingly, mitochondria are more fused also in *Sacs* KO MEFs and *SACS* KO HeLa cells compared to WT samples (Fig. Results 10 D-G). These findings strongly indicate that the mitochondrial hyperfusion is due to the loss of sacsin function.
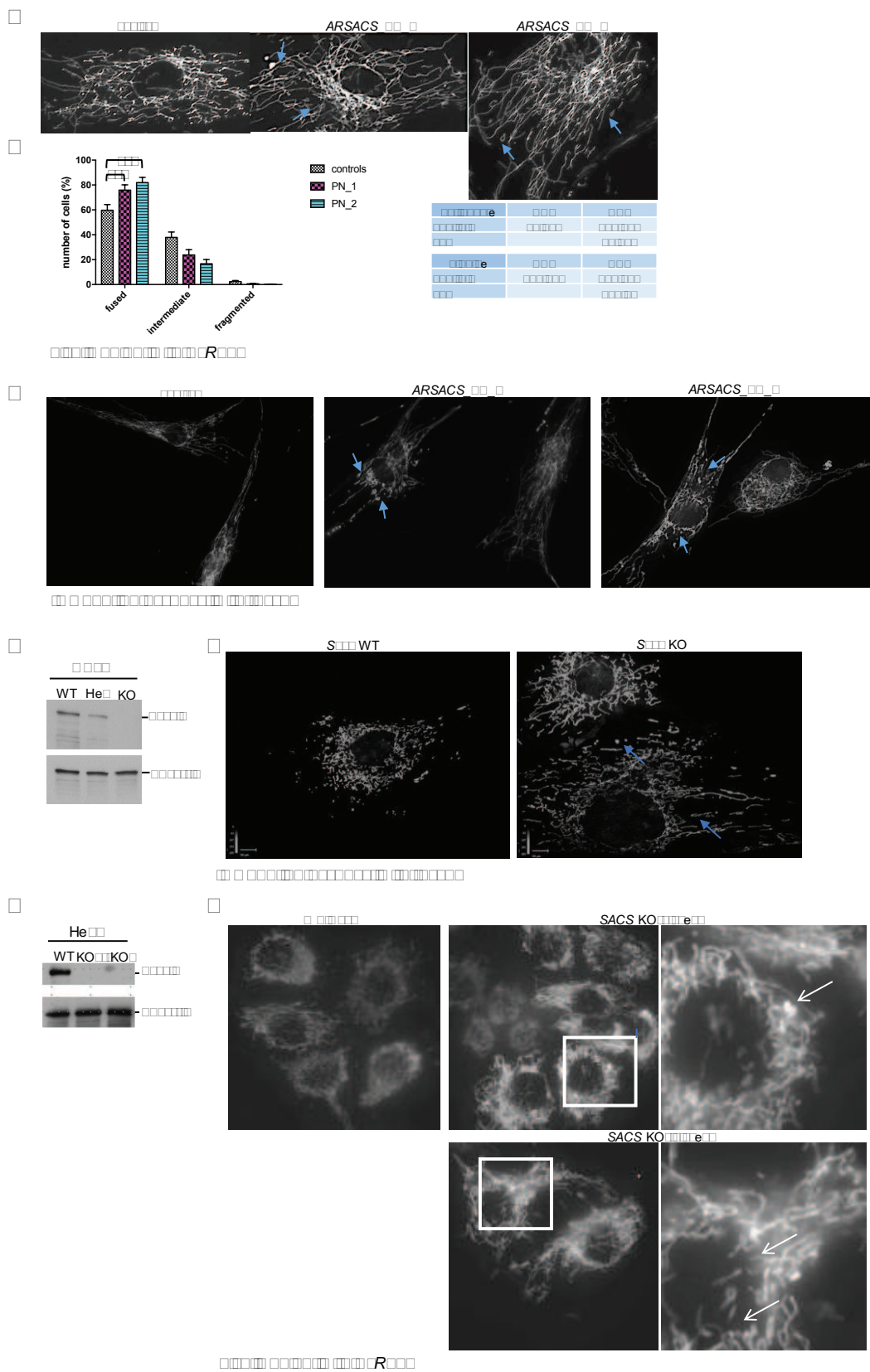
Fig. Results 10. Mitochondrial hyperfusion is a phenotype shared by ARSACS patient fibroblasts, *Sacs* KO MEFs and *SACS* KO HeLa cells. (A) Live imaging experiments and (B) quantification of mitochondrial network categories (☐SEM) with statistical ☐-square

analysis. (C) IF images of mitochondria labelled with Mitotracker Red. (D) WB of sacsin levels and (E) representative IF images of mitochondria in *Sacs* WT and KO MEFs. (F) WB of sacsin levels and (G) representative IF images of mitochondria in WT and CRISPR/Cas9 *SACS* KO HeLa cells we generated.

ARSACS fibroblasts show decreased DRP1 recruitment on mitochondria

Mitochondria continuously change their shape through the combined actions of fission, fusion, and movement along cytoskeletal tracks, in a process called mitochondrial dynamics. The mitochondrial network is determined by the balance between fission and fusion rates (Tilokani et al., 2018). Three members of the Dynamin superfamily are key components of the fission and fusion machineries. Mitofusins (i) mediate outer mitochondrial membrane (OMM) fusion in mammals. Optic Atrophy 1-OPA1- (ii) mediates inner mitochondrial membrane (IMM) fusion. Dynamin-related protein 1-DRP1- (iii), which cycles between the cytosol and OMM, mediates mitochondrial fission (Tilokani et al., 2018). In particular, once recruited, DRP1 further assembles around the mitochondrial tubule to form oligomeric rings (high order complexes) that constrict the mitochondrion in a GTP-dependent process (Liu and Chan, 2015) (Fig. Results 11 A). To shed light on the molecular event leading to mitochondrial alteration towards fusion in ARSACS cells, we tested levels of OPA1, MFNs and DRP1 in patient fibroblasts versus controls, but we did not detect significant alterations (Fig. Results 11 B).

We investigated in details DRP1-mediated fission in ARSACS patient fibroblasts PN_1, PN_2 also considering a previous paper, which found decreased incidence of mitochondrial associated DRP1 foci in *SACS* knockdown cells (Bradshaw et al., 2015). Interestingly, biochemical analysis of DRP1 relocalization on the OMM, where the active fraction of DRP1 is recruited to mediate mitochondrial fission (Tilokani et al., 2018), showed reduced recruitment in patients compared to controls, as highlighted by DRP1 levels in patient mitochondrial fraction (Fig. Results 11 C). Moreover, we analyzed DRP1 high order complexes by Native-

PAGE, which result slightly reduced in ARSACS patient PN_1, PN_2 (Fig. Results 11 D).

Immunoprecipitation of endogenous sacsin in HeLa cells revealed that sacsin does not co-immunoprecipitate with DRP1 (Fig. Results 11 E). The results indicate that mitochondrial hyperfusion in ARSACS cells is due to decreased fission mechanism, rather than enhanced fusion and that molecularly, the fission impairment is driven by reduced DRP1 relocalization on OMM. Being no direct interaction, DRP1 relocalization on OMM is not caused by a direct effect of mutant sacsin on DRP1.
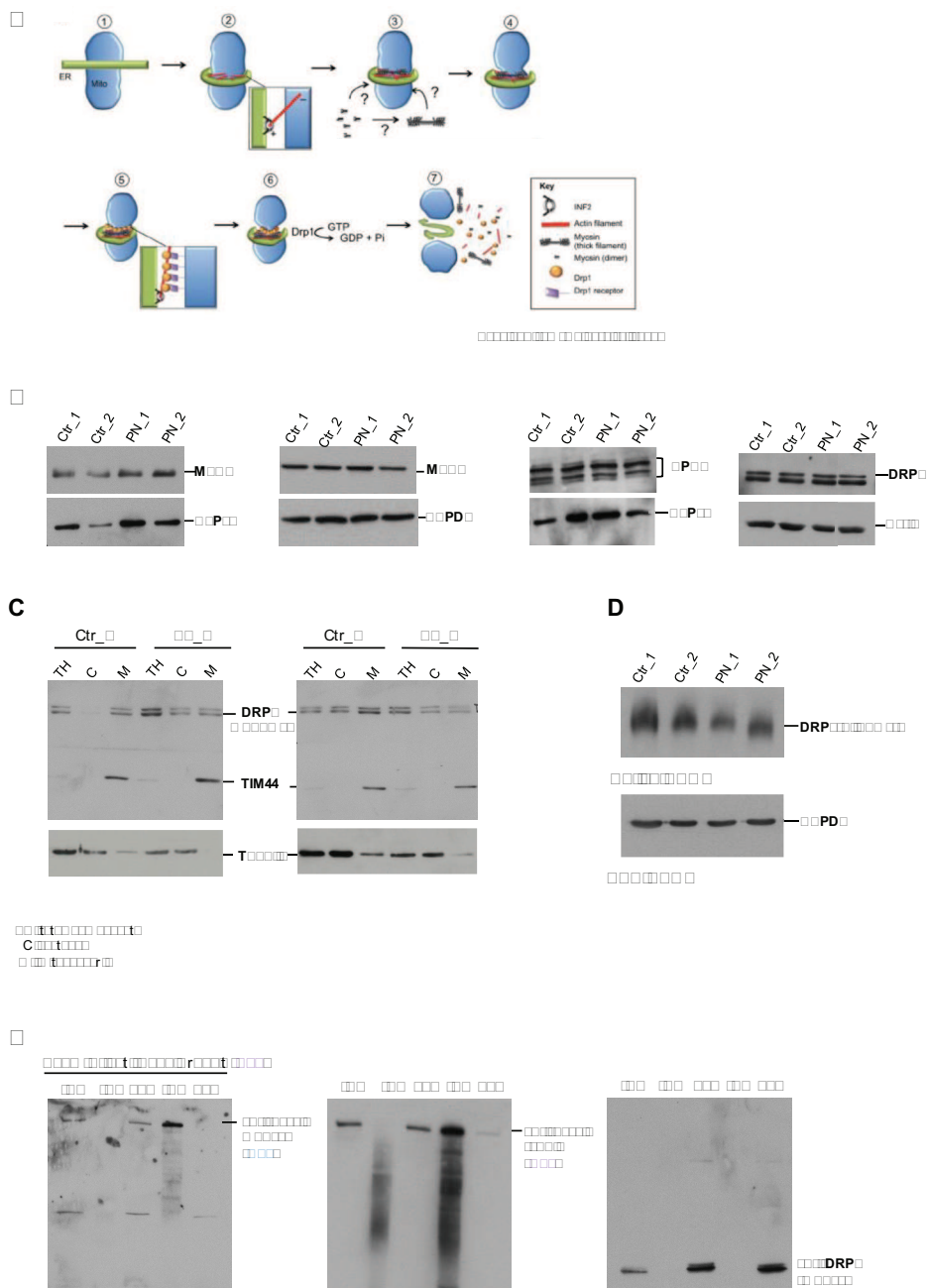
Fig. Results 11. The mechanism of ARSACS mitochondrial hyperfusion is based on reduced DRP1-mediated mitochondrial fission. (A) Cartoon showing the mechanism of DRP1 mediated mitochondrial fission, involving ER, filamentous actin (F-actin), myosin and DRP1 (Hatch et al., 2014). (B) WB analyses of mitochondrial dynamics players in controls versus ARSACS patient fibroblasts. (C) WB of DRP1 recruitment on mitochondria, in ARSACS patient and control mitochondrial and cytosolic fractions. (D) Native-PAGE showing active DRP1 high order oligomers in ARSACS patient and control fibroblasts. (E) WB of endogenous sacsin immunoprecipitation performed with anti-sacsin Ab2 and revealed with anti-sacsin Ab1 (left), anti-sacsin Ab2 (middle) and anti-DRP1 (right).

☐☐ ☐☐☐☐ ☐O ☐ur☐in☐e cells sho☐ mitochon☐rial retention in neuronal soma☐

To analyze the consequences of sacsin absence on mitochondrial morphology in neurons, a colleague in the lab studied possible mitochondrial dynamics alteration on primary Purkinje cells derived from *Sacs* KO mouse. In agreement with our data showing mitochondrial hyperfusion in ARSACS fibroblasts and in sacsin KO cells, IF experiments on *Sacs* KO Purkinje cells showed that mitochondria tend to cluster in the cell soma and barely enter the dendritic trees, while in WT and *Sacs* heterozygous (Het) Purkinje cells mitochondria entirely fill the dendrites (Fig. Results 12 A).

Indeed, the volumetric quantification of mitochondria in *Sacs* KO Purkinje cell dendrites revealed that they are reduced compared to WT and Het, indicating that these organelles are not properly transported (Fig. Results 12 B). Indeed, analyzing the whole cell volume, the quantification revealed that the total volume of mitochondria (both in dendrites and soma) is unchanged in *Sacs* KO Purkinje cells (normalized on its relative Purkinje cell volume, data not shown) suggesting that mitophagy or mitochondrial biogenesis are unaffected in the absence of sacsin.

Moreover, from Fig. Results 12 A, it is strongly appreciable that mature (DIV15) *Sacs* KO Purkinje cells are smaller compared to WT and Het and exhibit thinner, less branched dendritic trees with fewer spines. WT and *Sacs* Het Purkinje cells, instead, showed a huge soma and elaborate dendritic arbors with many spines and this likely indicates a defect in the development or a premature degeneration of neural processes.
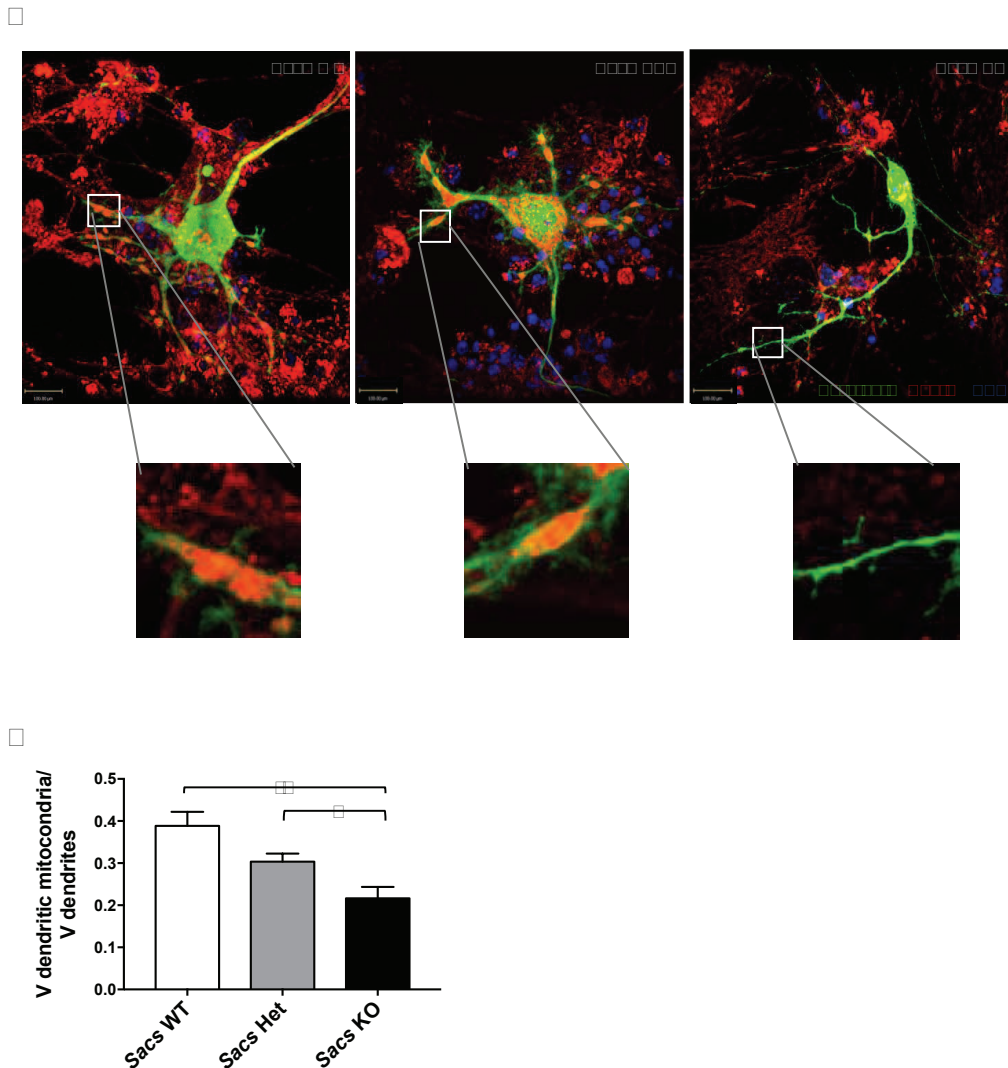
Fig. Results 12. *Sacs* KO primary Purkinje neurons show reduced mitochondria in dendrites. (A) Representative IF images of WT, *Sacs* Het and *Sacs* KO primary Purkinje cells at DIV 15, using calbindin as Purkinje cell marker (green) and COX-IV (red) as mitochondrial marker, analyzed with 63X confocal imaging. (B) Graph showing the ratio between volume of dendritic mitochondria and volume of dendrites as mean□SEM. n□ at least 7 Purkinje cells per genotype. □p□0,05, □□p□0,01 by two tailed t-test.

□□□ En□ogenous sacsin immunoprecipitation in mouse cere□ellum reveals AR□C□as putative sacsin interactor□

Our previous results show that sacsin plays a role on mitochondrial morphology. To shed light on the mechanisms by which sacsin regulates mitochondrial dynamics, we investigated sacsin interactors/substrates and its possible link to mitochondrial morphology.

We performed sacsin immunoprecipitation in mouse cerebellum and subsequent tandem mass spectrometry (LC-MS/MS). Fig. Results 13 A shows the checking in WB of a representative immunoprecipitation experiment, performed with Ab2 and revealed with Ab3 (from a different species). Interestingly, as putative sacsin interactor, we found Actin-Related Protein 2/3 Complex Subunit 2 (ARPC2) (Fig. Results 13 B), which is a subunit of the actin nucleator ARP2/3 complex (Goley and Welch, 2006). We carried out two biological independent immunoprecipitation experiments, identifying ARPC2 as sacsin interactor. The amino acid covering shows different peptides on ARPC2 sequence in each experiment. Each sacsin immunoprecipitation was done in technical replicate.

ARPC2 is an actin-modifying protein involved in F-actin remodelling and a role of these kind of proteins have been recently discovered in the process of mitochondrial fission (Hatch et al., 2014). ARPC2 may be the mediator through which sacsin plays a role on DRP1-mediated mitochondrial fission.

B

(CBB SDS first experiment)

	Protein	Accession	#Exclusive unique peptides	Coverage		Identified amino acids
Sequence Coverage						
		E			a	

	Protein	Accession	#Exclusive unique peptides	Coverage		Identified amino acids
Sequence Coverage	Actin ... A...	C			a	

(CBB SDS second experiment)

	Protein	Accession	#Exclusive unique peptides	Coverage		Identified amino acids
Sequence Coverage		E			a	

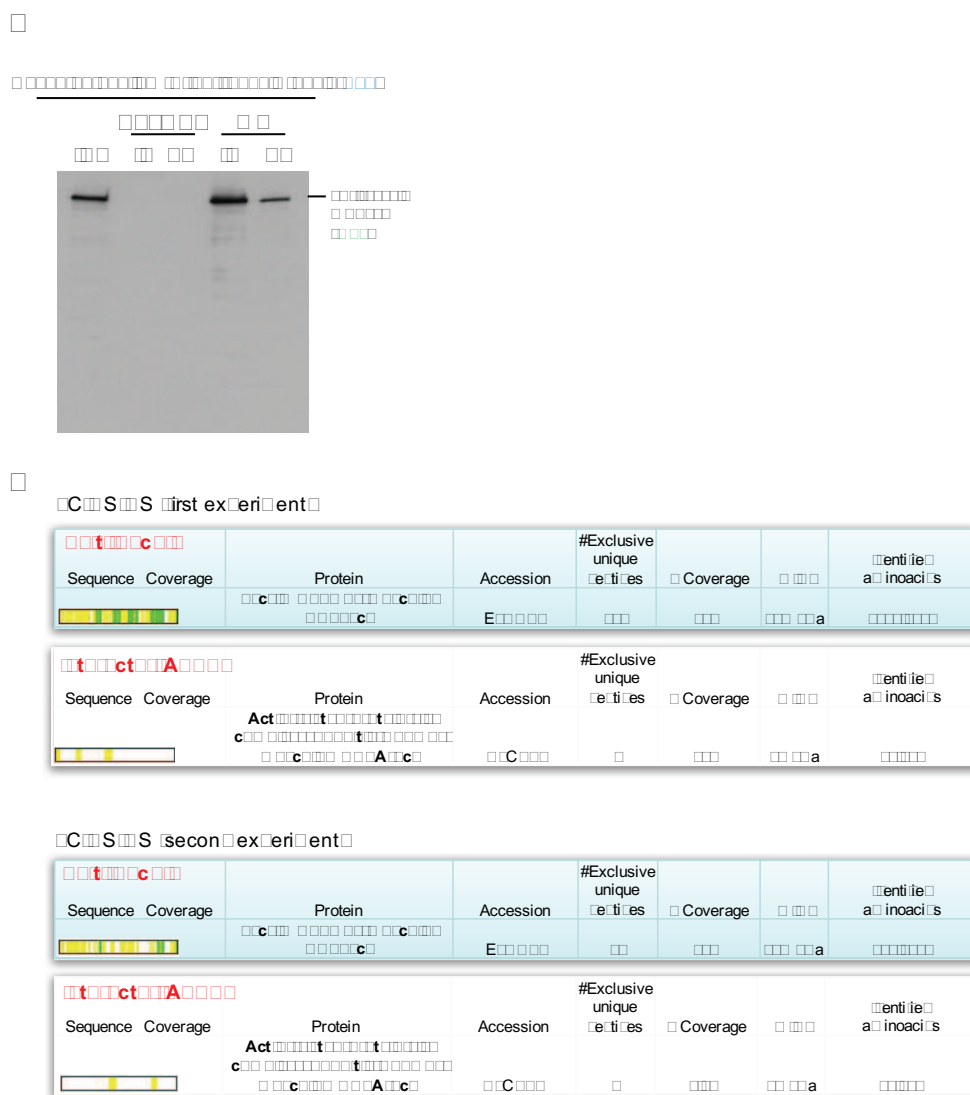|	Protein	Accession	#Exclusive unique peptides	Coverage		Identified amino acids
Sequence Coverage	Actin ... A...	C			a	

Fig. Results 13. Endogenous immunoprecipitation of sacsin in cerebellum reveals ARPC2 as putative sacsin interactor. (A) Representative WB of endogenous sacsin immunoprecipitation in mouse cerebellum performed with anti-sacsin Ab2 and revealed with anti-sacsin Ab3. (B) Mass spectrometry output (first experiment up, and second bottom) using Scaffold software, showing the bait (sacsin) and the interactor (ARPC2) and the unique peptides with which they have been detected by the MS analysis. In the two independent immunoprecipitations, both the bait and the interactor have been recognized with different unique peptides. OS: organism species GN: gene, m.w.: molecular weight.

Chapter □

□□ Investigating the outcomes of sacsin a□sence □ii□ cytos□eletal re□istri□ution□

□□□ Sacsin mutations□a□sence lea□ to cytos□eletal vimentin re□istri□ution□

While we studied mitochondrial network morphology in ARSACS fibroblasts (see Chapter 2, Fig. Results 10 A), we noticed peculiar empty areas in several patient cells, forming a sort of □hole' in the mito-DsRed2 labelled mitochondrial network (Fig. Results 14 A). To understand the nature of these holes, we performed IF experiments testing a panel of different organellar and cytoskeletal markers. Interestingly, we discovered that empty areas found in ARSACS cells were filled with intermediate filament-vimentin signal, which presented as recurrent cytoplasmic perinuclear areas forming a kind of □cage-like' structures from which mitochondria were excluded (Fig. Results 14 B). The reorganization of vimentin architecture in patient cells' was detected in about 60□ of the cells, both in PN_1 and PN_2 (Fig. Results 14 C). We published these data in collaboration with an English group (Duncan et al., 2017).

To verify that the vimentin remodelling detected in ARSACS fibroblasts was due to sacsin mutations/absence, we performed vimentin IF experiments in primary MEFs derived from *Sacs* KO mice. In these cells, we appreciated the presence of intermediate filament-vimentin reorganization, sometimes similar to the □cage-like' appearance found in human ARSACS patient fibroblasts and sometimes having a more bundling-like shape, even surrounding the nucleus (Fig. Results 15 A-B, dashed arrows indicating vimentin bundling and normal arrows vimentin cages). Accordingly, CRISPR/Cas9 *SACS* KO HeLa cells present this striking vimentin remodelling phenotype (Fig. Results 15 C-D).
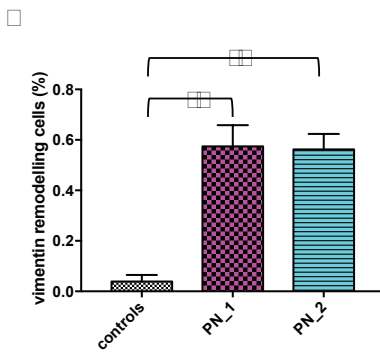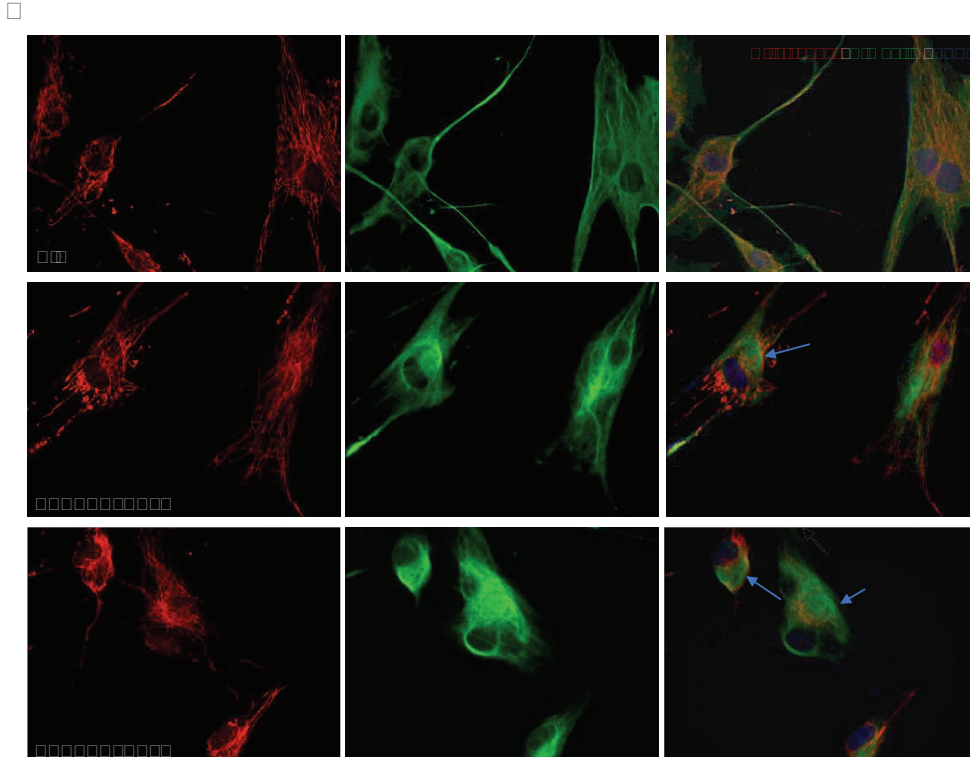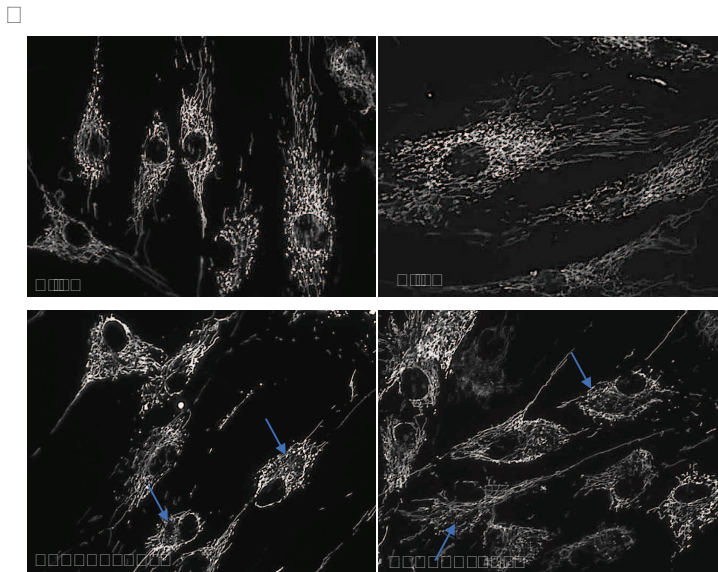
Fig. Results 14. Cytoskeletal redistribution of vimentin in ARSACS fibroblasts. (A) Representative images of mito-DsRed2 live imaging delimiting a hole near the nucleus in ARSACS patient fibroblast cells (arrows). (B) IF of vimentin demonstrates perinuclear accumulation and (C) quantification of vimentin phenotype in ARSACS cells, as mean SEM, two-tailed t test, p 0,005).

Fig. Results 15. The vimentin reorganization phenotype is shared by *Sacs* KO MEFs and *SACS* KO HeLa cells. (A) Vimentin and Mitotracker stainings in WT and KO MEFs, showing perinuclear accumulation of vimentin which excludes mitochondria and (B) quantification of vimentin remodelling in MEFs, expressed as mean□ □SEM. (C) Vimentin IF in HeLa cells (WT and CRISPR/Cas9 *SACS* KO clones) and (D) quantification.

In order to provide an in-depth characterization of the peculiar vimentin remodelling observed in ARSACS cells, we carried out electron microscopy (EM) experi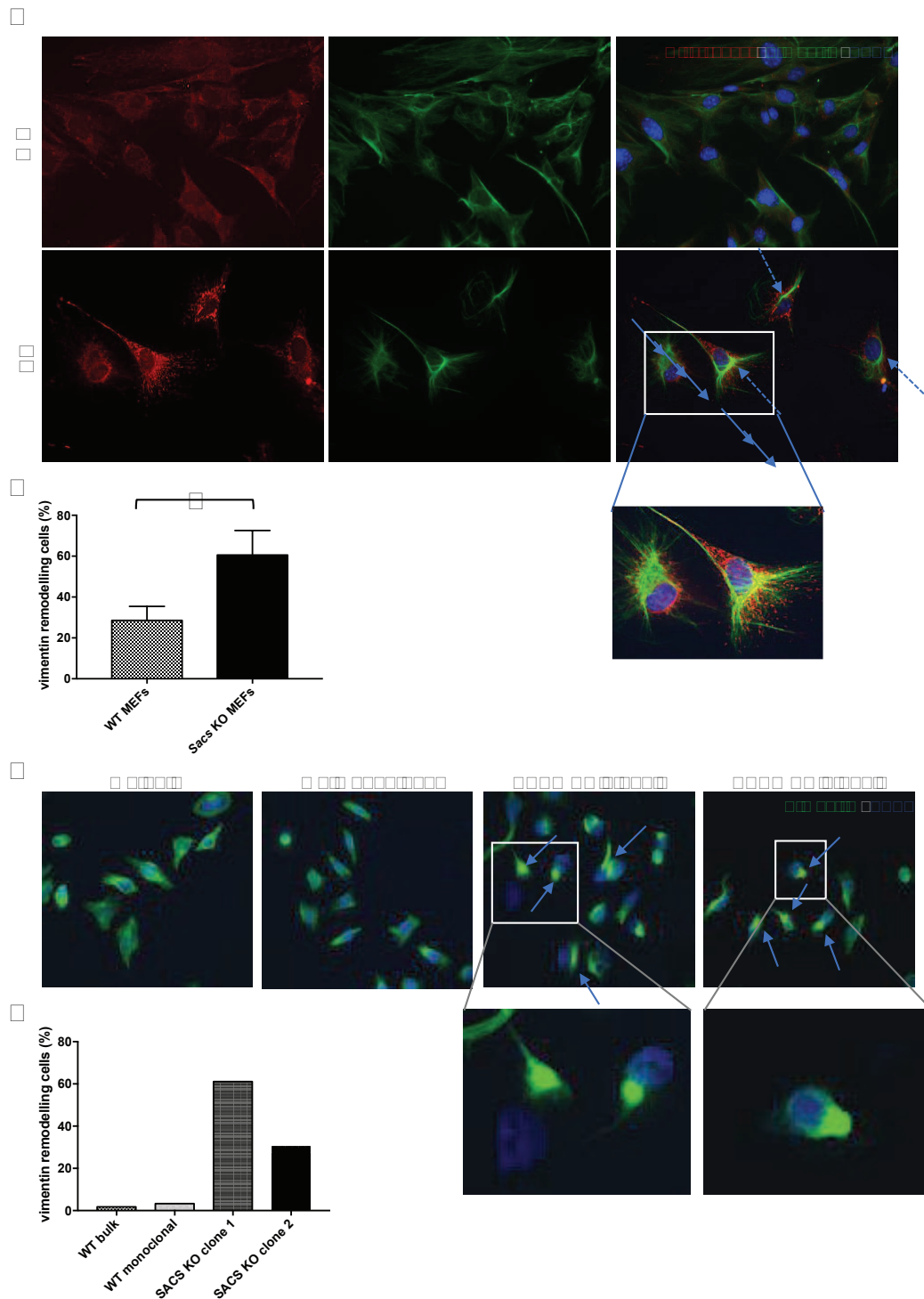ments in collaboration with the microscopy facility of San Raffaele Scientific Institute. By analyzing the EM images, we were able to detect about 10 nm filamentous structure accumulations in ARSACS cells (exactly compatible with the size of intermediate filaments (Lodish et al., 2000), by using EM higher magnification at 150 000X), forming the same perinuclear area of vimentin we found in IF experiments (Fig. Results 19 C). We performed these experiments on very early passages of ARSACS patient and control fibroblasts to exclude cell senescence and suffering signs.

□□ NFs accumulate in □□□□ □O mouse□

To investigate if the intermediate filament remodelling we observed in ARSACS fibroblasts and sacsin-depleted cells was a phenotype confirmable in central nervous tissues, we studied the cytoskeletal components also in *Sacs* KO mouse cerebellum. Differently from microfilaments and microtubules, intermediate filament classes are widely divergent in sequence and their expression is characteristic of a certain tissue or cell type. The intermediate filament cytoskeleton of CNS is made of type IV of intermediate filaments, which are NFs ((Lodish et al., 2000) and Results Table 4). By WB analyses, we interestingly found a strong accumulation of NFs in *Sacs* KO cerebellum compared to WT mice. In particular, we detected increased levels of non-phosphorylated subunits of heavy NFs (npNFH) and light NFs (NFL).

This phenotype is strongly evident starting from three months of age of *Sacs* KO mice and clearly reconfirmed at six months of age (Fig. Results 16 A-B).

IF Protein	MW (10^{-3})*	Tissue Distribution
TYPE I[†]		
Acidic keratins	40–57	Epithelia
TYPE II[†]		
Basic keratins	53–67	Epithelia
TYPE III		
Vimentin	57	Mesenchyme
Desmin	53	Muscle
Glial fibrillary acidic protein	50	Glial cells and astrocytes
Peripherin	57	Peripheral and central neurons
TYPE IV[‡]		
NF-L	62	Mature neurons
NF-M	102	Mature neurons
NF-H	110	Mature neurons
Internexin	66	Developing central nervous system
NONSTANDARD TYPE IV		
Filensin	83	Lens fiber cells
Phakinin	45	
TYPE V		
Lamin A	70	Nucleus of all cells
Lamin B	67	Nucleus of all cells
Lamin C	67	Nucleus of all cells

* *IFs show species-dependent variations in molecular weight (MW).*

† *More than 15 isoforms of both acidic and basic keratins are known.*

‡ *NF=neurofilament; L, M, and H=low, medium, and high molecular weight.*

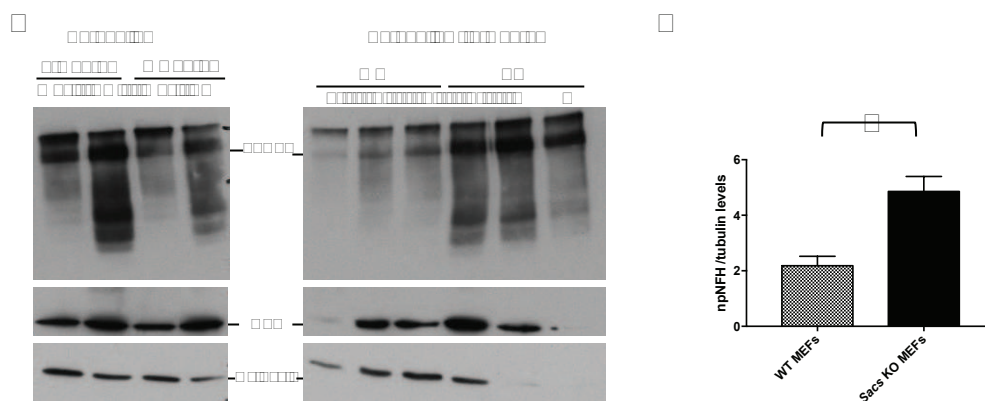Results Table 4. Intermediate filament types in mammals (Lodish et al., 2000).

Fig. Results 16. NF accumulation in *Sacs* KO cerebellum. (A) WB analysis of NFs (npNFH and NFL) in mouse cerebellum from *Sacs* WT and KO, normalized on calnexin (compatible with sample loading). (B) Quantification shows increased levels of npNFH in *Sacs* KO cerebellum (mean SEM, two-tailed t test p 0,05).

5.6 Testing the aggresomal pathway hypothesis: proteasomal machinery is not overwhelmed in ARSACS fibroblasts and Sacs KO mouse CNS tissues.

From literature, it is known that the intermediate filament remodelling occurs in cells in different situations, as in microtubule alterations (Hookway et al., 2015), phosphorylation of intermediate filaments due to mitosis-related events (Sihag et al., 2007) and when there is aggresome formation, due to an accumulation of misfolding proteins and/or the proteasome is impaired/overwhelmed (Johnston et al., 1998). In order to understand which was the cause of vimentin remodelling, we analyzed the microtubule network, but did not find any difference between ARSACS patients and controls (Fig. Results 17 A). The second hypothesis regarding vimentin phosphorylation was the less plausible, since this is an event mostly mitosis-related. Indeed, phosphorylation-mediated regulation of vimentin dynamics is integral for both mitosis and cell architecture/motility in interphase (Sihag et al., 2007) and we did not notice any modification in the ability of ARSACS cells to divide and proliferate. Moreover, for NFs, the phosphorylation has a completely different role because they are the intermediate filaments constitutive of post mitotic cells. Phosphorylation of NFs has been suspected to play roles in forming cross-bridges between NFs and microtubules, slowing axonal transport and promoting their integration into cytoskeleton lattice and in doing so, to control axonal caliber and stabilize the axon (Sihag et al., 2007). Furthermore, we found increased levels on non-phosphorylated subunits of NFH, excluding a remodelling of NFs related to the phosphorylation of intermediate filaments.

Due to putative function of sacsin as molecular chaperone, the most thrilling hypothesis, which causes vimentin cage formation, is the activation of the aggresome pathway. In this situation, cells form a cage-like structure of intermediate filaments. This cage surrounds misfolded proteins and compartmentalizes aggregated proteins in an inert structure since they exceed the proteasomal capacity (Johnston et al., 1998).

Indeed, accumulation of ubiquitinated proteins is an hallmark of several diseases characterized by aggresome formation (Glickman and Ciechanover, 2002). Based on the hypothesis of aggresomal pathway activation in ARSACS, we first checked if there was accumulation of ubiquitinated conjugates in ARSACS patient cells by WB (Fig. Results 17 B) without finding any evidence on that.

The presence of both UbL and J domain in sacsin suggests that it may integrate the ubiquitin–proteasome system. In particular, sacsin sub region containing the UbL domain (residues 1-124) was shown to interact with 20S proteasomal alpha subunit C8 by co-immunoprecipation (see Introduction and (Parfitt et al., 2009)).

Based on this data, we performed an *ex □i□o* assay on *Sacs* KO and WT mouse CNS (cortex and cerebellum) to assess the activity of the 20S core component of the proteasome. The assay is based on detection of the fluorophore 7-Amino-4- methylcoumarin (AMC) after cleavage from the labelled substrate LLVY-AMC. The free AMC fluorescence is quantified by a fluorimeter and the Relative Fluorescence Units (RFU) are directly proportional to the intracellular proteasome activity of the samples.

We assayed cerebellum and cortex extracts from *Sacs* KO mouse (Fig. Results 17 C), without finding any evident impairment of proteasome activity compared to WT mice (data normalized on WB loading, not shown).
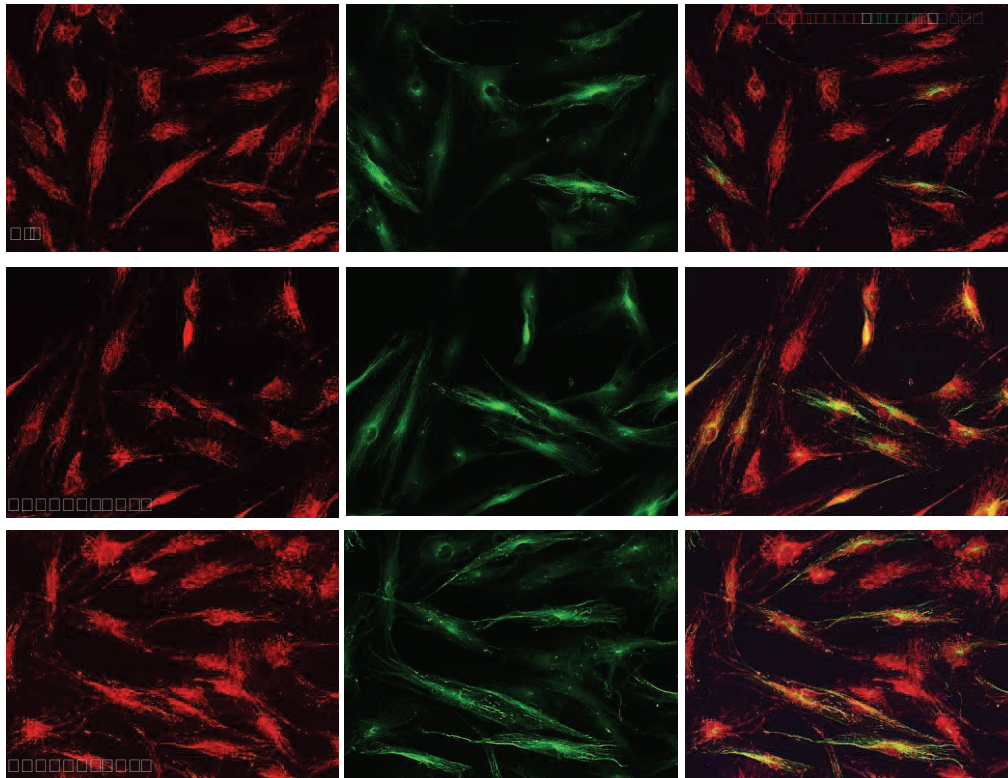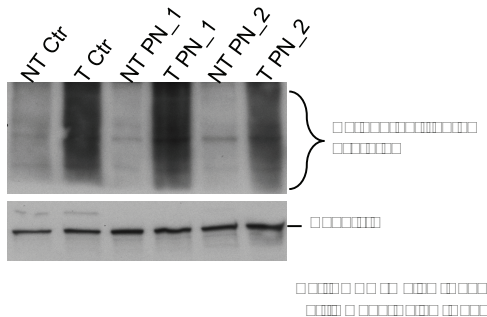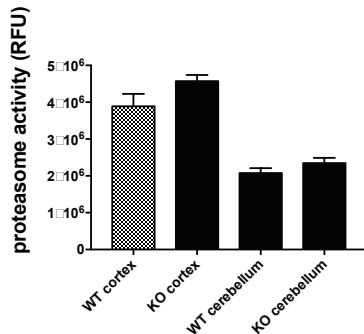
Fig. Results 17. Microtubule organization is conserved in ARSACS and the proteasome works correctly. (A) Representative images of microtubule staining (tubulin) showing no alteration of these cytoskeletal components. (B) WB of ubiquitinated proteins in patients and controls at steady state and upon MG132 treatment, normalized on spectrin levels.
(C) Proteasome activity assay quantification, showing no difference in the 20S proteasome activity of cerebellum and cortex in WT versus KO mice (mean☐SEM).

□□ Testing the aggresomal path□ay hypothesis□ aggregate□ structures are not evi□ent in ARSACS fi□ro□lasts an□ in □□□□ □O mouse□

To detect the presence of putative aggregates that in turn could give origin to the aggresome pathway, we used a method that allows the detection of aggresome-like structures in ARSACS fibroblasts. This technique employs a 488 nm excitable red fluorescent molecular rotor dye to specifically detect denatured protein cargo within aggresomes and aggresome-like inclusion bodies in fixed cells. In this procedure, the detection reagent allows the aggregate detection, since it becomes brightly fluorescent upon binding to aggregated proteins within vesicles produced during aggresome formation. By using the proteasome inhibitor MG132 as a positive aggresome-inducer on control fibroblasts, we performed aggresome detection experiments, comparing MG132-treated and untreated controls with ARSACS patient fibroblasts. We found some structures compatible with aggregated proteins, but we were unable to detect aggregates inside the area close to the nucleus, as we expected in the vimentin-cage (Fig. Results 18).

We also analyzed *Sacs* KO mouse cerebellum by EM experiments, without finding signatures typical of aggregates (Fig. Results 19 A).
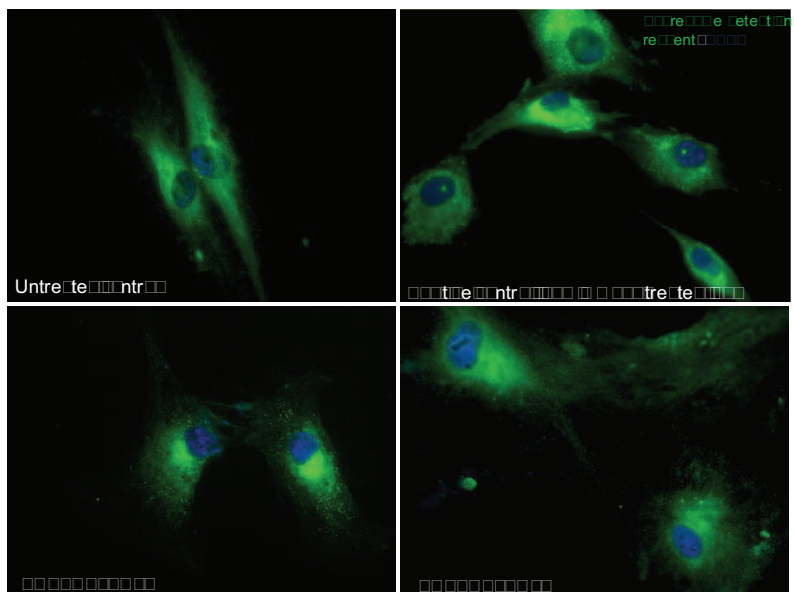
Fig. Results 18. Aggresomes are not clearly identified in ARSACS patient fibroblasts. IF showing punctate dots marking the aggregated proteins (the emission of the molecule was better revealed by using the green emission filter).
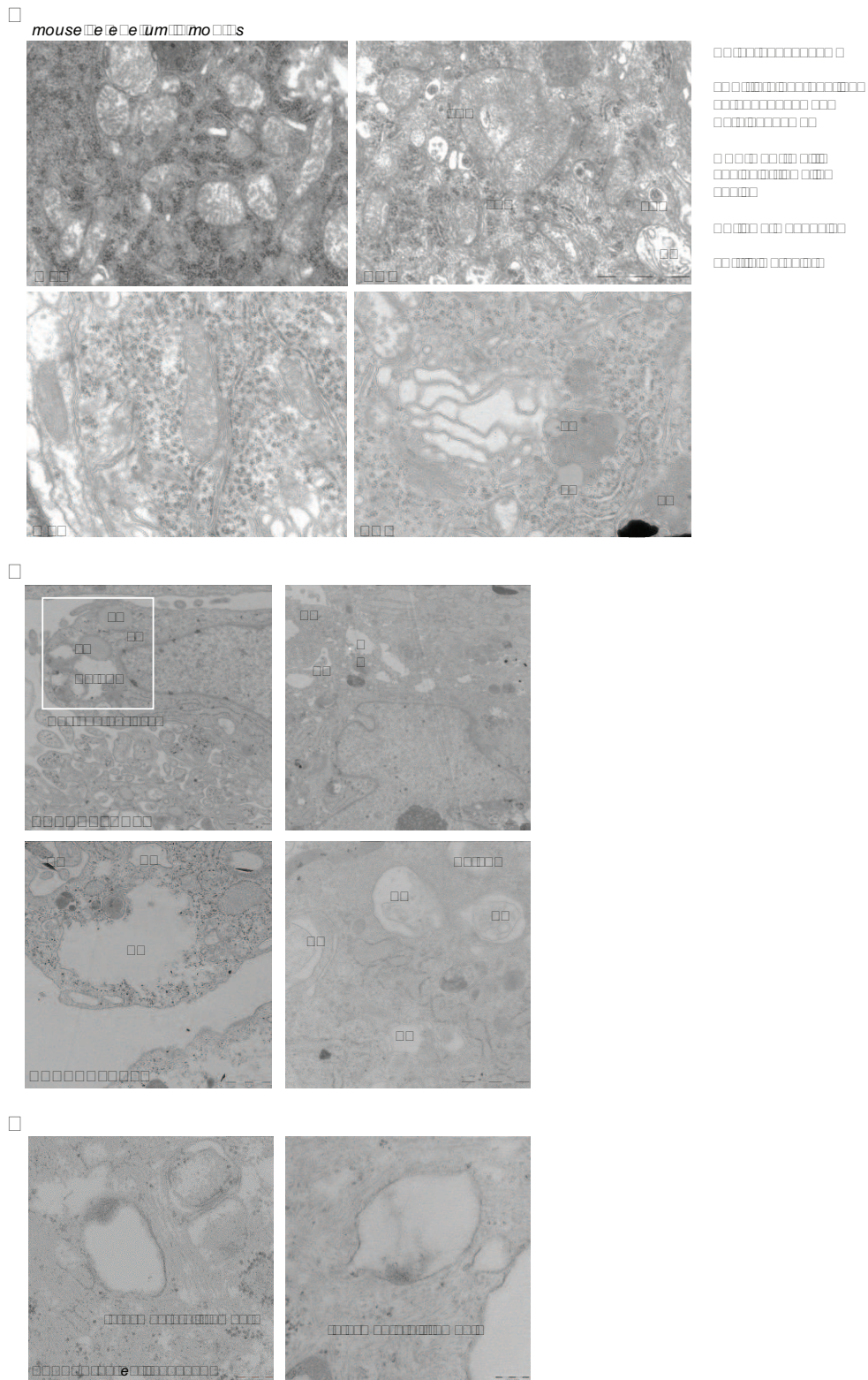
Fig. Results 19. Electron microscopy (EM) experiments show accumulation of autophagy related-structures in *Sacs* KO mouse cerebellum and ARSACS fibroblasts. (A) EM experiments on mouse cerebellum from WT and KO at 6 months of age, showing no signs of aggregated material, but increased number of autophagic structures. (B) EM experiments on ARSACS patient fibroblasts showing perinuclear areas with structures related to late stages of autophagy.

(C) EM enlargements showing intermediate filament bundling at higher magnification (15000X) plus autophagic structures in patient fibroblasts, surrounded by intermediate filaments.

ARSACS patient fibroblasts show increased autophagic flux

Although we did not detect clear-cut protein aggregates in EM experiments on ARSACS fibroblasts and *Sacs* KO mouse cerebellum, as those reported in literature (Johnston et al., 1998; Kopito, 2000), EM experiments revealed a strongly evident accumulation of late stages of autophagic structures. In particular, we found autophagic structures like double membraned-autophagosomes full of organelles, single membraned-autolysosomes with partially digested organelles and late degradative autophagic vacuoles. Together with these structures, we noticed an increased number of multi-lamellar- and vesicular- bodies, and lipid droplets, probably related to autophagy as advanced stage structures and source of membranes respectively (Cermelli et al., 2006; Shatz et al., 2016). On the contrary, control cells appeared with a conserved ultrastructure (Fig. Results 19 B). Moreover, patient cells present evident signs of cell suffering, i.e. structures sometimes membraned and sometimes not, sometimes with electron dense material or sometimes very large and totally empty (Fig. Results 19 B).

The detection of vimentin filament bundling allowed the identification of some late degradative autophagic vacuoles surrounded by intermediate filaments (Fig. Results 19 C). These vacuoles are recognizable as late stages of autophagic pathway and are often filled with electron dense material, which can somehow retrieve how protein aggregates look like in EM of experimentally induced aggregates from literature (Kopito, 2000).

To understand if the accumulation of autophagic structures in ARSACS patients was the result of impaired or, conversely, of enhanced autophagic flux, we performed biochemical analysis of autophagic flux by following LC3-I and LC3-II levels (Fig. Results 20 A). At steady state level, LC3-II amount is strikingly reduced in patients versus controls (Fig. Results 20 B). Considering the higher presence of autolysosomes detected by EM in

patients, this likely indicates a higher autophagic flux with a more rapid turnover of LC3-II, rather than an impairment of autophagosomes formation. To verify this hypothesis, we treated fibroblasts in culture with autophagic enhancers and inhibitors, i.e. C☐ to block lysosomal acidification and so degradation at the late stages of autophagy and HBSS to promote starvation-induced autophagy. We found that in patient cells upon C☐ treatment there was a statistical significant increase of LC3-II compared to controls, consistent with an increased number of pre-existing autophagic vacuoles in ARSACS cells (Fig. Results 20 C-D). Starving cells, in ARSCAS cells the situation is revertes to the WT one: patient cells are able to efficiently degrade autophagosomes, as appreciable by reduced levels of LC3-II (Fig. Results 20 C-D).

Excluding the activation of the canonical aggresomal pathway as the cause of intermediate filament remodelling and accumulation, our working hypothesis is that sacsin absence could impact on the post-translational turnover of intermediate filaments.
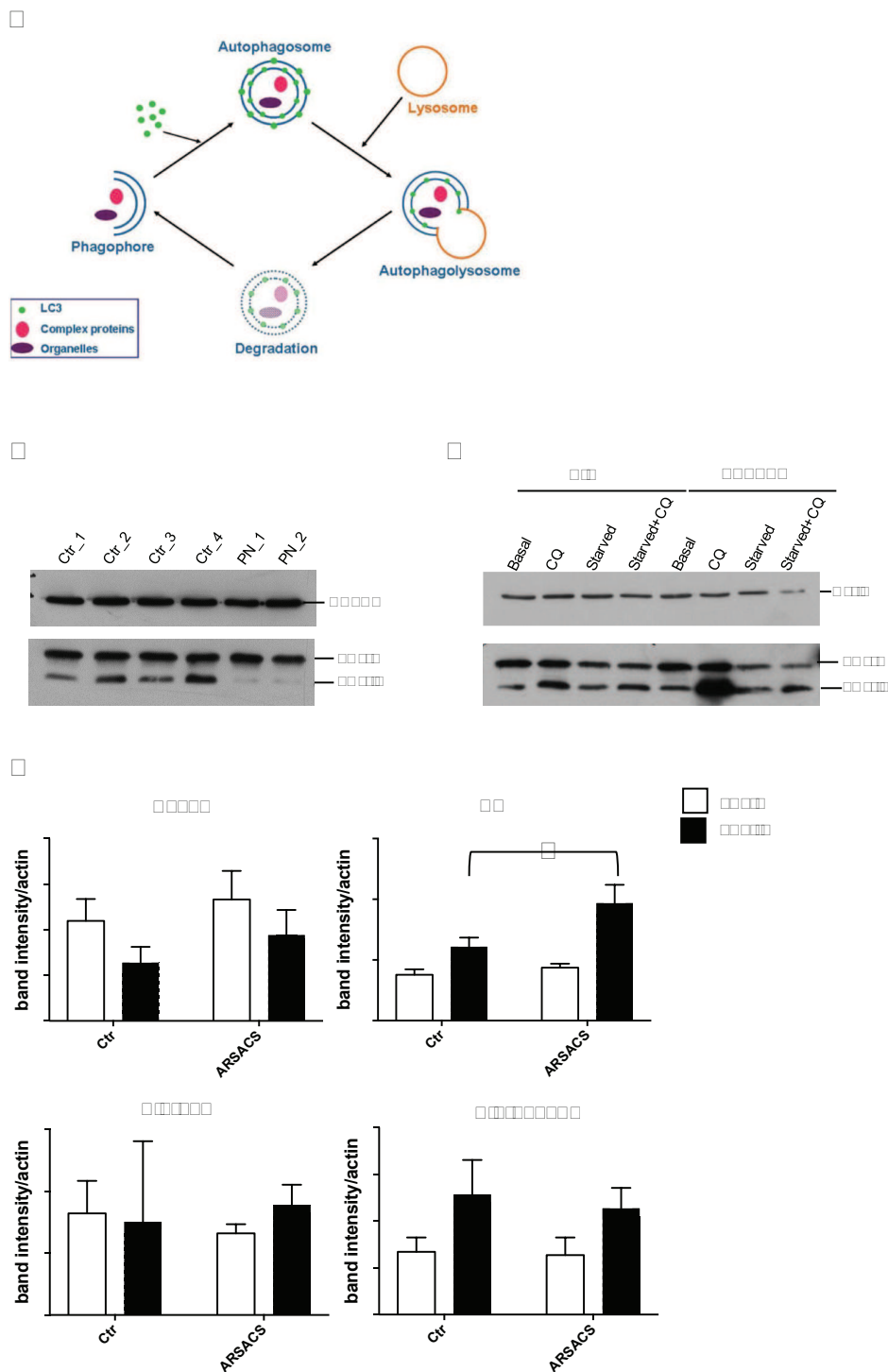
Fig. Results 20. Autophagic flux is increased in ARSACS patient fibroblasts. (A) Overview of selective autophagy in mammalian cells. (B) LC3 steady state WB experiment showing the faster turnover of LC3-II in patients compared to controls. (C) Autophagic flux representative experiment. Cell lysates were collected from untreated cells, C☐ treated, HBSS treated cells, and cells HBSS+C☐ treated cells (treatment conditions: 10 ☐M C☐ + HBSS for 24 hours). Actin was used as a loading control. (D) Densitometric analyses were performed and mean LC3-I and LC3-II levels relative to actin were calculated for each treatment in control and ARSACS fibroblasts (n☐5, mean☐SEM, two-tailed t test, ☐p☐0,05).

Discussion

With this work, we tried to fill some gaps that have been remained unexplored on sacsin protein knowledge, the protein mutated in ARSACS disease, shedding light on new aspects of the molecular mechanisms underlying ARSACS pathogenesis. We tried (i) to decipher the still missing genotype-phenotype correlation in ARSACS, addressing how different ARSACS-causing mutations lead to the disease and impact on the level of sacsin protein; (ii) to shed light on sacsin subcellular localization both by employing biochemical methods of cellular co-fractionation and generating new tools to tag endogenous sacsin in cells; (iii) to understand sacsin molecular function by studying the outcomes of sacsin loss of function in different tools depleted for sacsin.

The detailed discussion of each part of the thesis follows, subdivided in the same three chapters as the results.

Analyzing the genotype-phenotype correlation of sacsin mutations in ARSACS disease.

In the first chapter of my work, I have been interested in studying how different kinds of *SACS* mutations lead to ARSACS. Indeed, a still unresolved, open field in ARSACS is the genotype-phenotype correlation. Up to now more than 200 pathogenetic ARSACS causing-mutations have been identified worldwide and they range from missense, nonsense, frameshift, to small or gross deletions. ARSACS causing-mutations are all recessively inherited. They can affect *SACS* gene in homozygous or compound heterozygous state and they cover the entire length of the gene as expected for a loss of function disease. However, ARSACS clinical disease severity and symptoms seem not to be linked either to the nature or to the position of the mutation on *SACS* gene (Baets et al., 2010; Synofzik et al., 2013). Besides the intrinsic human variability in front of the neurodegenerative diseases, however, any kind of analysis of residual mutant sacsin in ARSACS patients has never been performed.

We focused on how specific *SACS* mutations affect the amount of sacsin protein. In this context, we used fibroblasts from two ARSACS patients (PN_1 and PN_2) carrying two identical missense mutations on one allele (p.R3636□; p.P3652T) and a different frameshift mutation on the other allele (PN_1: p.L3745fs; PN_2: p.C72fs). We surprisingly found that sacsin is drastically reduced independently from the nature of the mutation. Indeed, from the nature of *SACS* mutations above cited, we expected half amount of full-length sacsin protein in both patients, at least as contribute of the missense mutation-carrying allele. Same results derive from other compound heterozygous ARSACS patients, as they totally lack the protein although presenting missense mutations on one allele. For example, patient p.F2780C; p.S3892fs and patient p.R4331□; p.K1715fs, analyzed in supplemental material of our collaborative paper (Duncan et al., 2017).

Indeed, we reasoned that in an autosomal recessive disorder, such as ARSACS, mutations resulting in premature stop codons (insertions or deletions, generating frameshifts or pure nonsense) may abolish sacsin function by preventing the production of the protein at mRNA level by the NMD mechanism. On the other hand, the abolishment of protein function can derive from degradation of truncated/aberrant protein after translation.

To investigate these two quality control mechanisms as causative of sacsin absence in patient cells, we analyzed if *SACS* mRNA was stable, by qRT-PCR. Our results indicate that mutant *SACS* mRNA is not degraded in its entirety (and it is not halved). However, our results do not distinguish between the two patient alleles, since reasonably they do not behave in the same way. This is because one allele for each patient presents a frameshift (expected to cause NMD) and the other allele presents missense mutations, never reported to trigger NMD.

On the other hand, as anticipated, subtle changes, such as missense mutations, are not expected to hamper efficient translation, thus they can cause sacsin function abolishment by faster post-translational degradation or can give origin to mutated aggregation-prone protein products. To investigate the first possibility, we studied mutant sacsin protein stability in

terms of post-translational degradation, without finding mutant sacsin rescue upon inhibition of proteasome, autophagy or specific proteases. We corroborated these data also by performing long-lasting combined treatments of proteasome and autophagy inhibition and obtaining the same results. The hypothesis we then explored was the possible mutant sacsin aggregation. Since we failed in detecting any kind of mutant sacsin aggregate, we drew the conclusion that our data exclude a potential post-translational problem as the cause of mutant sacsin absence (degradation or aggregation). In conclusion, rejecting a transcriptional regulation of mutant *SACS* mRNA or a post-translational degradation/aggregation of mutant sacsin in patient cells, our current hypothesis converges on possible regulation of the mutant protein at the co-translational level.

Increasing evidence suggests that beyond mRNA quality control pathways, a compelling role of the ribosome as hub for nascent polypeptide quality control exists in cells. In some cases, and only for some proteins, protein synthesis can be tightly coupled with ubiquitination and degradation of nascent polypeptides (Wang et al., 2015). Indeed, it is intuitive that the cell benefits from detecting and removing errors at the earliest opportunity. Thus, in addition to the canonical post-translational protein □C pathways (e.g. proteasomal degradation and autophagy), co-translational □C pathway is commissioned to degrade aberrant proteins in the meantime they are being translated. In this way, nascent polypeptidic chains can be tagged for destruction before they leave the ribosome, thus avoiding complete translation, and more importantly, their possible post-translational aggregation (Pechmann et al., 2013; Inada, 2017). This mechanism must be especially considered in case of big and multi-domain proteins, such as sacsin protein, whose translation and folding is extremely time and energy consuming for the cell. In support of this last concept, a recently described model proposes that polypeptides undergo □domain-wise□ co-translational quality surveillance, where a protein domain corresponds to individual folding unit. In other words, a domain before the full-length protein, constitutes the minimal quality control unit,

being checked primarily at co-translational level (Wang et al., 2015). The emerging scenario provides two different co-translational quality controls: one acts on stalled ribosomes and is, at least in part, associated to mRNA degradation; the other targets actively translating polypeptides that are not able to achieve their native conformation (Comyn et al., 2014). For the first □C, the molecular players have been clearly identified in yeast and mammal and contemplates: (i) a specific E3 ubiquitin ligase (Listerin) that operates ubiquitination of nascent polypeptides; (ii) a nuclear export mediator factor (NEMF), which binds Listerin and stabilizes its association to ribosomes (Pechmann et al., 2013; Inada, 2017); (iii) a valosin-containing-protein (VCP) complex, extracting nascent chains and targeting them to proteasome for rapid degradation (Lykke-Andersen and Bennett, 2014). For the second co-translational □C, sensing the folding state of nascent polypeptides, the steps are the same; some potential E3 ligases and proteasomal targeting proteins intervene, but they have yet not been clarified.

Our working model of co-translational □C on mutant sacsin is also supported by recent data that we obtained by expanding the panel of ARSACS patients in which we analyzed residual sacsin levels. These ARSACS patients carry diverse ARSACS-causing mutations. Sacsin is again mostly absent, independently from the nature of the mutations. Indeed, we expected half amount of sacsin in patient p.L2374S; deleted_allele [Terracciano et al., 2009]; as contribute of the missense mutated allele; and full-length protein in patient p.G188E + p.S2465L ; p.L3916W, carrying only missense mutations, but we did not detect not even half sacsin quantity. Accordingly, this is not a problem in transcription, as *SACS* mRNA is stable in patient p.L2374S; deleted_allele [Terracciano et al., 2009] and, more interestingly, it even increases in patient p.G188E + p.S2465L; p.L3916W. This can be perfectly in line with the co-translational □C pathway we propose for mutant sacsin, which acts by actively translating polypeptides that are not associated to their mRNA instability.

These results indicate that ARSACS-causing mutations lead to the absence of sacsin protein probably because of a mechanism that involves this specific type of co-translational □C pathway. And, more intriguingly, no loss of function mechanism acting through this pathway has ever been described in any physiopathological conditions, as in a human disease. Furthermore, being the loss of sacsin function the cause of ARSACS, partially restoring sacsin protein, for example trying to overcome translational obstacles and producing it, although mutated, could recover some sacsin functions. Moreover, preliminary unpublished data from our collaborator B. Brais show that a new *Sacs* KI mouse model, carrying a homozygous pathogenetic mutation in the UbL domain of sacsin, has a phenotype which is intermediate between the WT and the *Sacs* KO mouse at the neurological level. This correlates with a halved residual amount of sacsin protein, and maybe, being positioned at the beginning of the protein, it might not affect a sacsin folding unit. This mouse model phenotype suggests that having even a small amount of the protein, although mutated, could be beneficial for ARSACS. Indeed, multidomain feature of sacsin protein suggests that conserving one or more functional domains can be better than completely lacking the protein, ameliorating the clinical phenotype.

□**erspectives**

To address the issue of mutant sacsin stability in details, perspectives of our ongoing work are directed to study mutant *SACS* mRNA in a wide panel of ARSACS patients, by performing allele-specific PCR to discriminate possible NMD of only frameshift-carrying alleles of *SACS* mRNA.

We want to investigate also mutant sacsin degradation in the enlarged panel of ARSACS patients we collected.

To unravel the hypothesis of co-translational □C of mutant sacsin, we want to verify the existence of polyubiquitinated-sacsin nascent chains in ARSACS fibroblasts. We will also study the potential residual amount of sacsin protein originated from truncating mutations upstream the exon 10

by generating a new N-terminal sacsin Ab, in the panel of ARSACS cells we have further expanded with truncating mutations.

On the other hand, for *SACS* missense mutation-carrying cells, we are studying the activation of co-translational ☐C, by performing polysome fractionation experiments to discern if mutant *SACS* mRNA is accumulating at the ribosomal level.

☐☐Investigating the outcomes of sacsin a☐sence i☐☐mitochon☐rial net☐or☐hyperfusion☐

In the second chapter, we became interested in shedding light on one major unsolved issues in the field of sacsin knowledge, which is sacsin subcellular localization. As stated previously, sacsin's big dimension has hampered experimental studies over time. Contrarily to what reported in literature, imaging of the endogenous protein failed due to lack of antibodies able to recognize sacsin in IF. Indeed, data reported by other authors, who were able to detect sacsin diffused in the cytosol with punctate spots in the nucleus and on mitochondria in IF with different antibodies (Parfitt et al., 2009; Girard et al., 2012), were not reproducible in our lab and in the next literature. Regardless, by performing bioinformatic analyses, we found cytosolic localization of sacsin and excluded mitochondrial internalization, due to the absence of mitochondrial targeting sequences. Given sacsin's huge size, it is also likely that it stays in the cytosol, rather than being translocated in other organelles.

We revealed that the prediction of sacsin nuclear co-localization was not strictly faithful to the real sacsin localization. Actually, by having excellently WB working-antibodies, our wet data unequivocally demonstrated that sacsin is totally absent from the nuclear fraction. Moreover, the nuclear component is not reported consistently by different prediction algorithms and softwares.

In this context, the design of a new molecular strategy to tag endogenous sacsin by CRISPR/Cas9-mediated HDR, able to generate a sacsin protein

fused with a tag, has the aim to shed light on the ultrastructural level of the sacsin localization and has the potentiality to make feasible sacsin cellular imaging. By this approach, we overcome problems due to exogenous overexpression, as the tag would be inserted in the same sacsin open reading frame, therefore, under the same endogenous transcriptional control.

We set up the system in HeLa cells using as tag the HA peptide. By employing a donor template encoding the Linker-HA-STOP construct flanked by sacsin homology arms, we obtained extremely high homology recombination efficiency with integration of the tag at genomic locus in at most 5□. Extensive screening of monoclonal cell lines derived from the nucleofected population ended up with the identification of two clones that integrated HA peptide. Characterization of these clones is now ongoing, together with the generation of *SACS*-HA KI SHSY5Y (neuronal-like cells). We have already set up a strategy that can also be used to tag endogenous sacsin with a fluorescent protein, like GFP, thus allowing live cellular imaging. Furthermore, GFP insertion or Halo tag insertion can make possible Correlative and Light Electron Microscopy (CLEM) coupled approach, to in depth analyze sacsin co-localization with mitochondria, as it can be only close to the OMM or can interact with OMM through mitochondrial receptors. Determining if sacsin is physically associated to the OMM or in close proximity to is an important starting point to understand the role played by sacsin in the regulation of mitochondrial fitness.

The HA tag also provides a suitable system to perform immunoprecipitation analysis, to isolate and identify sacsin interactors or substrates, thus enlarging the spectrum of application for studying sacsin physiological role inside the cell beyond its spatial localization.

Given that sacsin probably associates to mitochondria, in the second part of Chapter 2, we investigated the role of sacsin absence on mitochondrial function. Since we found increased number of cells presenting fused mitochondria in ARSACS patient fibroblasts, in *SACS* KO Hela cells and in

Sacs KO MEFS, we deduced these data are strictly dependent on sacsin loss of function. Accordingly, Girard et al. noticed ARSACS patient cells showing mitochondria bulbed structures in IF. Mechanistically, hyperfusion of mitochondrial network could be caused by enhanced fusion or decreased fission (Tilokani et al., 2018). Therefore, to discriminate between the two mechanisms, we investigated the levels of proteins involved in mitochondrial dynamics in ARSACS cells and we found a reduced DRP1 recruitment onto mitochondria, accompanied by a slightly reduced DRP1 oligomerization in ARSACS fibroblasts compared to controls. DRP1 is the key mediator of mitochondrial fission, cycling between the cytosol and OMM, where it oligomerizes and mediates mitochondrial fission (Tilokani et al., 2018). Our data clearly demonstrates that in ARSACS cells there is a defective fission process, as sacsin regulates mitochondrial fission rather than fusion. In agreement with our findings, IF data from another lab showed reduced localization of DRP1 foci to mitochondria in sacsin knockdown cells and ARSACS fibroblasts carrying different mutations (Bradshaw et al., 2015). However, previous data did not provide any hint either on the mechanism or on the functional consequences on mitochondria in sacsin-depleted cells.

To dissect mechanistically how sacsin regulates mitochondrial dynamics, we found that sacsin is not directly interacting with DRP1 as we did not find DRP1 immunoprecipitating with sacsin, highlighting that sacsin acts on DRP1 recruitment onto mitochondria in an indirect manner, probably through a mediator. This data disagrees with previously published finding showing an interaction between a sub cloned portion of sacsin (the N-terminal 1368 amino acids, encompassing the UbL domain and first SRR) and DRP1 (Girard et al., 2012).

The relevance of mitochondrial involvement in ARSACS pathogenesis is highlighted by the deregulation of mitochondrial distribution in *Sacs* KO primary Purkinje neurons that we found. As shown, mitochondria in *Sacs* KO Purkinje cells do not reach distal dendrites, presumably due to the mitochondrial dynamics alteration, i.e. the unbalance towards fusion. The

reduction of mitochondria specifically in dendrites of *Sacs* KO Purkinje cells suggests a problem in mitochondrial transport in distal neural processes, where the need for mitochondria is presumably the highest. Mitochondrial transport in neurons has crucial role as mitochondria should become stationary or pause both in regions that have a high metabolic demand and regions that need to buffer increased calcium concentrations deriving from excitatory glutamatergic stimuli. Maintaining intact mitochondrial dynamics is critical, as mitochondria should move again rapidly in response to physiological changes. Indeed, defects in mitochondrial transport are implicated in the pathogenesis of several major neurological disorders (Sheng and Cai, 2012). Since Purkinje cells receive mainly glutamatergic stimuli on their super arborized dendritic trees, they are subjected to the highest calcium concentrations compared to other neuronal populations. Thus, proper mitochondrial distribution throughout all Purkinje cell dendrites becomes very crucial. In ARSACS pathogenesis, the defective mitochondrial transport could be causal of the main dysfunction of the disease that is the Purkinje cell loss.

In the lab, we are also investigating the applicability of potential translational approaches to improve mitochondrial dynamics per se in Purkinje cells and alternatively, to restore the consequent calcium dysregulation we found in Purkinje cells, which can be causal of the premature loss of these neurons in ARSACS.

Since we excluded that sacsin directly interacts with DRP1, to uncover the molecular mechanism by which sacsin absence lead to a decreased DRP1 recruitment, we performed endogenous sacsin immunoprecipitation and LC-MS/MS. We interestingly found a putative sacsin interactor, which is the ARPC2 subunit of the ARP2/3 complex. ARP2/3 complex is an actin nucleator complex, involved in creating branched actin networks, by giving origin to newly directional actin filaments. F-actin chain modifying-proteins have been recently shown to play a role in mitochondrial division (Li et al., 2015a). Growing evidence on mitochondrial division demonstrated this process is regulated at many levels and is triggered by a complex cascade

of events. These events include 1) contacts between ER and mitochondria defining 'mitochondria pre-constriction sites'; 2) subsequent actin polymerization; and 3) final DRP1 recruitment to the OMM, mediated by F-actin nucleation and polymerization at mitochondria-ER contact sites, leading in the end to mitochondrial division (Prudent and McBride, 2016; Tilokani et al., 2018). Both linear F-actin and branched F-actin modifying proteins are involved in DRP1 dependent mitochondrial fission (Hatch et al., 2014). As other branched F-actin modifying-proteins (for example cortactin, cofilin), downregulation of ARP2/3 complex has been shown to lead to a dramatic elongation of mitochondria (Li et al., 2015a), making suggestive the hypothesis of impaired F-actin mitochondrial association in sacsin absence. Therefore, this in turn could trigger impaired F-actin-mediated DRP1 recruitment, ultimately explaining the mechanism underlying the defective mitochondrial fission in ARSACS.

Perspectives

For this second part of the work, we want to in depth dissect the molecular link between sacsin absence and mitochondrial alteration. Indeed, besides our preliminary data showing a putative interaction between sacsin and actin cytoskeleton (ARPC2), the cascade of events leading to decreased mitochondrial recruitment of DRP1 remains still unidentified. We want to analyze sacsin interaction with mitochondria at the ultrastructural level, by using CRISPR/Cas9 endogenous sacsin-HA tagged HeLa cells we generated. This approach will clarify sacsin localization at the ultrastructural level, e.g. if it physically interacts with or it is juxtaposed to mitochondrial outer membrane.

We are interested in identifying the failing step in mitochondrial fission cascade in sacsin-depleted cells by studying i) ER-mitochondria interaction that is involved in labelling the 'pre-constriction sites' of mitochondrial fission, (ii) F-actin polymerization and its involvement in DRP1 recruitment. Starting from our preliminary results showing the ARPC2-sacsin putative interaction, we want to analyze the spatial relationship between F-actin and mitochondria in cells depleted for sacsin.

Investigating the outcomes of sacsin absence iii cytoskeletal redistribution.

In the last chapter, we wanted to uncover the gap regarding sacsin role on cytoskeletal organization. Our data show significant alteration and remodelling of cytoskeletal network in sacsin depleted cells, i.e. accumulation of intermediate filament subunits and increased autophagy, highlighting a specific role of intermediate filament cytoskeleton in defining ARSACS pathogenesis.

We found that in ARSACS fibroblasts, perinuclear areas left devoid of mitochondria were filled with vimentin, the major component of intermediate filaments in mesenchymal cells. In ARSACS cells, but also in *Sacs* KO MEFs and *SACS* KO Hela cells, vimentin shows an abnormal perinuclear accumulation with cage-like appearance. Accumulation of filamentous structures, that were intermediate filament size-compatible, was also identified in high magnifications of EM experiments. This phenotype seems to be highly relevant for the mechanism of the disease, excluding it could be only related to the type of the cells we were looking at. Indeed, we also found different NF subunits (npNFH and NFL) accumulating in *Sacs* KO mouse cerebellar extracts (the NFs are the intermediate filaments mainly constituting CNS). In support to our findings, in literature it has been also shown that loss of sacsin results in the accumulation of nonphosphorylated NFs in vulnerable neuronal populations of *Sacs* KO mouse and in ARSACS patient brain (Larivière et al., 2015).

To explain the intermediate filament phenotype we observed, we referred to the literature and what we found is that a remodelling of vimentin similar to that we found can be a consequence of microtubule depolymerization (Hookway et al., 2015), vimentin phosphorylation –mostly during mitotic events – (Sihag et al., 2007) or aggresome formation (Johnston et al., 1998; Kopito, 2000; Kopito and Sitia, 2000). We excluded the first hypotheses, since we did not observe evident signs of alterations of

microtubule network organization or problems in mitosis-related events in ARSACS cells. Given that sacsin is predicted to work as a molecular chaperone, we hypothesized that the most plausible reason of the vimentin cage origin is the aggresome pathway activation.

Aggresomes are juxta-nuclear accumulations of misfolded proteins or aggregates that form when chaperone refolding system and the ubiquitin-proteasome degradation pathway are overwhelmed. Aggresomal response is present in several pathological conditions as described for many neurodegenerative disorders with accumulation of toxic aggregates (Johnston et al., 1998; Kopito, 2000; Kopito and Sitia, 2000). The aggresome hypothesis was intriguing also based on putative chaperone-like function of sacsin because sacsin has diverse motifs recalling chaperone functions as Hsp90 and Hsp40 homologous regions and a J domain. From these domains, it could be inferred that sacsin exerts a role in proteostatic □C. In the scenario of sacsin loss, putative sacsin substrates or clients can be misfolded or unfolded and can form the aggregates surrounded by the vimentin cage.

In order to investigate aggresomal pathway activation, we checked for ubiquitinated protein levels in ARSACS patient cells, being the proteasome exceeded capacity the first hallmark of aggresome formation (Johnston et al., 1998; Glickman and Ciechanover, 2002). Accumulation of ubiquitin conjugates, indeed, have been reported in a broad array of chronic neurodegenerative diseases characterized by aggregate formation, such as the neurofibrillary tangles of Alzheimer's disease (AD), brain stem Lewy bodies (LBs), the neuropathological hallmark in Parkinson's disease (PD), LBs in LB dementia, nuclear inclusions in CAG repeat expansion (polyglutamine extension) disorders, such as Huntington's disease and spinocerebellar ataxias (SCAs) (Glickman and Ciechanover, 2002). However, we did not detect accumulation of ubiquitinated proteins in ARSACS cells. We also studied directly proteasomal activity in *Sacs* KO mouse CNS, which is interesting to assess also due to the presence of UbL domain in sacsin protein.

Moreover, N-terminal portion of sacsin has been reported to co-immunoprecipitate with the proteasome (Parfitt et al., 2009) and in general, it has been shown that some proteins containing UbL domain are able to bind the proteasome (Hartmann-Petersen and Gordon, 2004). We did not find the ubiquitin proteasome system to be compromised. These data indicate that vimentin network rearrangement is not the result of a problem with clearance of ubiquitinated proteins, as the canonical aggresomal pathway is reported to originate from. To detect putative aggregates, we performed selective aggresome detection experiments, but we did not observe aggregated proteins co-localizing in the vimentin cage area. Furthermore, EM experiments did not reveal cytosolic electron dense material referable to protein aggregates, as conventionally described. In EM, we noticed late stages of autophagic structures filled with electron dense material, which could be suggestive of protein aggregates.

Interestingly, the accumulation of autophagy-related structures in EM images (autophagosomes, autolysosomes, lipid droplets) co-localizes in a specific area close to the nucleus, recalling exactly the vimentin cage found in IF experiments.

The detailed autophagic flux analysis demonstrates an upregulation of autophagy in ARSACS fibroblasts. Supporting evidence, from the paper we published in collaboration, showed multiple components of the proteostasis machinery, among which Hsp70 and lysosomal proteins, relocalizing to the perinuclear region of vimentin accumulation (Duncan et al., 2017). These findings suggest functional changes in autophagy-lysosome pathways. These results could be in line with a role for sacsin in protein C and in maintenance of proteostasis.

The organization of vimentin as a cage' in ARSACS fibroblasts and *SACS* KO HeLa, and as bundles in *SACS* KO MEFs and in primary neuron dendrites (NFs) (Duncan et al., 2017), can reflect a difference in the organization of cell specific cytoskeleton architecture.

Based on our results, we can affirm that loss of sacsin drastically affects organization of intermediate filament network and probably it does not cause the activation of aggresomal pathway in the canonical way. Rather we believe that sacsin can regulate directly intermediate filament dynamics and/or assembly. Sacsin may have a pure direct role (being the chaperone that fold them) or a more indirect role (acting via a mediator) on intermediate filament reorganization. The precise molecular link between sacsin and intermediate filaments is still under investigation.

Perspectives

Future perspectives aimed at dissecting the role of sacsin on intermediate filament cytoskeleton have main objectives. First, they are focused on falsifying the hypothesis of aggresome formation in ARSACS. To do so, we will perform EM of 'aggresomal fraction' and upon aggresome induction (proteasome inhibition) and vimentin cage correlative IF-EM experiments. Second, to identify sacsin substrates, by cloning sacsin, carrying out immunoprecipitation in mouse cerebellum and mass spectrometry and complementing the results with proteomics analysis in *SACS* KO SHSY5Y we recently generated in our lab.

SACS KO SHSY5Y also provide an excellent tool for ARSACS study, as they are neuronal-like cells maintaining easiness in manipulation, but can be differentiated into post mitotic neurons, allowing proteomics studies and avoiding the intrinsic variability when using animal models. On *SACS* KO SHSY5Y, we want to dissect the molecular basis of intermediate filament cytoskeleton remodelling and to define the link between sacsin absence and neurodegeneration.

Conclusion

In our hypothetical model, the first point regards how sacsin mutations affect sacsin function/level and we found that all sacsin mutations lead to a mostly absent mutant protein. The cause of sacsin absence is probably not related to mutant sacsin mRNA stability or protein faster post-translational degradation, but converges towards possible co-translational ☐C mechanisms.

Approaching sacsin absence from the other side, particularly looking at the consequences it causes on cells depleted for sacsin and on *Sacs* KO mouse model, we obtained strong evidence about molecular events underlying ARSACS pathogenesis. On one hand, we have intermediate filament network reorganization. It is probably caused by a straightforward action of sacsin on intermediate filament network architecture or through a direct interaction or via a mediator. On the other hand, we found mitochondrial hyperfusion. It acts through a reduced DRP1 relocalization to the OMM. These two phenotypes can proceed in parallel, considering preliminary evidence underlying a role of sacsin in direct interaction with ARPC2 and so, on actin recruitment of DRP1 during the mitochondrial fission cascade. Alternatively, these two phenotypes may be dependent on each other; the impaired DRP1 trafficking towards the OMM may be secondary to the traffic jam caused by intermediate filament remodelling.

The impaired DRP1 recruitment onto OMM is of particular relevance for Purkinje cells, the primary site affected by ARSACS, where we found a deregulation in mitochondrial proper distribution in distal dendrites.

Going in details of the intermediate filament remodelling phenotype that we observed, it could be an attempt of the cell to compartmentalize misfolded/aggregated proteins. These accumulating proteins can be directly caused by sacsin dysfunction/absence, due to its hypothetical chaperone-like function. While we did not observe evident signs of aggregated proteins, we cannot exclude that sacsin absence leads to a form of aggresome pathway divergent from the canonical one. Indeed, we

did not attain clear-cut evidence of the presence of aggregates both in ARSACS cells and mouse cerebellar tissue. A more realistic explanation is the direct role of sacsin in the remodelling of intermediate filaments (interacting with intermediate filaments, e.g. governing their post-translational folding, or acting through a mediator; or maybe regulating their expression at the transcriptional level). Increased autophagy could be reconciled with a specific response of ARSACS cells to redistribute and functionally modify autophagy components, as consequence to some proteostatic stress (Fig. Conclusion 1).

In summary, our findings identify sacsin crucial role in the fine regulation of mitochondrial and cytoskeletal dynamics. Considering the complex architecture of sacsin functional domains, it is very fascinating the need to evolve such elaborate protein exactly in the high vertebrates of the evolutionary tree. Sacsin's complexity in addition to its major expression in the CNS can lead us to suppose that sacsin is involved in very finely-tuned evolutionarily superior functions.

Fig. Conclusion 1. Hypothetical model summarizing all thesis results.

References

Anderson JF, Siller E, Barral JM. The Sacsin Repeating Region (SRR): A Novel Hsp90-Related Supra-Domain Associated with Neurodegeneration. J. Mol. Biol. 2010; 400: 665–674.

Baets J, Deconinck T, Smets K, Goossens D, Van Den Bergh P, Dahan K, et al. Mutations in SACS cause atypical and late-onset forms of ARSACS. Neurology 2010; 75: 1181–1188.

Bouchard RW, Bouchard JP, Bouchard R, Barbeau A. Electroencephalographic Findings in Friedreich's Ataxia and Autosomal Recessive Spastic Ataxia of Charlevoix-Saguenay (ARSACS). Can. J. Neurol. Sci. / J. Can. des Sci. Neurol. 1979

Bouhlal Y, Amouri R, El Euch-Fayeche G, Hentati F. Autosomal recessive spastic ataxia of Charlevoix-Saguenay: An overview. Park. Relat. Disord. 2011; 17: 418–422.

Bradshaw TY, Romano LEL, Duncan EJ, Nethisinghe S, Abeti R, Michael GJ, et al. A reduction in Drp1-mediated fission compromises mitochondrial health in autosomal recessive spastic ataxia of Charlevoix Saguenay. Hum. Mol. Genet. 2015

Brandman O, Hegde RS. Ribosome-associated protein quality control. Nat. Struct. Mol. Biol. 2016

Cermelli S, Guo Y, Gross SP, Welte MA. The Lipid-Droplet Proteome Reveals that Droplets Are a Protein-Storage Depot. Curr. Biol. 2006; 16: 1783–1795.

Chen H, Chan DC. Mitochondrial dynamics-fusion, fission, movement, and mitophagy-in neurodegenerative diseases. Hum. Mol. Genet. 2009

Chen X, ☐aro JL, Shen WC. Fusion protein linkers: Property, design and functionality. Adv. Drug Deliv. Rev. 2013

Comyn SA, Chan GT, Mayor T. False start: Cotranslational protein ubiquitination and cytosolic protein quality control. J. Proteomics 2014

Duncan EJ, Larivi☐re R, Bradshaw TY, Longo F, Sgarioto N, Hayes MJ, et al. Altered organization of the intermediate filament cytoskeleton and relocalization of proteostasis modulators in cells lacking the ataxia protein sacsin. Hum. Mol. Genet. 2017; 26

Elliott B, Richardson C, Winderbaum J, Nickoloff JA, Jasin M. Gene conversion tracts from double-strand break repair in mammalian cells. Mol. Cell. Biol. 1998

Engert JC, B☐rub☐ P, Mercier J, Dor☐ C, Lepage P, Ge B, et al. ARSACS, a spastic ataxia common in northeastern ☐u☐bec, is caused by mutations in a new gene encoding an 11.5-kb ORF. Nat. Genet. 2000; 24: 120–125.

Franko A, Baris OR, Bergschneider E, Von Toerne C, Hauck SM, Aichler M, et al. Efficient isolation of pure and functional mitochondria from mouse tissues using automated tissue disruption and enrichment with anti-TOM22 magnetic beads. PLoS One 2013

Girard M, Larivi☐re R, Parfitt DA, Deane EC, Gaudet R, Nossova N, et al. Mitochondrial dysfunction and Purkinje cell loss in autosomal recessive spastic ataxia of Charlevoix-Saguenay (ARSACS). Proc. Natl. Acad. Sci. U. S. A. 2012; 109: 1661–6.

Glickman MH, Ciechanover A. The Ubiquitin-Proteasome Proteolytic Pathway: Destruction for the Sake of Construction. Physiol. Rev. 2002

Goley ED, Welch MD. The ARP2/3 complex: An actin nucleator comes of age. Nat. Rev. Mol. Cell Biol. 2006

Greer PL, Hanayama R, Bloodgood BL, Mardinly AR, Lipton DM, Flavell SW, et al. The Angelman Syndrome Protein Ube3A Regulates Synapse Development by Ubiquitinating Arc. Cell 2010; 140: 704–716.

Grynberg M, Erlandsen H, Godzik A. HEPN: A common domain in bacterial drug resistance and human neurodegenerative proteins. Trends Biochem. Sci. 2003

Hartmann-Petersen R, Gordon C. Integral UBL domain proteins: A family of proteasome interacting proteins. Semin. Cell Dev. Biol. 2004

Hatch AL, Gurel PS, Higgs HN. Novel roles for actin in mitochondrial fission. J. Cell Sci. 2014

Hookway C, Ding L, Davidson MW, Rappoport J□, Danuser G, Gelfand VI. Microtubule-dependent transport and dynamics of vimentin intermediate filaments. Mol. Biol. Cell 2015

Horton P, Park KJ, Obayashi T, Fujita N, Harada H, Adams-Collier CJ, et al. WoLF PSORT: Protein localization predictor. Nucleic Acids Res. 2007

Inada T. The Ribosome as a Platform for mRNA and Nascent Polypeptide □uality Control. Trends Biochem. Sci. 2017; 42: 5–15.

Johnston JA, Ward CL, Kopito RR. Aggresomes: A cellular response to misfolded proteins. J. Cell Biol. 1998; 143: 1883–1898.

Kamionka M, Feigon J. Structure of the XPC binding domain of hHR23A reveals hydrophobic patches for protein interaction. Protein Sci. 2004

Klein JS, Jiang S, Galimidi RP, Keeffe JR, Bjorkman PJ, Regan L. Design and characterization of structured protein linkers with differing flexibilities. In: Protein Engineering, Design and Selection. 2014.

Komor AC, Badran AH, Liu DR, Guilinger JP, Bessen JL, Hu JH, et al. CRISPR-based technologies for the manipulation of eukaryotic genomes. Cell 2017

Kopito RR. Aggresomes, inclusion bodies and protein aggregation. Trends Cell Biol. 2000; 10: 524–530.

Kopito RR, Sitia R. Aggresomes and Russell bodies. Symptoms of cellular indigestion□EMBO Rep. 2000; 1: 225–31.

Kozlov G, Denisov AY, Girard M, Dicaire MJ, Hamlin J, McPherson PS, et al. Structural basis of defects in the sacsin HEPN domain responsible for Autosomal Recessive Spastic Ataxia of Charlevoix-Saguenay (ARSACS). J. Biol. Chem. 2011; 286: 20407–20412.

Kraus F, Ryan MT. The constriction and scission machineries involved in mitochondrial fission. J. Cell Sci. 2017

Larivi□re R, Gaudet R, Gentil BJ, Girard M, Conte TC, Minotti S, et al. Sacs knockout mice present pathophysiological defects underlying autosomal recessive spastic ataxia of charlevoix-saguenay. Hum. Mol. Genet. 2015; 24: 727–739.

Li □, Wang K. InterVar: Clinical Interpretation of Genetic Variants by the 2015 ACMG-AMP Guidelines. Am. J. Hum. Genet. 2017; 100: 267–280.

Li S, Xu S, Roelofs BA, Boyman L, Jonathan Lederer W, Sesaki H, et al. Transient assembly of F-actin on the outer mitochondrial membrane contributes to mitochondrial fission. J. Cell Biol. 2015a

Li X, M□nade M, Kozlov G, Hu □, Dai □, McPherson PS, et al. High-throughput screening for ligands of the HEPN domain of sacsin. PLoS One 2015b

Liu R, Chan DC. The mitochondrial fission receptor Mff selectively recruits oligomerized Drp1. Mol. Biol. Cell 2015

Lodish H, Berk A, □ipursky SL, Matsudaira P, Baltimore D, Darnell J. Molecular Cell Biology. 4th edition. Section 19.6, Intermediate Filaments. 2000.

Lowery J, Kuczmarski ER, Herrmann H, Goldma RD. Intermediate filaments play a pivotal role in regulating cell architecture and function. J. Biol. Chem. 2015

Lykke-Andersen J, Bennett EJ. Protecting the proteome: Eukaryotic cotranslational quality control pathways. J. Cell Biol. 2014

Mao □, Bozzella M, Seluanov A, Gorbunova V. Comparison of nonhomologous end joining and homologous recombination in human cells. DNA Repair (Amst). 2008

Morimoto RI, Cuervo AM. Proteostasis and the aging proteome in health and disease. Journals Gerontol. - Ser. A Biol. Sci. Med. Sci. 2014; 69: S33–S38.

Nasif S, Contu L, M□hlemann O. Beyond quality control: The role of nonsense-mediated mRNA decay (NMD) in regulating gene expression. Semin. Cell Dev. Biol. 2017

Paquet D, Kwart D, Chen A, Sproul A, Jacob S, Teo S, et al. Efficient introduction of specific homozygous and heterozygous mutations using CRISPR/Cas9. Nature 2016

Parfitt DA, Michael GJ, Vermeulen EGM, Prodromou N V., Webb TR, Gallo JM, et al. The ataxia protein sacsin is a functional co-chaperone that protects against polyglutamine-expanded ataxin-1. Hum. Mol. Genet. 2009; 18: 1556–1565.

Pechmann S, Willmund F, Frydman J. The Ribosome as a Hub for Protein ☐uality Control. Mol. Cell 2013

Prudent J, McBride HM. Mitochondrial Dynamics: ER Actin Tightens the Drp1 Noose. Curr. Biol. 2016

Ratz M, Testa I, Hell SW, Jakobs S. CRISPR/Cas9-mediated endogenous protein tagging for RESOLFT super-resolution microscopy of living human cells. Sci. Rep. 2015

Renaud JB, Boix C, Charpentier M, De Cian A, Cochennec J, Duvernois-Berthet E, et al. Improved Genome Editing Efficiency and Flexibility Using Modified Oligonucleotides with TALEN and CRISPR-Cas9 Nucleases. Cell Rep. 2016

Richardson CD, Ray GJ, DeWitt MA, Curie GL, Corn JE. Enhancing homology-directed genome editing by catalytically active and inactive CRISPR-Cas9 using asymmetric donor DNA. Nat. Biotechnol. 2016

Roberts B, Haupt A, Tucker A, Grancharova T, Arakaki J, Fuqua MA, et al. Systematic gene tagging using CRISPR/Cas9 in human stem cells to illuminate cell organization. Mol. Biol. Cell 2017

Robinson BH. Mitochondrial Biogenesis and Genetics Part B. 1996.

Romano A, Tessa A, Barca A, Fattori F, Fulvia de Leva M, Terracciano A, et al. Comparative Analysis and Functional Mapping of SACS Mutations Reveal Novel Insights into Sacsin Repeated Architecture. Hum. Mutat. 2013; 34: 525–537.

Schauber C, Chen L, Tongaonkar P, Vega I, Lambertson D, Potts W, et al. Rad23 links DNA repair to the ubiquitin/proteasome pathway. Nature 1998

Shatz O, Holland P, Elazar ☐, Simonsen A. Complex Relations Between Phospholipids, Autophagy, and Neutral Lipids. Trends Biochem. Sci. 2016; 41: 907–923.

Sheng ☐H, Cai ☐. Mitochondrial transport in neurons: Impact on synaptic homeostasis and neurodegeneration. Nat. Rev. Neurosci. 2012

Sihag RK, Inagaki M, Yamaguchi T, Shea TB, Pant HC. Role of phosphorylation on the structural dynamics and function of types III and IV intermediate filaments. Exp. Cell Res. 2007

Silvestri G, Masciullo M, Santorelli FM. Autosomal recessive spastic ataxia of Charlevoix-Saguenay in the time of next-generation sequencing. Arch. Neurol. 2012

Song F, Stieger K. Optimizing the DNA Donor Template for Homology-Directed Repair of Double-Strand Breaks. Mol. Ther. - Nucleic Acids 2017

Synofzik M, Soehn AS, Gburek-Augustat J, Schicks J, Karle KN, Sch☐le R, et al. Autosomal recessive spastic ataxia of Charlevoix Saguenay (ARSACS): expanding the genetic, clinical and imaging spectrum. Orphanet J. Rare Dis. 2013; 8: 41.

Terracciano A, Casali C, Grieco GS, Orteschi D, Di Giandomenico S, Seminara L, et al. An inherited large-scale rearrangement in SACS associated with spastic ataxia and hearing loss. Neurogenetics 2009

Tilokani L, Nagashima S, Paupe V, Prudent J. Mitochondrial dynamics: overview of molecular mechanisms. Essays Biochem. 2018

Wai T, Langer T, Vafai SB, Mootha VK, Liesa M, Shirihai OS, et al. Mitochondrial Dynamics and Metabolic Regulation. Trends Endocrinol. Metab. 2016

Wang F, Canadeo LA, Huibregtse JM. Ubiquitination of newly synthesized proteins at the ribosome. Biochimie 2015

Weiss A, Klein C, Woodman B, Sathasivam K, Bibel M, R☐gulier E, et al. Sensitive biochemical aggregate detection reveals aggregation onset before symptom development in cellular and murine models of Huntington's disease. J. Neurochem. 2008

Xu X, Gao D, Wang P, Chen J, Ruan J, Xu J, et al. Efficient homology-directed gene editing by CRISPR/Cas9 in human stem and primary cells using tube electroporation. Sci. Rep. 2018

Youle RJ, Narendra DP. Mechanisms of mitophagy. Nat. Rev. Mol. Cell Biol. 2011

❑u❑lications

❑n re❑ision: Severe DRP1 axonal neuropathy by impaired turnover of hyperfused mitochondria and peroxisomes.

Longo F, Benedetti S, ❑ambon A, Natali Sora MG, Di Resta C, ❑uattrini A, Maltecca F, Ferrari M and Previtali SC. *❑eurolog❑ 2❑1❑*

❑ Altered organization of the intermediate filament cytoskeleton and relocalisation of proteostasis modulators in cells lacking the ataxia protein sacsin.

Duncan EJ, Larivi❑re R, Bradshaw TY, **Longo F**, Sgarioto N, Hayes MJ, Romano LEL, Nethisinghe S, Giunti P, Bruntraeger MB, Durham HD, Brais B, Maltecca F, Gentil BJ, Chapple JP. Hum Mol Genet. 2017 May 23

❑Myosin IXa Binds AMPAR and Regulates Synaptic Structure, LTP, and Cognitive Function.

Folci A, Murru L, Vezzoli E, Ponzoni L, Gerosa L, Moretto E, **Longo F**, ❑apata J, Braida D, Pistillo F, B❑hler M, Francolini M, Sala M, Bassani S. Front Mol Neurosci. 2016 Jan 20.

Some of my PhD thesis results were published in the paper above indicated (Duncan et al., 2017).